

214
12-4-74

Dr-1083

MASTER

Y-1957

**ORTHOTROPIC PHOTOELASTICITY FOR FIBER-
REINFORCED COMPOSITE MATERIALS**

C. E. Knight, Jr

November 1974



OAK RIDGE Y-12 PLANT
OAK RIDGE, TENNESSEE

*prepared for the U.S. ATOMIC ENERGY COMMISSION
under U.S. GOVERNMENT Contract W-7405 eng 26*

DISTRIBUTION OF THIS DOCUMENT IS UNLIMITED

DISCLAIMER

This report was prepared as an account of work sponsored by an agency of the United States Government. Neither the United States Government nor any agency Thereof, nor any of their employees, makes any warranty, express or implied, or assumes any legal liability or responsibility for the accuracy, completeness, or usefulness of any information, apparatus, product, or process disclosed, or represents that its use would not infringe privately owned rights. Reference herein to any specific commercial product, process, or service by trade name, trademark, manufacturer, or otherwise does not necessarily constitute or imply its endorsement, recommendation, or favoring by the United States Government or any agency thereof. The views and opinions of authors expressed herein do not necessarily state or reflect those of the United States Government or any agency thereof.

DISCLAIMER

Portions of this document may be illegible in electronic image products. Images are produced from the best available original document.

Reference to a company or product name does not imply approval or recommendation of the product by Union Carbide Corporation or the U.S. Atomic Energy Commission to the exclusion of others that may meet specifications.

Printed in the United States of America. Available from
National Technical Information Service
U.S. Department of Commerce
5285 Port Royal Road, Springfield, Virginia 22151
Price: Printed Copy \$5.45; Microfiche \$2.25

This report was prepared as an account of work sponsored by the United States Government. Neither the United States nor the United States Atomic Energy Commission, nor any of their employees, nor any of their contractors, subcontractors, or their employees, makes any warranty, express or implied, or assumes any legal liability or responsibility for the accuracy, completeness or usefulness of any information, apparatus, product or process disclosed, or represents that its use would not infringe privately owned rights.

MASTER

Date of Issue: **November 22, 1974**
Distribution Category: **UC-25**

Report Number: **Y-1957**

ORTHOTROPIC PHOTOELASTICITY FOR FIBER-REINFORCED COMPOSITE MATERIALS

C. E. Knight, Jr

Fabrication Systems Development Department
Y-12 Development Division

NOTICE

This report was prepared as an account of work sponsored by the United States Government. Neither the United States nor the United States Atomic Energy Commission, nor any of their employees, nor any of their contractors, subcontractors, or their employees, makes any warranty, express or implied, or assumes any legal liability or responsibility for the accuracy, completeness or usefulness of any information, apparatus, product or process disclosed, or represents that its use would not infringe privately owned rights.


Adapted from a dissertation that was submitted to The University of Tennessee in partial fulfillment of the requirements for the Degree Doctor of Philosophy.

Oak Ridge Y-12 Plant

P.O. Box Y, Oak Ridge, Tennessee 37830

Prepared for the U.S. Atomic Energy Commission
Under U.S. Government Contract W-7405-eng-26

DISTRIBUTION OF THIS DOCUMENT IS UNLIMITED



ABSTRACT

This study was concerned with the development of orthotropic photoelasticity as a viable means of experimentally analyzing the stresses in orthotropic material structures. Theoretical formulation of the governing equations and verification experiments for the theory were investigated. Material with sufficient transparency and uniformity was prepared.

Theoretical relationships were derived by utilizing the tensorial nature of stress, strain, and birefringence in the material. The relations were condensed to provide the equations needed for plane-stress analysis. Experiments were carried out on special biaxial stress fields created in off-axis uniaxial tensile-stress specimens. Material properties were determined experimentally and calculated from a microstructure finite-element model.

The experiments conducted support the theoretical orthotropic photoelasticity formulation. A plane-stress problem solution by orthotropic photoelasticity showed good correlation with finite-element and elasticity solutions. A model material of fiberglass and epoxy was produced with a low void content and matched refractive indexes to give adequate transparency. Material properties were reasonably predictable from the microstructure model.

CONTENTS

SUMMARY	5
INTRODUCTION	7
ORTHOTROPIC PHOTOELASTICITY	11
Theoretical Development	11
Birefringent Crystal Theory	11
Two-Dimensional Photoelastic Property Tensor Relations	15
Transformation of Photoelastic Tensor	15
Stress-Optic Law for Orthotropic Materials	20
Theoretical Prediction of Properties	23
Finite-Element Model for Normal Stress	24
Finite-Element Analysis for Normal Stress	24
Finite-Element Model for Shear Stress	31
Finite-Element Analysis for Shear Stress	32
Material Fabrication and Model Preparation	34
Selection of Constituent Materials	35
Winding Method	36
Impregnation Procedure for Dry Winding	38
Model Preparation	39
Experimental Evaluation of Material Properties and Stress-Optic Laws	43
Test Methods and Equipment	43
Experimental Determination of Photoelastic Properties	46
Experimental Determination of Elastic Properties	47
Uniaxial Loading Evaluation of Stress-Optic Laws	49
Shear-Difference Method for Orthotropic Photoelasticity	50
Development of Equations	51
Application Along the Arbitrary Axes	54
Application Along the Principal Material Axes	54
Application of Orthotropic Photoelasticity to a Plane-Stress Problem	55
Statement of the Problem	55
Analytical Solution	55
Photoelastic Solution	56
Comparison of Solutions	57
CONCLUSIONS	60
REFERENCES	61
APPENDIX A	63
Finite Element Computer Program for Normal Stress Properties	63

APPENDIX B	81
Finite Element Computer Program for Shear Stress Properties	81
APPENDIX C	89
Extraction of Initial Birefringence	89
ACKNOWLEDGEMENTS	91

SUMMARY

Tensor relations were explored to find stress-optic relations which are most easily applied to problem solution. The general relations were formulated and resolved to two-dimensional space. Transformation equations for the photoelastic property tensor were developed, which resolved the property components in the principal material directions to correspond to any coordinate axes that were chosen.

Symmetries that exist in the material and the combination of tensor components reduced the tensor equations to two basic stress-optic equations for two-dimensional space. These equations were written in terms of the three plane-stress components: photoelastic properties, birefringence, and the isoclinic angle. These two equations may be combined to yield one equation in terms of birefringence, stresses, and photoelastic properties; and a second equation in terms of isoclinic angle, stresses, and properties.

A composite material for photoelastic analysis was fabricated from components with a good match of refractive indexes. The material was free of voids to produce acceptable transparency. The process developed for producing the material began by dry winding fiberglass strands onto a flat, steel mandrel. When the winding was complete, the plate was evacuated in a chamber to remove the air. The epoxy resin was introduced by backfilling the evacuated space in the dry, fiber plate. The composite was cured in a platen press where the composite plate thickness was controlled. Room-temperature curing resins were chosen to minimize the initial birefringence in the material.

Prediction of material elastic and photoelastic properties was made by finite-element methods. Models of the fiber/matrix composite consisted of regular arrays of fibers such as the square array and hexagonal array. Analyses were made for longitudinal and transverse normal stresses and for longitudinal shear stress. Experimental evaluation of the properties was conducted on tensile coupons cut from the material sheet. Experimentally determined values correlated well with the analytical results for both photoelastic and elastic properties. Curves were prepared to show the relationship between constituent properties and composite properties.

The stress-optic relations derived from the tensor equations were verified by experiment. A special biaxial stress field existed in tensile coupons which had the fiber oriented in a known angular direction with respect to the applied load direction. From data taken for 0 and 90-degree orientation along with data at one intermediate angle, the response at all other intermediate angles was predicted from the theory. Experimental data correlated well with the analytical prediction of birefringence and isoclinic angle.

Some of the conventional methods of normal stress separation in isotropic photoelasticity were evaluated for application to orthotropic photoelasticity. Most of the methods did not readily apply, but the shear difference method was developed into a form suitable for use with the orthotropic stress-optic relations. This equation is of the general form so that it may be applied in an arbitrary direction with respect to the material axes. The general equation is simplified considerably if it is applied along the principal material axes.

In order to further validate the theory proposed in this study, analysis of a tensile strip with a central hole was conducted photoelastically and theoretically. Models were fabricated with three fiber orientations: 0, 30, and 90 degrees with respect to the load direction. Material properties (elastic and photoelastic) were obtained from data measured in areas away from the hole on the model. Finite-element models and elasticity solutions provided the theoretical analysis. The proposed stress-optic laws and the shear-difference methods applied to the photoelastic data yielded the experimental solution. In general, the results agreed very well.

INTRODUCTION

Composite materials are finding increased use where high structural performance is required. As the general level of technology is advanced, more demands are placed on the materials selected for use in many applications. High strength-to-weight ratios and/or high stiffness-to-weight ratios are sought for some of the applications. In recent years, development of high-performance fibers and their combination with a suitable matrix or binder to fabricate a composite material has produced some of the needed materials. Efficient application of composite materials can be managed by utilizing accurate analysis and design methods.

Because of the orthotropic nature of fiber-reinforced composite materials, many of the traditional methods of analytical and experimental stress analysis for isotropic materials must be reformulated. High-modulus fibers are usually combined with a lower-modulus matrix to form a composite material. The fibers are usually aligned in a chosen direction; thus, the composite becomes an anisotropic, nonhomogeneous material. On the macroscale, the individual fibers are so small that the material normally is assumed to be homogeneous, but it is still anisotropic. If the fibers are aligned so that there are three orthogonal planes of material symmetry, the material is termed "orthotropic". Anisotropic response is usually not accounted for in traditional methods of analysis.

Photoelasticity is one of the traditional experimental methods. Photoelasticity has been used for many years to analyze stress problems using transparent materials. Models of the structure are fabricated from these materials which are mostly plastics. The stress-optic relations, stated very simply, linearly relate the principal stress difference to the birefringence produced in the model when loaded. The material for the model before loading is both elastically and optically isotropic. The basic photoelastic method is applied to plane-stress problems. Utilization of the isoclinic angle (principal stress direction) and other equations of elasticity with the stress-optic law leads to the complete stress solution.

The stress-optic relations of standard photoelasticity do not apply to orthotropic materials. Materials are termed "orthotropic" because of their elastic orthogonal symmetry. However, this characteristic does not preclude use of photoelasticity methods. It is expected, and easily verified experimentally, that these materials are optically orthotropic as well. Since the material is optically orthotropic, new stress-optic relations are required.

The stress-optic laws for composite materials must be developed analytically and verified experimentally, and must account for this optical orthotropy. The tensorial properties of stress and birefringence are utilized in the formulation of the orthotropic stress-optic laws. The stress-optic relations are verified by experiments from cases of known uniaxial and biaxial stress states. A plane-stress problem of a tensile strip with a central hole is solved photoelastically to demonstrate the validity of the laws.

Research on orthotropic photoelasticity was initiated by Pih and Knight⁽¹⁾ in which fundamental experiments on uniaxial loading were conducted. A composite material of fiber glass with an epoxy matrix was developed which is transparent enough to test photoelastically. Specimens were machined from flat sheets of material. The first

experiments were run on uniaxially stressed specimens with selected fiber orientations. These tests confirm the expected optical anisotropy. Results from the tests indicate a uniaxial-fringe-value curve as a function of the fiber orientation. This curve is very similar to the elastic-modulus curve as a function of the fiber orientation.

A simple proportioning stress-optic law was proposed using principal stresses. It was in the form:

$$N = \frac{t}{f} (C_1\sigma_1 - C_2\sigma_2) \quad (1)$$

where:

- N represents the fringe order,
- t the model thickness,
- f a material constant,
- C₁ the material fringe response in Direction 1,
- C₂ the material fringe response in Direction 2,
- σ₁ one principal stress, and
- σ₂ the second principal stress.

The stress-optic law relates the difference between the birefringence produced by one principal stress and that produced by the second principal stress to the resultant birefringence. Experiments in biaxial loading were performed to check the proposed law. Small, square specimens with a known fiber orientation were loaded by compression rams on all four sides to a known biaxial stress condition. The biaxial stress ratio was varied to obtain a range of data for evaluating the stress-optic law. The data fit was reasonable, but not as accurate as desired.

Although the developed stress-optic law looked reasonable, the behavior of isoclinics was not explained. The isoclinic angle for a known state of stress was reasonably predictable. However, the meaning of the isoclinic was not understood well enough to be used to solve a plane-stress problem.

Sampson⁽²⁾ proposed a stress-optic relationship based on an analogy to Mohr's circle of stress. A Mohr's circle of birefringence was constructed. Construction of the circle was based on the assumption that birefringence components are analogous to stress components. In a cartesian coordinate system, the resultant birefringence is given by:

$$N = \sqrt{\left(\frac{\sigma_x}{f_x} - \frac{\sigma_y}{f_y}\right)^2 + \left(\frac{2\tau_{xy}}{f_{xy}}\right)^2} \quad (2)$$

where:

N represents the fringe order,

σ a normal stress,

τ a shear stress, and

f a material fringe value.

Components in the x and y planes are denoted by the subscripts. This stress-optic law reduces to the form given by Pih and Knight⁽¹⁾ if x and y are chosen along the principal stress directions. Sampson suggested that the shear-difference method can be applied along an axis aligned with the material principal direction. No experimental data were presented to confirm the proposed methods. This work shows the general application of three fringe constants, and experimental values for the material used are presented. The uniaxial-fringe-value curve for a variable fiber orientation has been developed from these data.

Dally and Prabhakaran⁽³⁾ further refined the stress-proportioning method. The material principal axes were chosen for the coordinate axes. Stress components in the material coordinate system were used instead of principal stresses. Various strength-of-materials models were used to estimate the photoelastic constants. These models provided approximate fiber and matrix stresses which were used to compute birefringence. The calculated birefringence was used with the average stress components in the material coordinate system to formulate the stress-optic relations. Birefringence response to uniaxial loading at a variable fiber orientation was predicted and determined experimentally with good agreement. The meaning of isoclinics was not discussed by these authors.

Bert⁽⁴⁾ introduced the application of tensor relations in the formulation of the stress-optic law by adapting the work of Bhagavantam⁽⁵⁾ on crystal theory. In this theory, stress and birefringence were shown as second-order tensors so that the photoelastic-properties tensor which relates stress and birefringence must be fourth order. Symmetry of an aligned fibrous composite was assumed to be representable by the orthorhombic crystal. Symmetry of the orthorhombic crystal and simplification of the three-dimensional tensor relations to two dimensions yield the stress-optic theory for the plane-stress condition. The two-dimensional tensor relations were reduced by use of the Mohr's-circle representation. The two resulting equations involve three photoelastic constants, birefringence, and isoclinic angle. However, these equations were not in a form that was practically suitable for solving general plane-stress problems. No experimental data were presented in this paper.

Pipes and Rose⁽⁶⁾ are proposing the use of strain-optic relations to account for the orthotropic material behavior. They assume that isotropic strain-optic laws apply, and reasonably verify this assumption with tests. Application of the orthotropic stress-strain relations determines the stresses. The material used for testing did not have a very high degree of orthotropy. It remains to be shown that this approach has general applicability for other materials.

Other experimental methods are also being applied to the analysis of orthotropic materials. Obviously, strain gages will be satisfactory for pointwise strain measurement if the self heating of the gage is properly resolved on these poorly conducting materials. Daniel, et al⁽⁷⁾ applied moire grids to plane-stress problems to determine surface strains. They were also successful at carrying the test beyond the linear material range. Dally and Alfirevich⁽⁸⁾ applied photoelastic coatings to composite plates with holes. The most serious problem encountered was the Poisson's ratio mismatch between coating and substrate near the structural boundaries.

Theoretical solutions may be obtained in many cases by the theory of elasticity, as shown in the book by Lekhnitskii⁽⁹⁾. Solutions may also be obtained by applying the finite-element method. This method is described in the book by Zienkiewicz⁽¹⁰⁾.

The study reported in this document was conducted at the Oak Ridge Y-12 Plant.^(a)

(a) Operated by the Union Carbide Corporation's Nuclear Division for the US Atomic Energy Commission.

ORTHOTROPIC PHOTOELASTICITY

THEORETICAL DEVELOPMENT

Birefringent Crystal Theory

In the approach by Bhagavantam⁽⁵⁾, a physical property can be used to relate two measurable physical quantities. Each of these physical quantities may be regarded as a tensor of appropriate rank. The tensorial nature of the applied and response quantities leads to an investigation of the theoretical relations by means of tensor equations. Stress and birefringence are second-rank tensors, as shown by Bhagavantam⁽⁵⁾. The photoelastic property tensor must then be of fourth rank. This condition is similar to the stress-strain relations, where stress and strain are second-rank tensors and the elastic property tensor is fourth rank. In the general, unsymmetrical, three-dimensional case, there are 36 independent photoelastic constants. The equation written in tensor (index) notation becomes:

$$N_{ij} = Q_{ijkl}\sigma_{kl} \quad (i \text{ and } j \text{ can equal } 1, 2, \text{ or } 3), \quad (3)$$

where:

N_{ij} represents the birefringence tensor,

Q_{ijkl} the photoelastic stress-optic properties tensor, and

σ_{kl} the stress tensor.

The tensor suffixes are frequently contracted for ease of writing and recognition⁽¹¹⁾. The contraction generally used is:

$$A_{11} = A_1, A_{22} = A_2, A_{33} = A_3, A_{23} = A_{32} = A_4, A_{13} = A_{31} = A_5, \text{ and } A_{12} = A_{21} = A_6. \quad (4)$$

where A_{ij} (i and j can equal 1, 2, or 3) represents a symmetric, second-rank tensor. Then, for the stress tensor:

$$\sigma_{11} = \sigma_1, \sigma_{22} = \sigma_2, \sigma_{33} = \sigma_3, \sigma_{23} = \sigma_4, \sigma_{13} = \sigma_5, \sigma_{12} = \sigma_6; \quad (5)$$

and, for the birefringence tensor:

$$N_{11} = N_1, N_{22} = N_2, N_{33} = N_3, N_{23} = N_4, N_{13} = N_5, N_{12} = N_6. \quad (6)$$

The strain tensor is usually defined differently as:

$$\epsilon_{11} = \epsilon_1, \epsilon_{22} = \epsilon_2, \epsilon_{33} = \epsilon_3, 2\epsilon_{23} = \epsilon_4, 2\epsilon_{13} = \epsilon_5, 2\epsilon_{12} = \epsilon_6. \quad (7)$$

This difference is caused by the difference between the definition for "tensorial" strain (strain transforming by tensor rules) and the definition for "engineering" strain. For example, the shear modulus, G_{12} , is given by:

$$G_{12} = \frac{\sigma_{12}}{2\epsilon_{12}} = \frac{\sigma_6}{\epsilon_6} \quad (8)$$

It is noted that the contracted notation makes the quantities no longer in tensor form so that if coordinate transformations are required, they must be performed using the original tensor notation.

The generalized Hooke's law, when written in index notation, is:

$$\sigma_{ij} = C_{ijkl}\epsilon_{kl}, \text{ or:} \quad (9)$$

$$\epsilon_{ij} = S_{ijkl}\sigma_{kl} \text{ (i, j, k, and l can equal 1, 2, or 3),} \quad (10)$$

where:

C_{ijkl} represents the elastic stiffnesses, and

S_{ijkl} the elastic compliances.

In contracted notation, Equations 9 and 10 become:

$$\sigma_q = C_{qr}\epsilon_r, \text{ and} \quad (11)$$

$$\epsilon_q = S_{qr}\sigma_r \text{ (q and r can equal any number from 1 through 6).} \quad (12)$$

Expanding Equation 9 for $i = j = l$:

$$\begin{aligned} \sigma_{11} = & C_{1111}\epsilon_{11} + C_{1112}\epsilon_{12} + C_{1113}\epsilon_{13} + C_{1121}\epsilon_{21} + C_{1122}\epsilon_{22} \\ & + C_{1123}\epsilon_{23} + C_{1131}\epsilon_{31} + C_{1132}\epsilon_{32} + C_{1133}\epsilon_{33}. \end{aligned} \quad (13)$$

Contracting the stresses and strains and using their symmetries:

$$\begin{aligned} \sigma_1 = & C_{1111}\epsilon_1 + 2C_{1112}\left(\frac{1}{2}\epsilon_6\right) + 2C_{1113}\left(\frac{1}{2}\epsilon_5\right) + C_{1122}\epsilon_2 + \\ & 2C_{1123}\left(\frac{1}{2}\epsilon_4\right) + C_{1133}\epsilon_3. \end{aligned} \quad (14)$$

Expanding Equation 11 and comparing terms:

$$\sigma_1 = C_{11}\epsilon_1 + C_{12}\epsilon_2 + C_{13}\epsilon_3 + C_{14}\epsilon_4 + C_{15}\epsilon_5 + C_{16}\epsilon_6, \text{ then:} \quad (15)$$

$$\begin{aligned}
C_{1111} = C_{11}, C_{1122} = C_{12}, C_{1133} = C_{13}, C_{1123} = \\
C_{14}, C_{1113} = C_{15}, C_{1112} = C_{16}.
\end{aligned} \tag{16}$$

Carrying this expansion and comparison through gives:

$$C_{ijkl} \rightarrow C_{qr}. \tag{17}$$

Expanding Equation 10 for $i = j = l$:

$$\begin{aligned}
\epsilon_{11} = S_{1111}\sigma_{11} + S_{1112}\sigma_{12} + S_{1113}\sigma_{13} + S_{1121}\sigma_{21} + S_{1122}\sigma_{22} + \\
S_{1123}\sigma_{23} + S_{1131}\sigma_{31} + S_{1132}\sigma_{32} + S_{1133}\sigma_{33}.
\end{aligned} \tag{18}$$

Contracting the stresses and strain:

$$\begin{aligned}
\epsilon_1 = S_{1111}\sigma_1 + 2S_{1112}\sigma_6 + 2S_{1113}\sigma_5 + S_{1122}\sigma_2 + \\
2S_{1123}\sigma_4 + S_{1133}\sigma_3.
\end{aligned} \tag{19}$$

Expanding Equation 12 and comparing terms:

$$\epsilon_1 = S_{11}\sigma_1 + S_{12}\sigma_2 + S_{13}\sigma_3 + S_{14}\sigma_4 + S_{15}\sigma_5 + S_{16}\sigma_6, \text{ then:} \tag{20}$$

$$\begin{aligned}
S_{1111} = S_{11}, S_{1122} = S_{12}, S_{1133} = S_{13}, 2S_{1123} = S_{14}, \\
2S_{1113} = S_{15}, 2S_{1112} = S_{16}.
\end{aligned} \tag{21}$$

Carrying through this expansion and comparison results in:

$$\left. \begin{aligned}
S_{ijkl} &\rightarrow S_{qr} \text{ (q and r can equal 1, 2, or 3)} \\
2S_{ijkl} &\rightarrow S_{qr} \text{ (q can equal 1, 2, or 3; r can equal 4, 5, or 6)} \\
4S_{ijkl} &\rightarrow S_{qr} \text{ (q and r can equal 4, 5, or 6)}
\end{aligned} \right\} \tag{22}$$

The relations between birefringence and stress, and birefringence and strain, may also be contracted. The stress-optic relations and the strain-optic relations may be written:

$$N_{ij} = Q_{ijkl}\sigma_{kl}, \text{ and} \tag{23}$$

$$N_{ij} = P_{ijkl}\epsilon_{kl} \text{ (i and j can equal 1, 2, or 3),} \tag{24}$$

where P_{ijkl} represents the strain-optic property tensor. The other terms are as defined previously.

By contracting, Equations 23 and 24 can be written:

$$N_q = Q_{qr}\sigma_r, \text{ and} \quad (25)$$

$$N_q = P_{qr}\epsilon_r \text{ (q and r can equal any number from 1 through 6).} \quad (26)$$

From Equations 11, 12, 25, and 26, the stress-optic and strain-optic properties can be related through the elastic stiffnesses or compliances. The resulting relations are:

$$P_{qs} = Q_{qr}C_{rs}, \text{ and} \quad (27)$$

$$Q_{qs} = P_{qr}S_{rs} \text{ (p, q, r, and s can equal any number from 1 through 6).} \quad (28)$$

Expanding Equations 23 through 26, and comparing terms as before, results in:

$$\left. \begin{aligned} Q_{ijkl} &\rightarrow Q_{qr} \text{ (when } q = 1 \text{ to } 6; r = 1, 2, \text{ or } 3) \\ 2Q_{ijkl} &\rightarrow Q_{qr} \text{ (when } q = 1 \text{ to } 6; r = 4, 5, \text{ or } 6) \\ P_{ijkl} &\rightarrow P_{qr} \text{ (q and r = 1 to 6)} \end{aligned} \right\} \quad (29)$$

It is important to note that P_{qr} and Q_{qr} do not have the full symmetry that C_{qr} and S_{qr} have, ie:

$$\left. \begin{aligned} C_{qr} &= C_{rq}, S_{qr} = S_{rq} \\ P_{qr} &\neq P_{rq}, Q_{qr} \neq Q_{rq} \end{aligned} \right\} \quad (30)$$

For the general unsymmetrical case, then, there are 36 independent photoelastic constants.

A large number of the two-dimensional problems encountered are likely to be plane-stress problems. Therefore, only the stress-optic relations are completely developed and used in this work. When the stress-optic relations of Equation 25 are written in matrix form, they become:

$$\begin{bmatrix} N_1 \\ N_2 \\ N_3 \\ N_4 \\ N_5 \\ N_6 \end{bmatrix} = \begin{bmatrix} Q_{11} & Q_{12} & Q_{13} & Q_{14} & Q_{15} & Q_{16} \\ Q_{21} & Q_{22} & Q_{23} & Q_{24} & Q_{25} & Q_{26} \\ Q_{31} & Q_{32} & Q_{33} & Q_{34} & Q_{35} & Q_{36} \\ Q_{41} & Q_{42} & Q_{43} & Q_{44} & Q_{45} & Q_{46} \\ Q_{51} & Q_{52} & Q_{53} & Q_{54} & Q_{55} & Q_{56} \\ Q_{61} & Q_{62} & Q_{63} & Q_{64} & Q_{65} & Q_{66} \end{bmatrix} \begin{bmatrix} \sigma_1 \\ \sigma_2 \\ \sigma_3 \\ \sigma_4 \\ \sigma_5 \\ \sigma_6 \end{bmatrix} \quad (31)$$

As proposed by Bert,⁽⁴⁾ the general fiber-reinforced composite material with unidirectionally aligned fibers may be considered similar to an orthorhombic crystal which has three principal material directions. This assumption reduces to 12 the number of photoelastic constants in three-dimensional space. Equation 31 then becomes:

$$\begin{bmatrix} N_1 \\ N_2 \\ N_3 \\ N_4 \\ N_5 \\ N_6 \end{bmatrix} = \begin{bmatrix} Q_{11} & Q_{12} & Q_{13} & 0 & 0 & 0 \\ Q_{21} & Q_{22} & Q_{23} & 0 & 0 & 0 \\ Q_{31} & Q_{32} & Q_{33} & 0 & 0 & 0 \\ 0 & 0 & 0 & Q_{44} & 0 & 0 \\ 0 & 0 & 0 & 0 & Q_{55} & 0 \\ 0 & 0 & 0 & 0 & 0 & Q_{66} \end{bmatrix} \begin{bmatrix} \sigma_1 \\ \sigma_2 \\ \sigma_3 \\ \sigma_4 \\ \sigma_5 \\ \sigma_6 \end{bmatrix} \quad (32)$$

Two-Dimensional Photoelastic Property Tensor Relations

The stress-optic relations may be simplified further by considering only two-dimensional problems and thus eliminating the third dimensional terms. In the 1-2 plane, then, Equation 32 becomes:

$$\begin{bmatrix} N_1 \\ N_2 \\ N_6 \end{bmatrix} = \begin{bmatrix} Q_{11} & Q_{12} & 0 \\ Q_{21} & Q_{22} & 0 \\ 0 & 0 & Q_{66} \end{bmatrix} \begin{bmatrix} \sigma_1 \\ \sigma_2 \\ \sigma_6 \end{bmatrix} \quad (33)$$

Transformation of Photoelastic Tensor

The photoelastic stress-optic property tensor may be transformed to another set of coordinates by the rules for tensor transformations. In indicial notation, the rule for transformation of a first-rank tensor (a vector) is given by:

$$V_i' = a_{ij} V_j, \quad (34)$$

where:

V_i' represents the transformed vector,

a_{ij} the transformation coefficients for a vector, and

V_j the original vector.

For rotation about the 3 axis through Angle θ , a_{ij} is:

$$[a] = \begin{pmatrix} m & n \\ -n & m \end{pmatrix}, \quad (35)$$

where:

[a] represents the transformation matrix,

$m = \cos \theta$, and

$n = \sin \theta$.

The transformation rule is generalized for higher-rank tensors such as the fourth-rank transformation:

$$Q'_{ijkl} = a_{im}a_{jn}a_{ko}a_{lp}Q_{mnop} \quad (36)$$

where:

Q'_{ijkl} represents the transformed fourth-rank tensor,

$a_{im} \dots a_{lp}$ the transformation coefficients for a vector, and

Q_{mnop} the original tensor.

As stated previously, the photoelastic property tensor is of fourth rank and thus transforms, as in Equation 36. The transformation must be applied to the uncontracted tensor, however, so that the original tensorial nature is maintained.

Hearmon⁽¹²⁾ presents a composite equation in tabular form for the general fourth-rank tensor transformation. Table 1 shows this form of the transformation relations. In the table, the numerical entries in the boxes are the subscripts of the original tensor (say, $mnop$ of Q_{mnop} in Equation 36). The lower-case, subscripted a's are the direction cosines from the transformation matrix. This table and the general fourth-rank tensor transformation represent 81 equations, each with 81 terms. For example, the coefficient of the Q_{3313} term in the equation for a transformed component of Q'_{ijkl} (say, Q'_{1231}) is $a_{13}^2 a_{23} a_{31}$.

For the tensor quantities used here, the number of equations and terms is reduced due to their symmetries. When the original coordinate system is aligned with the principal axes for an orthorhombic crystal, Table 1 may be simplified, as in Table 2. Table 2 represents the transformation equations for the elastic stiffnesses, C_{ijkl} , the elastic compliances, S_{ijkl} , the stress-optic coefficients, Q_{ijkl} , and the strain-optic coefficients, P_{ijkl} .

When the rotation is about one of the principal axes, further simplifications occur. If the 1-2 axes are rotated through Angle θ about the 3 axis in a positive direction, then:

$$\left. \begin{aligned} a_{11} = m, a_{12} = n, a_{21} = -n, a_{22} = m, a_{33} = 1 \\ a_{13} = a_{23} = a_{31} = a_{32} = 0 \end{aligned} \right\} \quad (37)$$

where:

$m = \cos \theta$ and $n = \sin \theta$.

Table 1
COMPOSITE EQUATION FOR TRANSFORMING A GENERAL, FOURTH-RANK TENSOR

	$a_{i_1 a_{j_1}}$	$a_{i_2 a_{j_2}}$	$a_{i_3 a_{j_3}}$	$a_{i_2 a_{j_3}}$	$a_{i_3 a_{j_2}}$	$a_{i_1 a_{j_3}}$	$a_{i_3 a_{j_1}}$	$a_{i_1 a_{j_2}}$	$a_{i_2 a_{j_1}}$	
$Q_{ijkl} =$	1111	2211	3311	2311	3211	1311	3111	1211	2111	$a_{k_1 a_{l_1}}$
	1122	2222	3322	2322	3222	1322	3122	1222	2122	$a_{k_2 a_{l_2}}$
	1133	2233	3333	2333	3233	1333	3133	1233	2133	$a_{k_3 a_{l_3}}$
	1123	2223	3323	2323	3223	1323	3123	1223	2123	$a_{k_2 a_{l_3}}$
	1132	2232	3332	2332	3232	1332	3132	1232	2132	$a_{k_3 a_{l_2}}$
	1113	2213	3313	2313	3213	1313	3113	1213	2113	$a_{k_1 a_{l_3}}$
	1131	2231	3331	2331	3231	1331	3131	1231	2131	$a_{k_3 a_{l_1}}$
	1112	2212	3312	2312	3212	1312	3112	1212	2112	$a_{k_1 a_{l_2}}$
	1121	2221	3321	2321	3221	1321	3121	1221	2121	$a_{k_2 a_{l_1}}$

Table 2
COMPOSITE EQUATION FOR TRANSFORMING AN ORTHORHOMBIC, FOURTH-RANK TENSOR

	$a_{i_1 a_{j_1}}$	$a_{i_2 a_{j_2}}$	$a_{i_3 a_{j_3}}$	$a_{i_2 a_{j_3}}$	$a_{i_3 a_{j_2}}$	$a_{i_1 a_{j_3}}$	$a_{i_3 a_{j_1}}$	$a_{i_1 a_{j_2}}$	$a_{i_2 a_{j_1}}$	
$Q_{ijkl} =$	1111	2211	3311	-	-	-	-	-	-	$a_{k_1 a_{l_1}}$
	1122	2222	3322	-	-	-	-	-	-	$a_{k_2 a_{l_2}}$
	1133	2233	3333	-	-	-	-	-	-	$a_{k_3 a_{l_3}}$
	-	-	-	2323	3223	-	-	-	-	$a_{k_2 a_{l_3}}$
	-	-	-	2332	3232	-	-	-	-	$a_{k_3 a_{l_2}}$
	-	-	-	-	-	1313	3113	-	-	$a_{k_1 a_{l_3}}$
	-	-	-	-	-	1331	3131	-	-	$a_{k_3 a_{l_1}}$
	-	-	-	-	-	-	-	1212	2112	$a_{k_1 a_{l_2}}$
	-	-	-	-	-	-	-	1221	2121	$a_{k_2 a_{l_1}}$

Expanding Table 2 and using contracted indexes, the elastic stiffnesses and elastic compliances may be transformed, as in Table 3.

Table 3
ELASTIC STIFFNESS AND COMPLIANCE TRANSFORMATION EQUATIONS

	Transformation Equation			
	S_{11} (C_{11})	S_{12} (C_{12})	S_{22} (C_{22})	S_{66} ($4C_{66}$)
S'_{11} (C'_{11})	m^4	$2m^2n^2$	n^4	m^2n^2
S'_{12} (C'_{12})	m^2n^2	m^4+n^4	m^2n^2	$-m^2n^2$
S'_{16} ($2C'_{16}$)	$-2m^3n$	$2(m^3n-mn^3)$	$2mn^3$	m^3n-mn^3
S'_{22} (C'_{22})	n^4	$2m^2n^2$	m^4	m^2n^2
S'_{26} ($2C'_{26}$)	$-2mn^3$	$2(mn^3-m^3n)$	$2m^3n$	mn^3-m^3n
S'_{66} ($4C'_{66}$)	$4m^2n^2$	$-8m^2n^2$	$4m^2n^2$	$(m^2-n^2)^2$
		S_{13} (C_{13})		S_{23} (C_{23})
S'_{13} (C'_{13})		m^2		n^2
S'_{23} (C'_{23})		n^2		m^2
S'_{36} ($2C'_{36}$)		$-2mn$		$2mn$
		S_{44} (C_{44})		S_{55} (C_{55})
S'_{44} (C'_{44})		m^2		n^2
S'_{45} (C'_{45})		mn		$-mn$
S'_{55} (C'_{55})		n^2		m^2

For example, from Table 3:

$$S'_{11} = m^4S_{11} + 2m^2n^2S_{12} + n^4S_{22} + m^2n^2S_{66}, \text{ and:} \quad (38)$$

$$2C'_{26} = -2mn^3C_{11} + 2(mn^3-m^3n)C_{12} + 2m^3nC_{22} + 4(mn^3-m^3n)C_{66}. \quad (39)$$

Expanding Table 2 and using contracted indexes for the stress-optic and strain-optic coefficients, yields Table 4.

For example, from Table 4:

$$Q'_{21} = m^2n^2Q_{11} + n^4Q_{12} + m^4Q_{21} + m^2n^2Q_{22} - 2m^2n^2Q_{66}, \text{ and} \quad (40)$$

$$P'_{16} = -m^3nP_{11} + m^3nP_{12} - mn^3P_{21} - mn^3P_{22} + 2mn(m^2 - n^2)P_{66} \quad (41)$$

Table 4
STRESS-OPTIC AND STRAIN-OPTIC COEFFICIENT
TRANSFORMATION EQUATIONS

Transformation Equations					
	$Q_{11} (P_{11})$	$Q_{12} (P_{12})$	$Q_{21} (P_{21})$	$Q_{22} (P_{22})$	$Q_{66} (2P_{66})$
$Q'_{11} (P'_{11})$	m^4	m^2n^2	m^2n^2	n^4	$2m^2n^2$
$Q'_{12} (P'_{12})$	m^2n^2	m^4	n^4	m^2n^2	$-2m^2n^2$
$Q'_{21} (P'_{21})$	m^2n^2	n^4	m^4	m^2n^2	$-2m^2n^2$
$Q'_{22} (P'_{22})$	n^4	m^2n^2	m^2n^2	m^4	$2m^2n^2$
$Q'_{16} (2P'_{16})$	$-2m^3n$	$2m^3n$	$-2mn^3$	$2mn^3$	$2mn(m^2-n^2)$
$Q'_{26} (2P'_{26})$	$-2mn^3$	$2mn^3$	$-2m^3n$	$2m^3n$	$-2mn(m^2-n^2)$
$Q'_{61} (P'_{61})$	$-m^3n$	$-mn^3$	m^3n	mn^3	$mn(m^2-n^2)$
$Q'_{62} (P'_{62})$	$-mn^3$	$-m^3n$	mn^3	m^3n	$-mn(m^2-n^2)$
$Q'_{66} (2P'_{66})$	$2m^2n^2$	$-2m^2n^2$	$-2m^2n^2$	$2m^2n^2$	$(m^2-n^2)^2$

	$Q_{13} (P_{13})$	$Q_{31} (P_{31})$	$Q_{23} (P_{23})$	$Q_{32} (P_{32})$
$Q'_{13} (P'_{13})$	m^2	-	n^2	-
$Q'_{31} (P'_{31})$	-	m^2	-	n^2
$Q'_{23} (P'_{23})$	n^2	-	m^2	-
$Q'_{32} (P'_{32})$	-	n^2	-	m^2
$Q'_{36} (2P'_{36})$	-	$-2mn$	-	$2mn$
$Q'_{63} (P'_{63})$	$-mn$	-	mn	-

	$Q_{44} (P_{44})$	$Q_{55} (P_{55})$
$Q'_{44} (P'_{44})$	m^2	n^2
$Q'_{45} (P'_{45})$	mn	$-mn$
$Q'_{54} (P'_{54})$	mn	$-mn$
$Q'_{55} (P'_{55})$	n^2	m^2

Stress-Optic Law for Orthotropic Materials

The birefringence tensor in Equation 33 is given by its components in the coordinate system, coinciding with the principal material directions (1, 2, 3 axes). In the general case, the reference coordinates may be arbitrarily chosen. In the polariscope, only the birefringence components in the plane normal to the light path have any effect. Orientation of the principal birefringence components in the plane is given by the isoclinic angle observed in the polariscope. By the second-rank tensor transformation, then, after selecting the 3 axis to be coaxial with the polariscope, Equation 33 becomes:

$$\begin{pmatrix} N_p \cos^2 \phi + N_q \sin^2 \phi \\ N_p \sin^2 \phi + N_q \cos^2 \phi \\ (N_q - N_p) \sin \phi \cos \phi \end{pmatrix} = \begin{pmatrix} Q'_{11} & Q'_{12} & Q'_{16} \\ Q'_{21} & Q'_{22} & Q'_{26} \\ Q'_{61} & Q'_{62} & Q'_{66} \end{pmatrix} \begin{pmatrix} \sigma_x \\ \sigma_y \\ \tau_{xy} \end{pmatrix} \quad (42)$$

where:

p and q represent the principal birefringence directions, and

ϕ the isoclinic angle in the polariscope referenced to the x axis. Q'_{ij} is defined in Table 4 (i and j can equal 1, 2, or 6).

The birefringence components, as defined by Bhagavantam,⁽⁵⁾ are:

$$N_p = \frac{1}{n_p^2} \quad \text{and} \quad N_q = \frac{1}{n_q^2} \quad (43)$$

where n represents the index of refraction.

The observed quantity in the polariscope is the relative retardation, which is proportional to $(n_p - n_q)$. The first two expressions of Equations 42 may be combined to yield:

$$(N_p - N_q) (\cos^2 \phi - \sin^2 \phi) = (Q'_{11} - Q'_{21}) \sigma_x - (Q'_{22} - Q'_{12}) \sigma_y + (Q'_{16} - Q'_{26}) \tau_{xy}, \quad (44)$$

and the third expression of Equation 42 gives:

$$(N_q - N_p) \sin \phi \cos \phi = Q'_{61} \sigma_x + Q'_{62} \sigma_y + Q'_{66} \tau_{xy} \quad (45)$$

From Equation 43:

$$(N_q - N_p) = \frac{1}{n_q^2} - \frac{1}{n_p^2} = \frac{n_p^2 - n_q^2}{n_p^2 n_q^2} \approx \frac{2(n_p - n_q)}{n_o^3} \quad (46)$$

since the refractive-index changes under stress are small compared to the index magnitude, and n_0 is the average index of refraction of the unstressed material. Substituting Equation 46 and lumping some of the constants together, Equations 44 and 45 become:

$$N \cos 2\phi = C_1\sigma_x - C_2\sigma_y + C_3\tau_{xy}, \text{ and} \quad (47)$$

$$N \sin 2\phi = -2[C_4\sigma_x + C_5\sigma_y + C_6\tau_{xy}] \quad (48)$$

where:

$$N = (n_q - n_p) \frac{2}{n_0^3},$$

$$C_1 = (Q'_{11} - Q'_{21}),$$

$$C_2 = (Q'_{22} - Q'_{12}),$$

$$C_3 = (Q'_{16} - Q'_{26}),$$

$$C_4 = Q'_{61},$$

$$C_5 = Q'_{62}, \text{ and}$$

$$C_6 = Q'_{66}.$$

From Table 4:

$$\left. \begin{aligned} C_1 &= m^2(m^2 - n^2)(Q_{11} - Q_{21}) - n^2(m^2 - n^2)(Q_{22} - Q_{12}) + 4m^2n^2Q_{66} \\ C_2 &= -[n^2(m^2 - n^2)(Q_{11} - Q_{21})] + [m^2(m^2 - n^2)(Q_{22} - Q_{12})] + [4m^2n^2Q_{66}] \\ C_3 &= -2mn(m^2 - n^2)(Q_{11} - Q_{21}) - 2mn(m^2 - n^2)(Q_{22} - Q_{12}) + 4mn(m^2 - n^2)Q_{66} \\ C_4 &= -m^3n(Q_{11} - Q_{21}) + mn^3(Q_{22} - Q_{12}) + mn(m^2 - n^2)Q_{66} \\ C_5 &= -mn^3(Q_{11} - Q_{21}) + m^3n(Q_{22} - Q_{12}) - mn(m^2 - n^2)Q_{66} \\ C_6 &= 2m^2n^2(Q_{11} - Q_{21}) + 2m^2n^2(Q_{22} - Q_{12}) + (m^2 - n^2)^2Q_{66} \end{aligned} \right\} (49)$$

Equations 47 and 48, along with the relations just given (49), form the basic, two-dimensional, stress-optic theory for orthotropic materials.

For the case where the coordinate system (x,y) is aligned with the material principal axes:

$$C_1^* = C_1 = Q_{11} - Q_{21}, C_2^* = C_2 = (Q_{22} - Q_{12}), C_6^* = C_6 = Q_{66}$$

(50)

$$C_3 = C_4 = C_5 = 0.$$

This development results in the following form for the stress-optic relations:

$$N \cos 2\phi = C_1^* \sigma_x - C_2^* \sigma_y, \text{ and} \quad (51)$$

$$N \sin 2\phi = -2C_6^* \tau_{xy}, \quad (52)$$

where the asterisk denotes properties in the material principal coordinates. Thus, for the general plane-stress problem, the photoelastic stress-optic relations can be applied with three basic properties: C_1^* , C_2^* , and C_6^* , since, in other coordinate systems, the properties (C_1 through C_6) can be obtained from Equations 49 and 50.

Physical interpretation of these properties is straightforward. If σ_x is the only nonzero stress and the x axis is aligned with the fiber direction in the composite (0 degree), then C_1^* is the slope of the stress-birefringence curve. It would be expected, and has been shown experimentally, that the isoclinic angle, ϕ equals 0 degree. The birefringence is linearly proportional to the material thickness, and the familiar photoelastic term (the material fringe value) is introduced here. The fringe value for this loading condition is:

$$f_1 = \frac{t}{C_1^*}, \quad (53)$$

where:

t represents the thickness, and

f_1 the material fringe value for uniaxial stress along the fiber direction.

Similarly:

$$f_2 = \frac{t}{C_2^*}, \quad (54)$$

where f_2 represents the material fringe value for a uniaxial stress transverse to the fiber direction.

For these two cases, the applied uniaxial stress has been coaxial or transverse to the fiber direction (the x,y coordinates). Thus, there was no shear stress, τ_{xy} . If the fiber is aligned at some intermediate angle with the applied uniaxial stress, there will be a shear stress, τ_{xy} , and the isoclinic angle will generally be between 0 and 90 degrees. In order to determine the shear constant, C_6^* , the uniaxial stress is applied at some angle, θ , to the fiber direction. Then, from Equation 52, $2C_6^*$ is the slope of the shear stress-birefringence curve multiplied by $\sin 2\phi$. The principal shear material fringe value is:

$$f_{12} = \frac{t}{C_6^*}. \quad (55)$$

The stress-optic relations may now be written in terms of material fringe values when the coordinate system coincides with the material principal axes. Equations 51 and 52 become:

$$N \cos 2\phi = t \left(\frac{\sigma_x}{f_1} - \frac{\sigma_y}{f_2} \right), \text{ and} \quad (56)$$

$$N \sin 2\phi = - 2t \frac{\tau_{xy}}{f_{12}} \quad (57)$$

Two other forms of the stress-optic relations may also be obtained. By squaring both sides of Equations 56 and 57, and adding:

$$N = t \sqrt{\left(\frac{\sigma_x}{f_1} - \frac{\sigma_y}{f_2} \right)^2 + \left(\frac{2\tau_{xy}}{f_{12}} \right)^2} \text{ is obtained.} \quad (58)$$

Dividing Equation 57 by Equation 56 gives:

$$\phi = \frac{1}{2} \tan^{-1} \frac{- \frac{2\tau_{xy}}{f_{12}}}{\frac{\sigma_x}{f_1} - \frac{\sigma_y}{f_2}} \quad (59)$$

It is noted that these forms of the stress-optic relations may be applied only when the x and y coordinates coincide with the material principal directions.

In summary, there are two equations with three unknowns (σ_x , σ_y , and τ_{xy}) and two measured quantities (N and ϕ), with three photoelastic properties (f_1 , f_2 , and f_{12}). Other relations must be used to determine the separate stress components. These relations are developed in a later section.

THEORETICAL PREDICTION OF PROPERTIES

In order to utilize the equations of mechanics or photomechanics; in most cases, the values of all the material properties must be known. In the case of isotropic materials, the number of properties is usually small and they are easily determined by tests. Fiber-reinforced composite materials, however, generally have more properties due to orthotropy. Properties vary with the fiber/matrix volume fractions as well as the constituent material properties. Generally, the continuous fiber-reinforced composites are transversely isotropic (isotropic in the plane normal to the fiber direction) or orthotropic (with three orthogonal axes of material symmetry). In either case, usually the two-dimensional problems of interest have two orthogonal axes of material symmetry.

The number of properties and their variation requires an extensive testing plan to fully evaluate the property values. Therefore, it is desirable to be able to predict the property values with a mathematical model and verify it with a limited number of tests.

Finite-Element Model for Normal Stress

The model that has been most successful for predicting the elastic properties of composite materials is the periodic array of fibers in a matrix. One arrangement used to model the composite is the square array of fibers, illustrated in Figure 1. In this array, the maximum fiber volume fraction is 78.5%, but this value is not of much significance since most composites do not reach this value. This square array may be elongated to a rectangular array if it seems appropriate to model the particular composite under study.

The most efficient packing of fibers can be realized with the hexagonal array, as outlined in Figure 2. The maximum fiber fraction in this array is 90.6%. In actuality, neither of these idealized arrays exactly model the real composite, so the effectiveness of the model must be judged by its correlation with experimental data.

From a regular array, a typical repeating section (as in Figures 1 or 2) is chosen to represent the model. In this section, a finite element quadrilateral mesh is generated, as indicated in Figure 3 for the square array. Outline of the fiber is clearly indicated, and the connectivity of the mesh across the fiber boundary implies a uniform bond between the fiber and matrix.

Since the section is removed from a symmetric field, the displacements of the boundaries must be uniform in order to maintain compatibility. These boundary conditions are easily applied in the finite-element stress-analysis method. The assumed displacements are indicated in Figure 3. As described later, combinations of these displacements are used to produce the desired loading conditions.

Finite-Element Analysis for Normal Stress

The analysis is performed by supplying this model and boundary conditions to a finite-element computer code (given in Appendix A) along with appropriate properties of the constituent materials. For a given set of boundary conditions, a state of stress and strain exists in the model. Photoelastically, when the model is stressed, the fiber and matrix have different photoelastic responses at every point in the model because, in general, the stress field is not uniform.

For a given loading condition, the stresses at each point produce a birefringence which must be integrated over the total light path through the model to obtain the overall effect. A differential area, dA in Figure 3, which represents the point has a birefringence of:

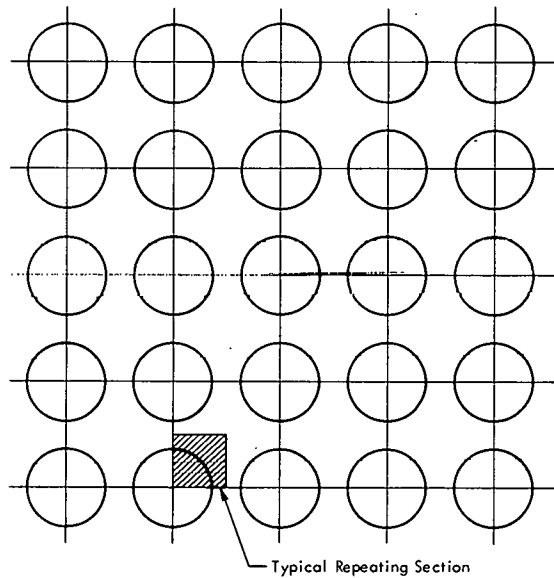


Figure 1. SQUARE ARRAY OF PARALLEL, CONTINUOUS FIBERS IN A MATRIX FORMING A COMPOSITE MATERIAL MODEL.

$$dN = (p - q) \frac{dZ}{f}, \quad (60)$$

where:

- dN represents the differential birefringence,
- dZ the incremental thickness in the direction of observation or the light path,
- $(p - q)$ the difference between the principal stresses in the RT plane, and
- f the material fringe value of the material in the differential area, dA .

Integrating Equation 60 gives the birefringence produced through the thickness at any given value of R . Since a point observable by eye covers a large number of fibers, the birefringence as a function of R may be replaced by its average value. Integrating with respect to R and dividing by R_{\max} ($R_{\max} = 1$ for the square array) gives this average. The macroscopic birefringence is given by:

$$N = \int \int (p - q) \frac{1}{f} dR dZ. \quad (61)$$

The finite-element program yields constant values of stress, material fringe value, and birefringence within each element. Thus, the integration can be replaced by a summation for all the elements. Equation 61 becomes:

$$N = \sum_{m=1}^M (p - q) \frac{1}{f} \Big|_m A_m, \quad (62)$$

where:

- N represents the average fringe order produced by an average stress state in the material,
- m refers to an element, and
- M represents the total number of elements.

As mentioned, the model is displacement controlled. When the model is subjected to known displacements, in general, a nonuniform stress exists along each boundary of the model. The average of this stress distribution must equal the applied stress in a macroscopic sense. By applying the correct displacements at the model boundaries, average stress states can be produced which may be used to calculate the elastic properties.

Several displacement combinations are used to determine the elastic properties in conjunction with the orthotropic stress-strain relations. In order to obtain three-dimensional

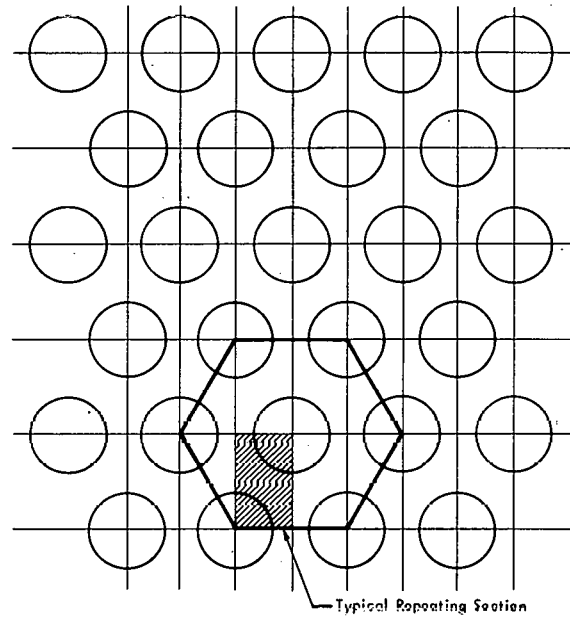


Figure 2. HEXAGONAL ARRAY OF PARALLEL, CONTINUOUS FIBERS IN A MATRIX FORMING A COMPOSITE MATERIAL MODEL.

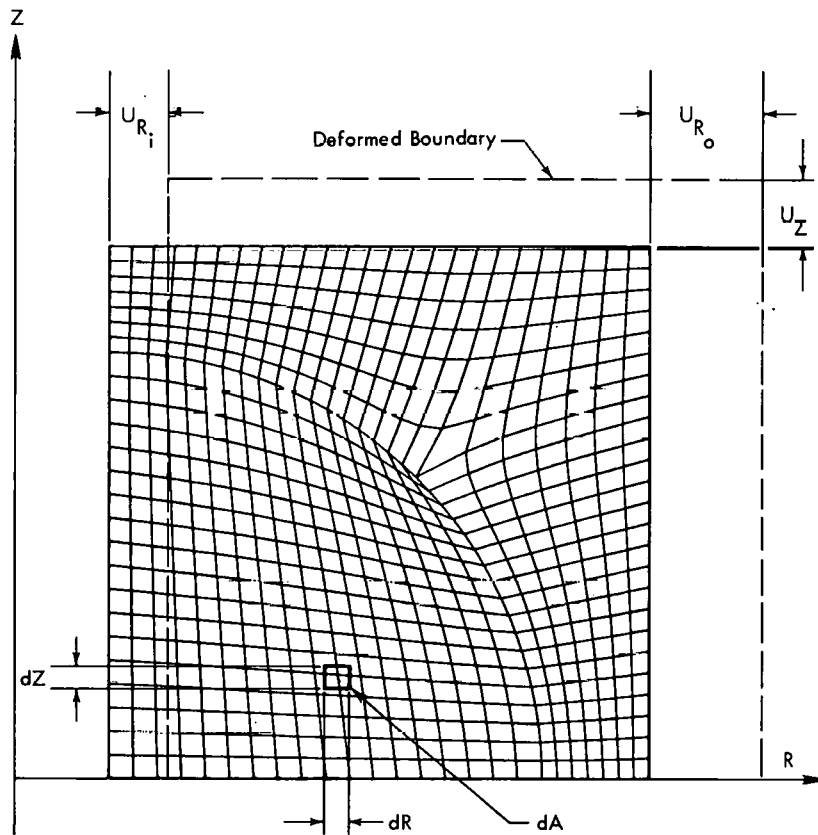


Figure 3. FINITE ELEMENT QUADRILATERAL MESH FOR A TYPICAL REPEATING SECTION FROM THE SQUARE ARRAY.

properties, the cross section in Figure 3 is not a plane model, but the cross section of an axisymmetric ring. R and Z displacements may then produce any state of normal stress desired (T strains are produced by average R displacement). The radius-to-thickness ratio is very high so that stress variation with R (due to cylindrical geometry) will not be significant.

The finite-element computer program is set up so that the sequential displacement loading steps required to determine all the normal stress constants are performed. The orthotropic stress-strain relations for normal stresses are given by:

$$\begin{pmatrix} \epsilon_R \\ \epsilon_Z \\ \epsilon_T \end{pmatrix} = \begin{pmatrix} \frac{1}{E_R} & \frac{-\nu_{RZ}}{E_R} & \frac{-\nu_{RT}}{E_R} \\ \frac{-\nu_{ZR}}{E_Z} & \frac{1}{E_Z} & \frac{-\nu_{ZT}}{E_Z} \\ \frac{-\nu_{TR}}{E_T} & \frac{-\nu_{TZ}}{E_T} & \frac{1}{E_T} \end{pmatrix} \begin{pmatrix} \sigma_R \\ \sigma_Z \\ \sigma_T \end{pmatrix} \quad (63)$$

where:

ϵ represents the normal strain,

E the modulus of elasticity, and

ν Poisson's ratio.

R, Z, and T are subscripts that indicate the component values.

For example, the Poisson's ratio, ν_{RZ} , is the ϵ_Z strain divided by the ϵ_R strain produced when a σ_R stress is applied. Also, use is made of the reciprocal relations:

$$\frac{\nu_{12}}{E_1} = \frac{\nu_{21}}{E_2}, \quad (64)$$

where the subscripts represent any R, Z, or T coordinates.

The first load step applies boundary displacements ($U_{R_0} - U_{R_1}$), so that:

$$(\epsilon_R)_1 = (e)_1, (\epsilon_Z)_1 = 0, (\epsilon_T)_1 = 0, \quad (65)$$

where the numerical subscripts refer to the load step number, and "e" is the applied strain. This expression produces three equations from Equation 63:

$$(e)_1 E_R = (\sigma_R)_1 - \nu_{RZ}(\sigma_Z)_1 - \nu_{RT}(\sigma_T)_1, \quad (66a)$$

$$0 = -\nu_{ZR}(\sigma_R)_1 + (\sigma_Z)_1 - \nu_{ZT}(\sigma_T)_1, \text{ and} \quad (66b)$$

$$0 = -\nu_{TR}(\sigma_R)_1 - \nu_{TZ}(\sigma_Z)_1 + (\sigma_T)_1. \quad (66c)$$

The second step applies displacements so that:

$$(\epsilon_Z)_2 = (e)_2, (\epsilon_R)_2 = 0, (\epsilon_T)_2 = 0. \quad (67)$$

The three resulting equations are:

$$0 = (\sigma_R)_2 - \nu_{RZ}(\sigma_Z)_2 - \nu_{RT}(\sigma_T)_2, \quad (68a)$$

$$(e)_2 E_Z = -\nu_{ZR}(\sigma_R)_2 + (\sigma_Z)_2 - \nu_{ZT}(\sigma_T)_2, \text{ and} \quad (68b)$$

$$0 = -\nu_{TR}(\sigma_R)_2 - \nu_{TZ}(\sigma_Z)_2 + (\sigma_T)_2. \quad (68c)$$

Equations 66c and 68c may be combined to give:

$$\nu_{TR} = \frac{(\sigma_T)_1(\sigma_Z)_2 - (\sigma_T)_2(\sigma_Z)_1}{(\sigma_R)_1(\sigma_Z)_2 - (\sigma_R)_2(\sigma_Z)_1}, \text{ and} \quad (69)$$

$$\nu_{TZ} = \frac{(\sigma_T)_1(\sigma_R)_2 - (\sigma_T)_2(\sigma_R)_1}{(\sigma_Z)_1(\sigma_R)_2 - (\sigma_Z)_2(\sigma_R)_1} \quad (70)$$

The third step applies:

$$(\epsilon_T)_3 = (e)_3, (\epsilon_R)_3 = -\nu_{TR}(e)_3, (\epsilon_Z)_3 = -\nu_{TZ}(e)_3, \quad (71)$$

which results in:

$$(\sigma_R)_3 = (\sigma_Z)_3 = 0. \quad (72)$$

Then:

$$E_T = \frac{(\sigma_T)_3}{(e)_3}. \quad (73)$$

Equations 66a and 68a may be combined to yield:

$$E_R = \frac{(\sigma_Z)_2(\sigma_R)_1 - (\sigma_R)_2(\sigma_Z)_1}{(\sigma_Z)_2(e)_1 - \nu_{TR} \frac{1}{E_T} [(\sigma_T)_2(\sigma_Z)_1 - (\sigma_T)_1(\sigma_Z)_2]}, \text{ and:} \quad (74)$$

$$\nu_{RZ} = \frac{(\sigma_R)_2 - \nu_{TR} \frac{E_R}{E_T} (\sigma_T)_2}{(\sigma_Z)_2} \quad (75)$$

Equation 68b then gives:

$$E_Z = \frac{(\sigma_Z)_2}{(e)_2 + \nu_{RZ} \frac{(\sigma_R)_2}{E_R} + \nu_{TZ} \frac{(\sigma_T)_2}{E_T}} \quad (76)$$

Also, from the third step, the material fringe value in the T direction (fiber axis) with the Z direction of observation is:

$$f_{TR} = \frac{(\sigma_T)_3}{(N_{TR})_3}, \quad (77)$$

where $(N_{TR})_3$ represents the average fringe order from Equation 62 with the direction of observation along the Z coordinate in Load Step 3. Similarly:

$$f_{TZ} = \frac{(\sigma_T)_3}{(N_{TZ})_3} \quad (78)$$

where $(N_{TZ})_3$ represents the average fringe order from Equation 62 with the direction of observation along the R coordinate in Load Step 3. Since the plane-stress problem with the fiber axis in the plane is considered here, only R and Z-direction observations need be made.

Step 4 applies:

$$(\epsilon_R)_4 = (e)_4, (\epsilon_Z)_4 = -\nu_{RZ}(e)_4, (\epsilon_T)_4 = -\nu_{RT}(e)_4, \quad (79)$$

which results in:

$$(\sigma_Z)_4 = (\sigma_T)_4 = 0. \quad (80)$$

The material fringe value for the R direction in the R-T plane is:

$$f_{RT} = \frac{(\sigma_R)_4}{(N_{RT})_4} \quad (81)$$

where $(N_{RT})_4$ represents the average fringe order from Equation 62 with the direction of observation along the Z coordinate in Load Step 4.

Step 5 applies:

$$(\epsilon_Z)_5 = (e)_5, (\epsilon_R)_5 = -\nu_{ZR}(e)_5, (\epsilon_T)_5 = -\nu_{ZT}(e)_5, \quad (82)$$

yielding:

$$(\sigma_R)_5 = (\sigma_T)_5 = 0, \quad (83)$$

and the material fringe value for the Z direction in the Z-T plane is:

$$f_{ZT} = \frac{(\sigma_Z)_5}{(N_{ZT})_5}, \quad (84)$$

where $(N_{ZT})_5$ represents the average fringe order from Equation 62 with the direction of observation along the R coordinate in Load Step 5.

Through the procedure just outlined, all of the elastic and photoelastic properties for normal stress loading are determined. The model of the fiber array is not required to be transversely isotropic in this procedure. The rectangular array is not transversely isotropic while the square array is isotropic. If the model is transversely isotropic, obviously the R and Z directions of observation are identical so that only Load Steps 1, 3, and 4 are required to determine all the properties.

The model for a square array of fibers may be mathematically transformed from a basic model for a 50% volume fraction fiber to cover a range from a 20 to 78% fiber volume. The transformation is accomplished by linearly increasing or decreasing the radial distance from the fiber center for all nodes within the fiber boundary; and, simultaneously, linearly decreasing or increasing the radial distance for nodal points outside the fiber boundary. This action eliminates the need for generating a new model for each fiber volume fraction. Finite-element meshes for various fiber volume fractions are illustrated in Figure 4 to show the transformation.

Calculated results are presented graphically, showing the functional relationships between properties of the fiber, matrix, and composite. These curves are prepared for the material constituents used in Material 2, identified later (Page 50). The modulated square-array model is analyzed in the finite-element computer program. Constituent-material properties are the input, and the composite elastic and photoelastic properties are the output of the program. Figure 5 gives the computed moduli of elasticity parallel and transverse to the fiber direction as functions of the fiber-volume fraction. As expected, the longitudinal modulus, E_1 , is practically linear, which agrees with rule-of-mixtures theory. The transverse modulus is lower because of the lower modulus of the matrix. However, it is always higher than the matrix modulus. The curves terminate at 78 volume percent fiber because the model is bounded by that value. The major Poisson's ratio, ν_{12} , in Figure 6 is also very linear; again, in agreement with the rule of mixtures. The curve is very slightly shifted with

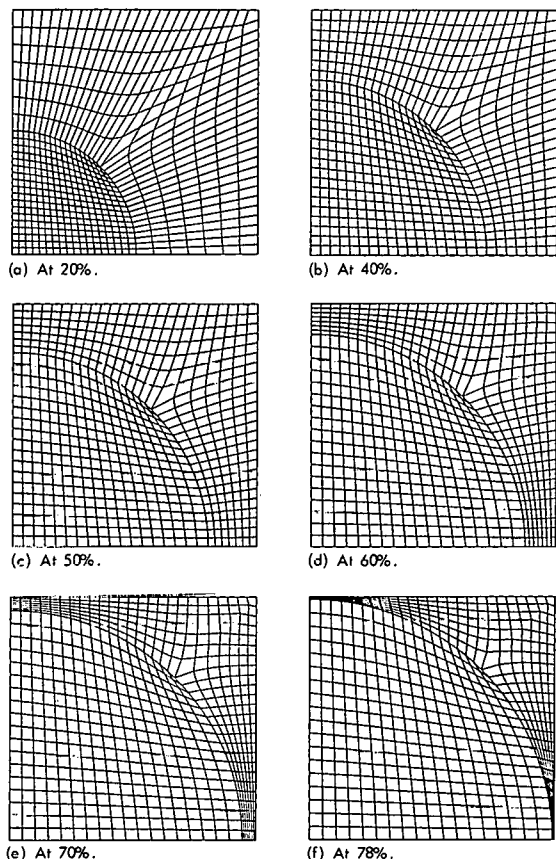


Figure 4. MODULATION OF THE 50 PERCENT FIBER VOLUME FRACTION SQUARE ARRAY MODEL FOR FIBER VOLUME FRACTIONS FROM 20 TO 78 PERCENT.

similar response with respect to the fiber volume fraction as those of the moduli in Figure 5. However, neither value is predictable by rule of mixtures. Experimental data are presented in a subsequent section (Page 43).

Finite-Element Model for Shear Stress

In-plane shear loading analysis will complete the calculated properties needed for analysis of two-dimensional problems. The sequence of analysis is very similar to the analysis described for normal stress. The composite is modeled as a regular array of fibers in a matrix, either square or hexagonal. A typical repeating section, as indicated in Figures 1 or 2, is chosen as the model and is approximated by a finite-element mesh. The mesh for shear loading is made up of a triangular element in order to be compatible with the computer program used. Again, displacement boundary conditions are imposed to maintain the geometric compatibility of the repeating sections.

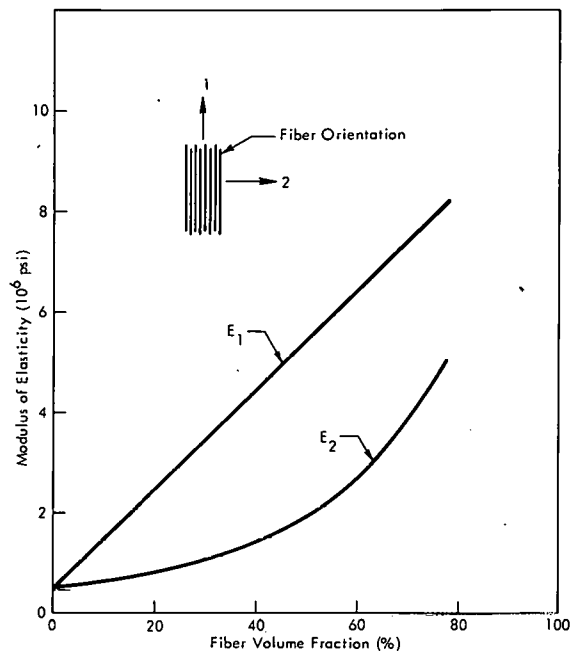


Figure 5. ORTHOTROPIC MODULI OF ELASTICITY FOR FIBER-REINFORCED COMPOSITE MATERIALS AS A FUNCTION OF THE FIBER VOLUME FRACTION.

respect to the rule-of-mixtures prediction so that the agreement between the two sets of values is not perfect. The photoelastic material fringe values parallel and transverse to the fiber direction are given in Figure 7.

The curves in Figure 7 show a somewhat

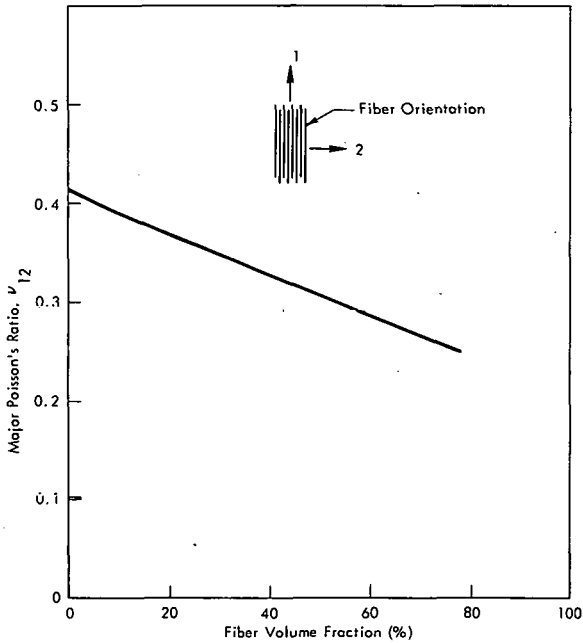


Figure 6. MAJOR POISSON'S RATIO FOR FIBER-REINFORCED COMPOSITE MATERIALS AS A FUNCTION OF THE FIBER VOLUME FRACTION.

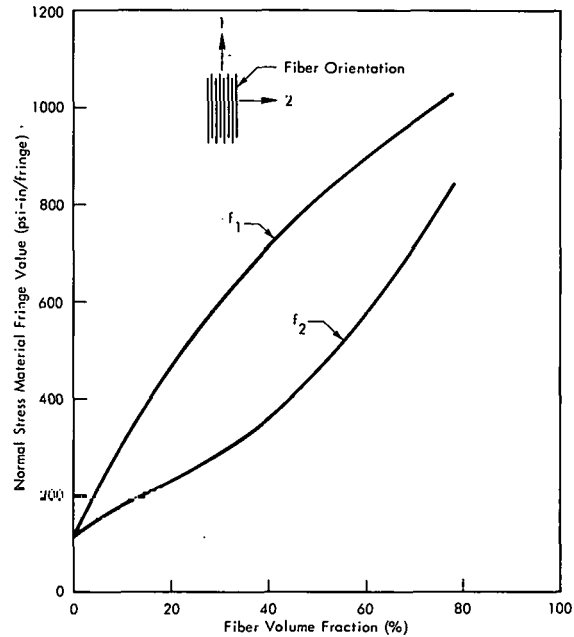


Figure 7. NORMAL STRESS MATERIAL FRINGE VALUES FOR FIBER-REINFORCED COMPOSITE MATERIALS AS A FUNCTION OF THE FIBER VOLUME FRACTION.

Finite-Element Analysis for Shear Stress

A finite-element program originally assembled for steady-state heat transfer is modified to analyze the shear-loading problem (given in Appendix B). It is shown that these are representable by the same mathematical problem.

The governing equations for pure shear loading are established from elasticity theory. Because of symmetry, the average longitudinal shear stress will cause a uniform axial displacement along the boundary on which it acts. The problem is defined by the displacement field:

$$u = v = 0, \quad w = w(x, y), \quad (85)$$

where u , v , and w are, respectively, the x , y , and z displacement components. For this problem, the only nonzero stress components are then:

$$\tau_{zx} = G \frac{\partial w}{\partial x}, \quad \tau_{zy} = G \frac{\partial w}{\partial y}, \quad (86)$$

where:

τ represents the shear stress, and

G the shear modulus of the material.

Equilibrium equations in the x and y directions are automatically satisfied, while equilibrium in the z direction requires that:

$$G \left(\frac{\partial^2 w}{\partial x^2} + \frac{\partial^2 w}{\partial y^2} \right) = 0. \quad (87)$$

To further define the problem, the boundary conditions are established so that only one of the shear-stress components is applied for a particular loading case. The body is assumed to be loaded at infinity by a uniform shear stress; however, in the micro scale, this condition is represented by a uniform edge displacement. The boundary conditions become, for τ_{zx} loading:

$$\left. \begin{aligned} w &= w^0 \text{ along } x = a \\ w &= 0 \text{ along } x = 0 \\ G \frac{\partial w}{\partial y} &= 0 \text{ along } y = 0, y = b \end{aligned} \right\} \quad (88)$$

After solving the problem, the shear-stress loading is determined by averaging the calculated shear stresses along the boundary $x = a$ or $x = 0$.

Rather than set up a computer program especially for this problem, it is noted that the mathematical problem is identical to that of the formulation for steady-state heat transfer. Boley and Weiner⁽¹³⁾ give the equation as:

$$k \left(\frac{\partial^2 T}{\partial x^2} + \frac{\partial^2 T}{\partial y^2} \right) = 0, \quad (89)$$

where:

k represents the thermal conductivity, and

T the temperature.

A finite-element program for evaluating this heat-transfer equation is modified to solve the shear-loading problem. A comparison of Equations 87 and 89 shows the analogous variables. These are:

$$\left. \begin{aligned} T &\rightarrow W \\ k &\rightarrow G \end{aligned} \right\} \quad (90)$$

The boundary conditions for the heat-transfer program corresponding to the shear-loading problem are:

$$\begin{aligned}
 T &= T^0 \text{ along } x = a \\
 T &= 0 \text{ along } x = 0 \\
 \frac{\partial T}{\partial y} &= 0 \text{ (insulated boundary) along } y = 0, b
 \end{aligned}
 \tag{91}$$

The shear stress corresponds to the heat flux:

$$\tau_{zx} = G \frac{\partial w}{\partial x} \rightarrow k \frac{\partial T}{\partial x} .
 \tag{92}$$

Some of the photoelastic quantities which have no counterpart in the heat-transfer problem and some other desired output are added to the existing program.

Curves are obtained for the shear modulus and principal shear photoelastic constant. Again, these curves are calculated from the constituent material properties of Material 2. The shear modulus, plotted in the graph of Figure 8, is seen to remain very low for the whole practical range of fiber fractions. The principal shear fringe value is given by Figure 9. The fringe value is defined by Equation 55. The fringe value does not remain low as did the shear modulus for increasing fiber-volume fractions.

By the methods described in this section, all the properties needed to solve the two-dimensional problem may be calculated from constituent properties. If the correlation between experimental and calculated values is reasonable, the amount of testing for property determination is greatly reduced. Comparisons with experimental data are presented in the section entitled: **EXPERIMENTAL EVALUATION OF MATERIAL PROPERTIES AND STRESS-OPTIC LAWS.** (Page 43).

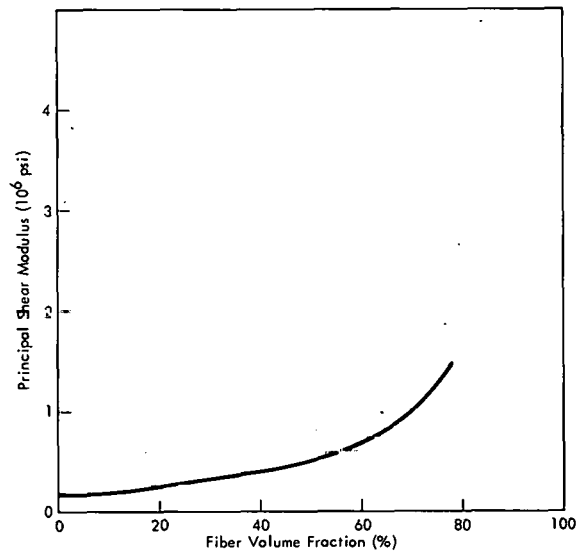


Figure 8. PRINCIPAL SHEAR MODULUS FOR FIBER-REINFORCED COMPOSITE MATERIALS AS A FUNCTION OF THE FIBER VOLUME FRACTION.

MATERIAL FABRICATION AND MODEL PREPARATION

The foremost requirement for a material for photoelastic work is that the material be transparent. In order to produce a transparent, fiber-reinforced composite material, each phase of the manufacturing process must be carefully controlled.

Selection of Constituent Materials

One of the most readily available fibers is fiberglass. Fiberglass comes in many forms, but the form most suitable for fabrication of unidirectionally reinforced material is called "roving" or "yarn". When the fiberglass is formed, a bundle of monofilaments are drawn simultaneously to form a threadlike string called a "single-end strand", which is collected on a high-speed cylindrical drum to form a "cake". All of the roving or yarn is then formed from this cake. Single-end roving is simply rewound from one cake onto a tube in an amount convenient for sales purposes. Twenty-end roving is formed by gathering the single ends from 20 cakes into one strand and rewinding onto a tube. Yarn is the same as roving except that it is twisted during the rewind operation. This step makes the fiber easier to handle when weaving into cloth.

There are also many different glass compositions, not all having the same degree of optical clarity. The fiberglass used in this study is obtained from Owens-Corning Fiberglas. One of their glass fibers, designated "W-1" clear glass, was used in some early composite materials work. The form of strand available is a 2040-filament bundle which forms a relatively large strand for winding purposes. The composition of this glass is almost identical to the more common "E" glass. "E" glass is as clear, but has a faint greenish tint. "E" glass is available in a variety of forms and sizes.

For this study it is concluded that "E" glass with the sizing removed is the best material to use. Typically, all glass yarn and rovings have a coating on the fiber known as the "finish" or "sizing". Finishes are defined as a coating designed to remain on the glass and promote bonding with a particular type of resin; sizings are defined as a coating designed to prevent fiber abrasion and breaking during handling processes such as cloth weaving. After weaving, the sizing is removed and a finish is applied. For highly transparent composites, the finish is undesirable because it may not be optically clear and/or the index of refraction may not match that of the fiberglass. The fiberglass material used in this study is single-end (2040-filament) "E" glass yarn with one twist per inch and a starch/oil sizing. The Owens-Corning product is identified as ECG-150-1/0-1.0Z, a standard product for Owens-Corning. The yarn bundle is small enough to wind a fairly uniform composite.

The other material required to make the composite bonds the fibers in position and forms a rigid material. It is called the "matrix material". The best matrix for most applications is a liquid resin (either polyester or epoxy) which will flow and fill the spaces between fibers

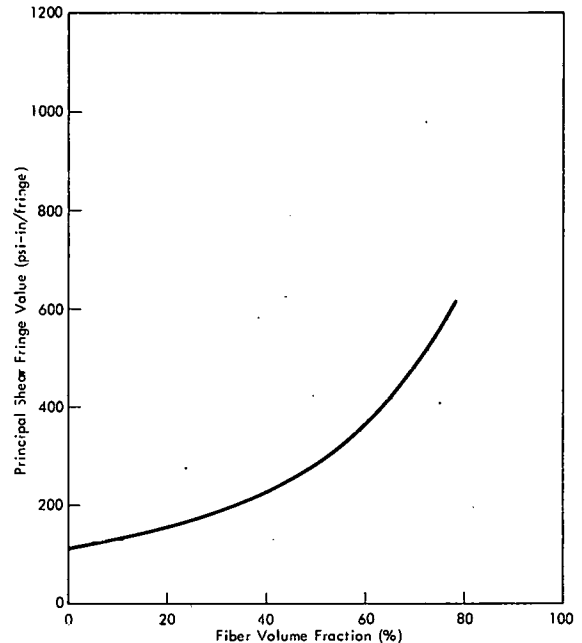


Figure 9. PRINCIPAL SHEAR-FRINGE VALUE FOR FIBER-REINFORCED COMPOSITE MATERIALS AS A FUNCTION OF THE FIBER VOLUME FRACTION.

before hardening. It is also desirable for it to have a low viscosity and a reasonably long pot life (time before gellation begins). Several other characteristics of the matrix are very important for producing transparent material.

For a low initial birefringence, room-temperature-cure resins with low shrinkage are required. In this study, only epoxy resins were seriously considered because their shrinkage is less than that of polyester, and more experience had been gained with epoxies. When the fiberglass strand is impregnated with the matrix and the curing begins, any difference in temperature from room temperature produces a differential expansion between the fiber and matrix because the expansion coefficients are different. Matrix shrinkage causes a similar effect and adds to the thermal component. In traditional isotropic photoelasticity, the material usually has negligible initial birefringence. In fiber-reinforced composite materials, the initial birefringence is very difficult to eliminate and must usually be accounted for in the analysis.

In order to achieve good transparency, the fiber and matrix indexes of refraction must match very well. The light path travels through several hundred fiber/matrix interfaces in a composite that is 0.100 to 0.200 inch thick. Thus, a small difference in the refractive index progressively distorts the path and diffuses the light. Refractive indexes were determined for eight epoxy resins which were suitable for use in other respects. The refractive indexes for these epoxies ranged from 1.512 to 1.587, while the fiber index was 1.548.

Maraglas 658 epoxy with Maraglas 558 hardener mixed 100/50 parts by weight, respectively, was the matrix that was selected for use. The resin is produced by the Marlette Corporation. Maraglas 658 is a room-temperature-cured, crystal-clear epoxy casting resin with a low exotherm. The cure time is 24 hours. The refractive index is 1.557, which matches that of the fiber to within 0.6%.

Winding Method

The most important factor in fabricating a transparent composite is the elimination of voids or air bubbles. Differences in the refractive index make the composite more translucent; but, if the voids are not eliminated, the composite is opaque.

In a typical filament-winding process using simple impregnation devices, minute air bubbles form in the resin and/or in the spaces between the fibers. These voids may occupy less than 5% of the material volume and yet still render the composite opaque. Special processes are required to reduce the void content to less than 1/2% for reasonable transparency. These special processes normally involve use of vacuum in some way.

One fabrication method for producing low-void composites is vacuum winding. There are several ways to apply the vacuum. As expected, the best results are achieved by the most difficult method.

The simplest approach uses only a vacuum impregnation device. The impregnation device has inlet and exit orifices for the fiber strand to pass through. The resin is in a cup inside the evacuated tank. The strand enters and is dry while being evacuated of air for a short length. It then passes through the resin to be wound onto the mandrel surface. Good, low-void

composites may be fabricated in this manner. The primary disadvantage of this method is that the winding speed needs to be slow so that the dry strand has enough time to evacuate before being impregnated by the resin. Also, fiber abrasion and consequent "fuzzballs" tend to clog the orifices and make it difficult to maintain smooth operation.

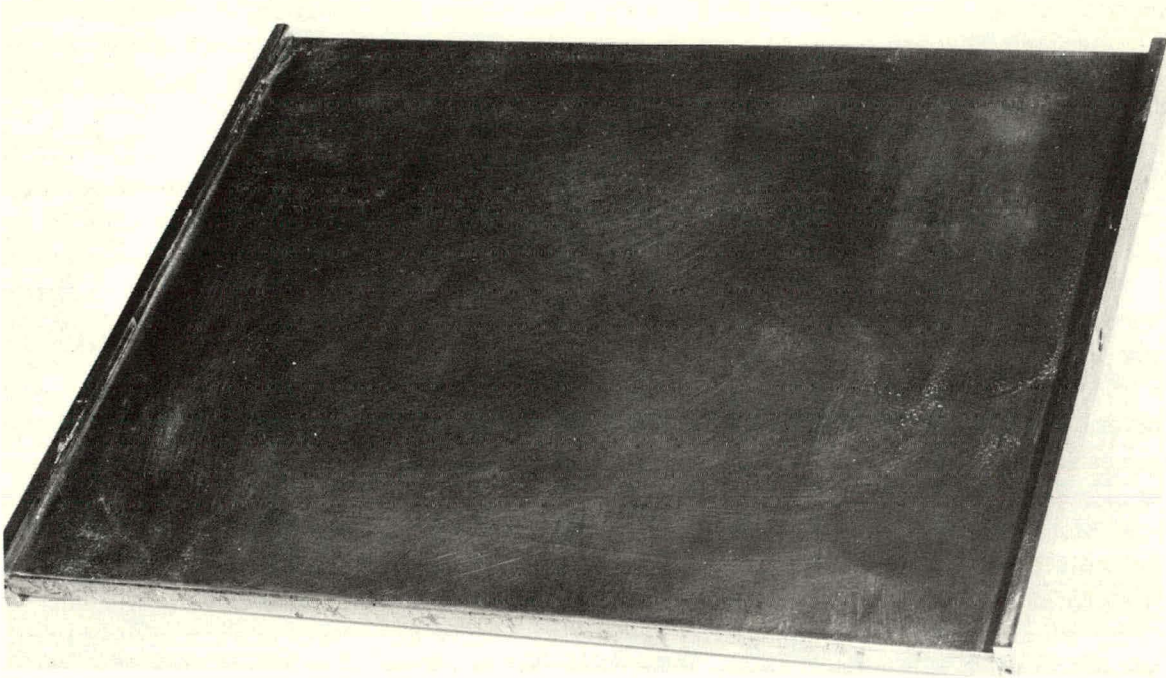
The next approach places the spool of fiber inside the evacuated tank. With the spool in a vacuum, the whole spool of fiber may be evacuated for a time before starting to wind. This action allows faster winding speeds. The tank is compartmentalized since any resin splatter on the spool makes it difficult to pull the strand off the spool. This process works very effectively as long as fiber breaks are minimal. Rings produced for residual stress studies⁽¹⁴⁾ were produced by this technique.

Enclosing the whole process in a vacuum chamber accomplishes the removal of all air sources which may contribute to voids in the composite. This approach would seem to be the ultimate method. However, additional complexities are involved. The winding machine is remotely controlled for all steps in the process. Mold releases on the mandrel as well as lubricants on the machinery require a long outgassing period. A large vacuum chamber is expensive and not readily available in most cases. Also, when a fiber breaks, the part is usually ruined because the chamber is opened to restart the strand and the reevacuation time is too long. Some winding has been done this way with good results, but the effort required hardly seemed justified. The finished parts to date are no better than parts produced by the other methods, although the potential part quality is better.

A completely different scheme for producing material is called "dry winding", with vacuum impregnation after the winding is finished. Dry winding is better suited for producing flat material. It is better to wind cylinders by wet winding (with resin) because dry windings lose tension, bulk up, and wrinkle during winding. Bulking results in a low fiber content, while wrinkling, due to tension relaxation when successive layers are applied, results in material of poor quality. Even though flat windings bulk up across the flat surface due to the lack of winding pressure against an infinite-radius-of-curvature surface, the material can be pressed to a uniform thickness in order for it to be of uniform consistency. Since the resin in a wet-wound plate is further "advanced" (meaning advanced on the polymerization cycle, making it more viscous), dry winding with vacuum impregnation is recommended. The flat material used in this study was produced by dry winding.

A flat mandrel with round edges provides the winding support. The yarn is wound around the mandrel. Fifty to 75 grams of tension on a single-end yarn (204 filaments) is applied to pull the fiber straight. The mandrel has a very short "H" cross-section design where the sides are used to enclose the winding and provide mechanical stops for thickness control in pressing. A view of the mandrel is given in Figure 10.

The sizing is "burned off" the yarn after winding on the mandrel. (The starch/oil sizing is effectively removed by heating to 650° F for 24 hours.) This high temperature requires the use of a stainless steel mandrel to prevent surface oxidation. The mold release on the mandrel is a high-temperature type—Peninsular Silicones, Inc, MR-22 Silicone. It is a liquid applied by wiping, brushing, or spraying. The mold-release curing cycle is 60 minutes at 400° F and 10 minutes at 600° F. After sizing removal, the fiberglass is vacuum impregnated.

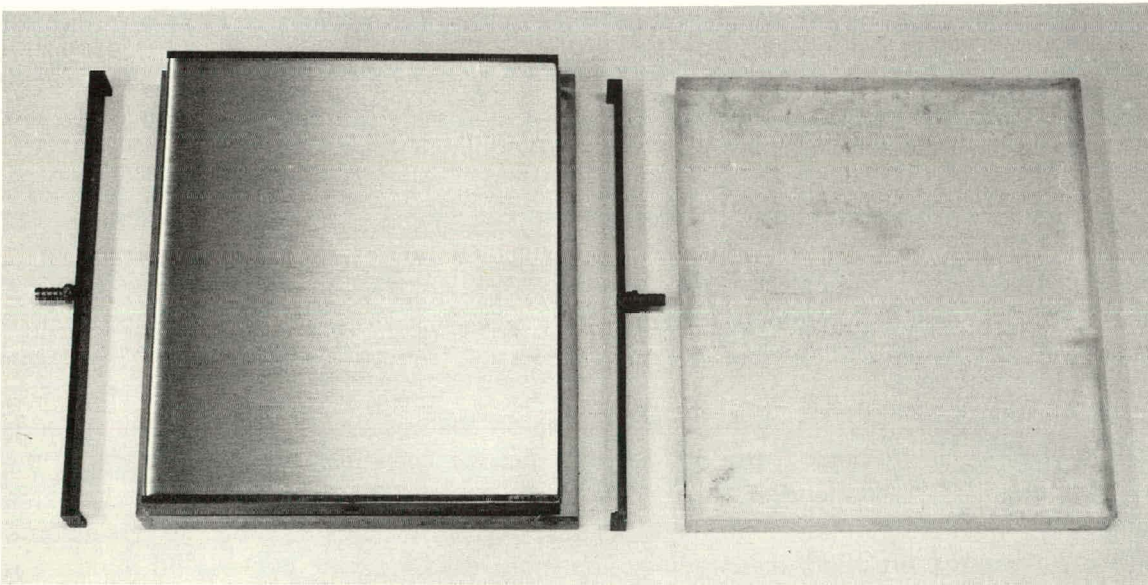


154397

Figure 10. H-SHAPED STAINLESS-STEEL MANDREL FOR WINDING DRY, UNIDIRECTIONAL, FLAT MATERIAL.

Impregnation Procedure for Dry Winding

The mandrel with winding is assembled with other components, as seen in Figure 11, to form a vacuum chamber around the winding. The U-shaped steel top and bottom pieces which have tube ports are bolted to the ends of the mandrel. Plexiglas plates are fitted over



152878

Figure 11. COMPONENTS OF THE ASSEMBLY USED TO VACUUM IMPREGNATE DRY FIBERGLASS WINDING WITH EPOXY RESIN.

the sides of the mandrel to complete the chamber. Any small cracks at the joints are sealed with a putty-like material called "duct seal". Hoses are connected to the tube ports. One hose goes through a resin trap to the vacuum source; the other hose is used to feed the epoxy resin.

The resin hose is clamped off and the vacuum applied. The dry winding is evacuated for an arbitrary minimum of 12 hours. This length of time is usually convenient for processing. Longer times have not seemed to yield any better results.

At this point, the resin is fed through the hose into the chamber. The chamber is filled and allowed to remain on vacuum until the fiberglass is impregnated. A view of the impregnation in progress is given in Figure 12. When dry, the fiberglass winding is white and opaque; when completely impregnated, the winding is green tinted and transparent. When impregnation is complete, the Plexiglas plates and steel U caps are removed.

Steel plates are positioned on each side against the impregnated winding in preparation for pressing. The assembly is loaded into the press and the desired pressure (up to 250 psi) is applied. The pressure is maintained to squeeze out any excess resin. To produce a composite of the desired fiber volume fraction, shim stock of the proper thickness is placed between the H-mandrel sides and the pressing-plate edges. The shims serve as mechanical stops to produce the desired composite thickness. A photograph of the assembly in the press is presented in Figure 13. The resin cures in the press for 24 hours at room temperature. The composite material sheets are then removed.

Model Preparation

The photoelastic model is cut from the flat sheets. Because it is a two-phase material with a hard and soft phase, the machining process is difficult. The best result is usually obtained with a grinding-type process. Most other processes leave a ragged, loose, fiber edge.

Diamond-coated tools have provided the most successful cutting edges. Straight edges are cut by a diamond-coated metal disc, mounted on a surface grinder, as seen in Figure 14. Diamond-coated core drills are used to bore holes. In all the machining processes it is necessary to keep the tool from loading up with the soft phase (epoxy resin) because this buildup prevents a clean cutting action. In most cases, water coolant is used to lubricate and cool the material and to prevent tool loading. The fiberglass/epoxy composite can be machined by these methods to yield a clean, smooth surface.

Part of this study involved testing for tensile-stress response as a function of the fiber orientation angle with respect to the tensile-stress direction. Tensile specimens were cut from the flat sheet following layouts made to efficiently utilize the material. Where possible, all the specimens were cut from one sheet of material. The sheet was clamped by two De-Sta-Co clamps onto a micarta plate on the surface grinder shown in Figure 14. Micarta serves as back support to prevent fiber splintering. Multiple passes distribute the cutting forces and generate heat, and prevent machining-edge stresses.

Another part of the study analyzed the photoelastic patterns produced in a tensile strip with a central hole. Straight edges of the strips were machined in the same manner as the tensile specimens. Holes were drilled by the diamond-coated core drill.

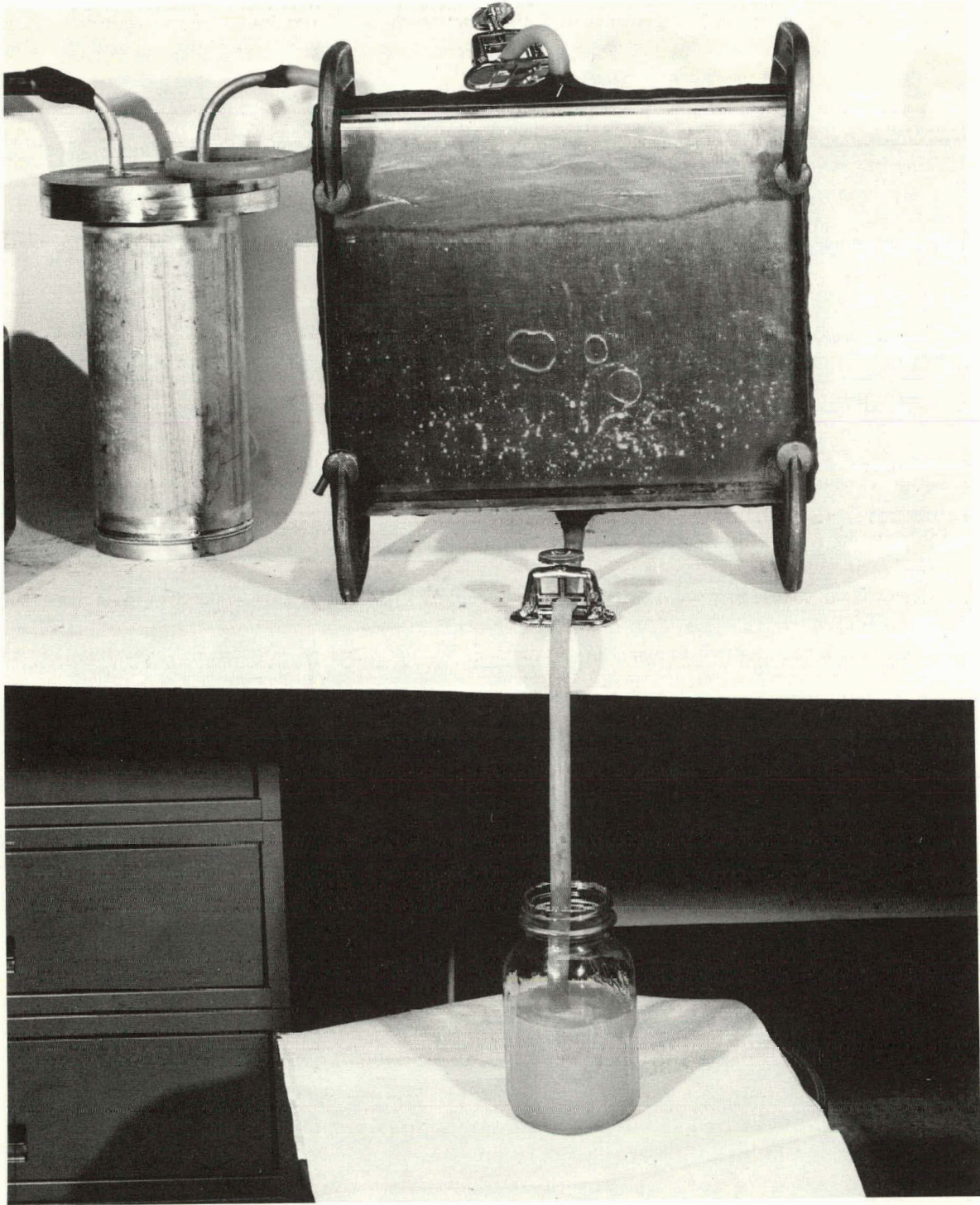


Figure 12. VACUUM IMPREGNATION IN PROGRESS.

152879

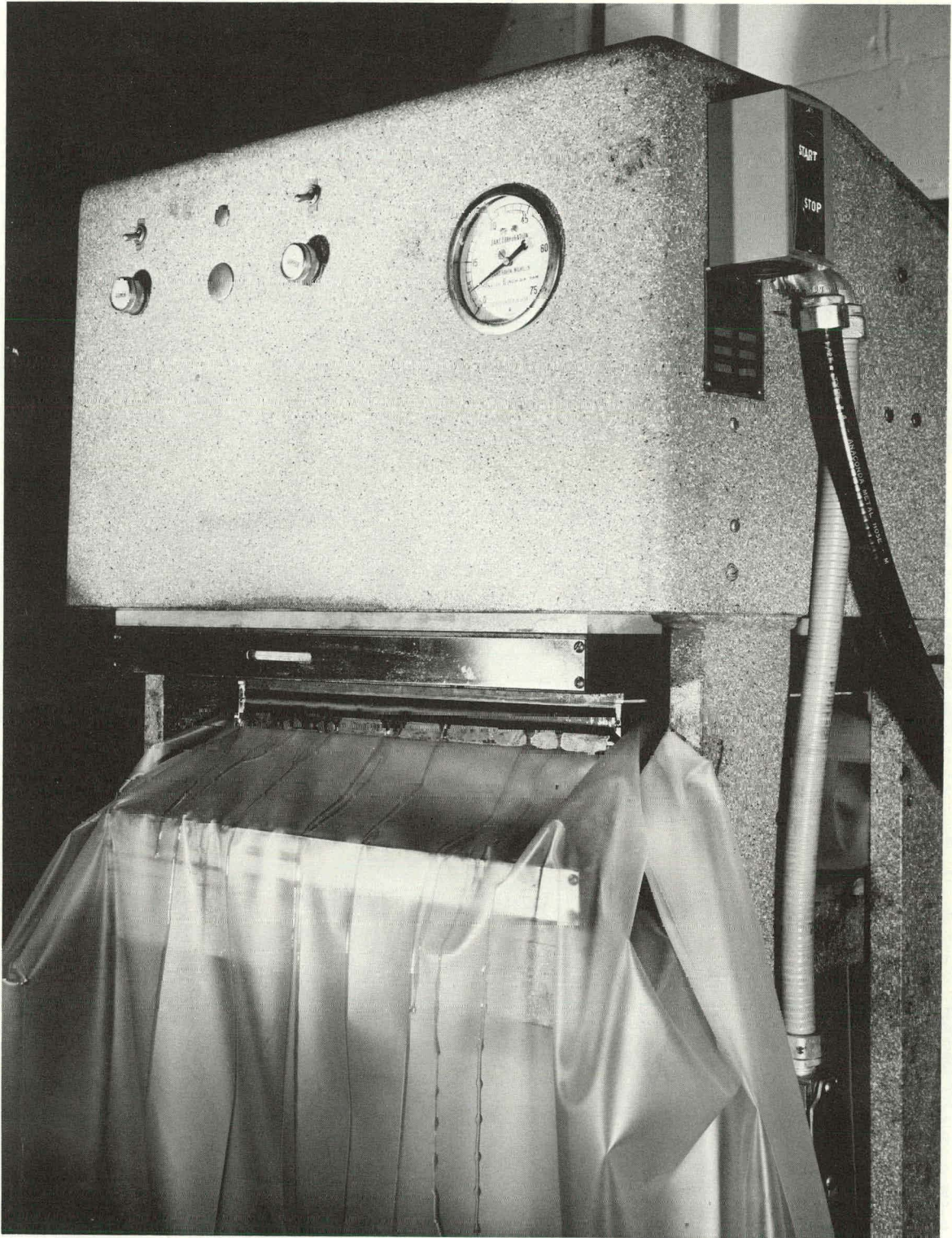


Figure 13. VACUUM-IMPREGNATED PLATE IN THE PLATEN PRESS FOR CURE.

152876

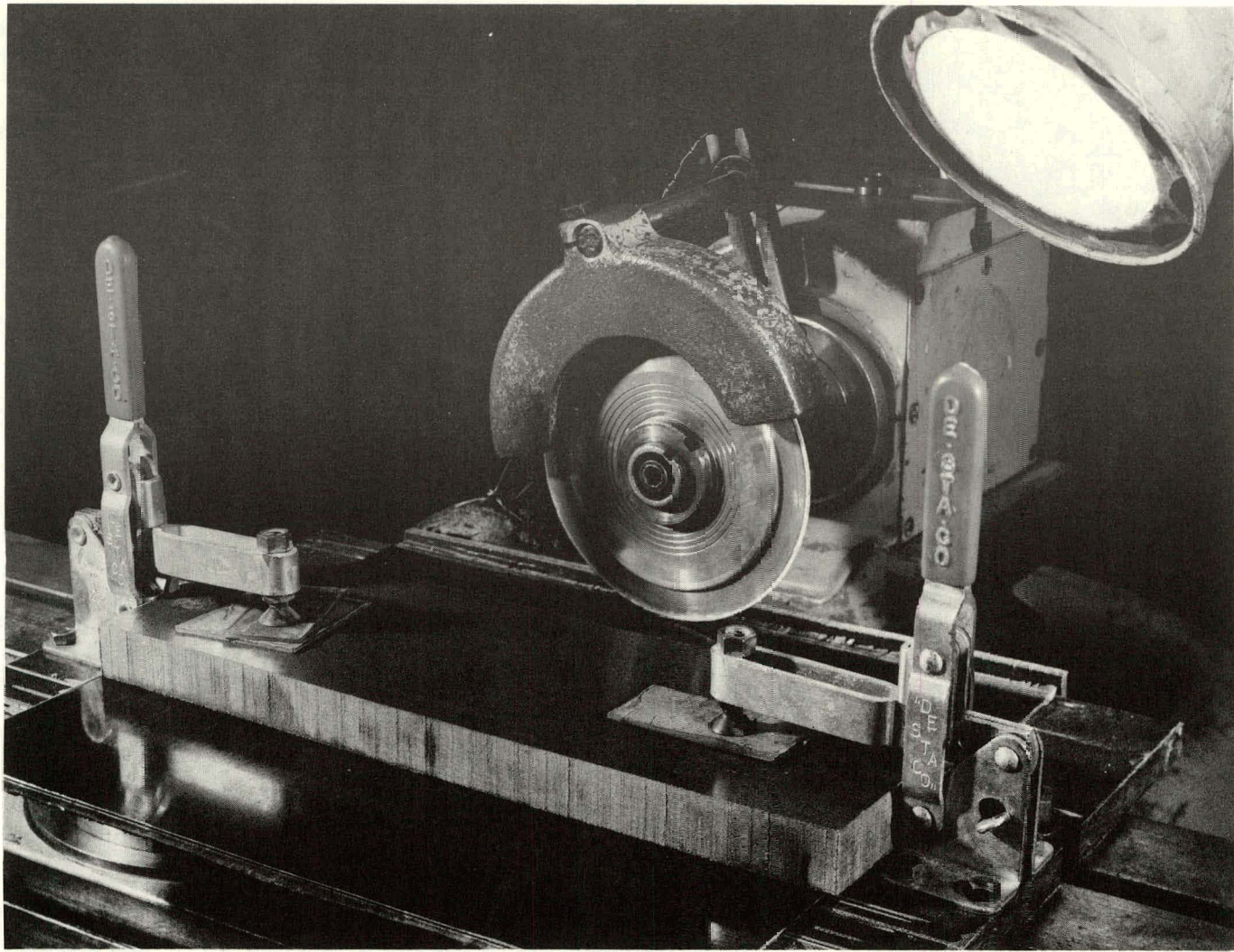


Figure 14. CURED FIBERGLASS PLATE IN THE SURFACE GRINDER FOR SPECIMEN CUTTING.

153060

EXPERIMENTAL EVALUATION OF MATERIAL PROPERTIES AND STRESS-OPTIC LAWS

One part of the experimental program used uniaxial tensile specimens to generate the required data for evaluation of the developed theory. The specimens of various fiber orientation were loaded in the loading frame in the polariscope. Photoelastic data and strain measurements were recorded for property determinations and theoretical evaluations.

Test Methods and Equipment

The polariscope used is Polarizing Instrument Company's Model 402, seen in Figure 15. It is a circular polariscope with a collimated light. The quarter-wave plates may slide out of the field to convert it into a plane polariscope.

Some of the other components and auxiliary equipment can be seen in Figure 16. The loading frame in the original setup is for dead-weight loading of the specimens through a lever arm. Since a large number of specimens were tested in this research, another loading device was adapted. An air-cylinder loading arrangement with a load cell provided more efficient operation. The cylinder, exerting the load in place of the dead weight, was much quicker and easier to load and unload.

The polarizer and analyzer were mechanically coupled to facilitate isoclinic determination. After reading the isoclinic angle, a Babinet-Soleil-type compensator was used to determine the fringe order. Photoelastic, Inc Model 232 compensator was used.

A photometer search unit was mounted on the projection screen behind an aperture. The point of interest in the model was located over the aperture. When the compensator was adjusted, the minimum light intensity was determined by the photometer. The photometer used was a Photovolt Corporation Model 520-M.

The tensile specimens were 0.500 inch wide by 0.100 inch thick by 6 inches long. Each end of the specimen was clamped between two aluminum plates. The clamping force was provided by cap screws through the plates. A central hole and pin were used to transmit the load from the loading frame. A universal-joint pin arrangement was used to prevent the specimen from bending. Foil-resistance strain gages were mounted on the specimen, and strain was read on a BLH Model 120 strain indicator. The specimen was incrementally loaded and data were recorded at each load level to establish the loading curve.

As described earlier, the properties were determined by normal-stress and shear-stress loadings. The normal-stress properties were readily determined from tensile specimens of the proper fiber orientation. It was desirable to determine the shear properties from a pure shear test, but very few loading methods for pure shear tests were in existence. The rail shear test was one method tried for testing shear properties; the other test used was the off-axis fiber orientation tensile specimen. The normal-stress properties were determined first in order to reduce the shear properties from this test.

In the tensile test, it was necessary to have a high length-to-width ratio.⁽¹⁵⁾ High length-to-width ratios (L/W) produce more uniform stress fields. For most materials,

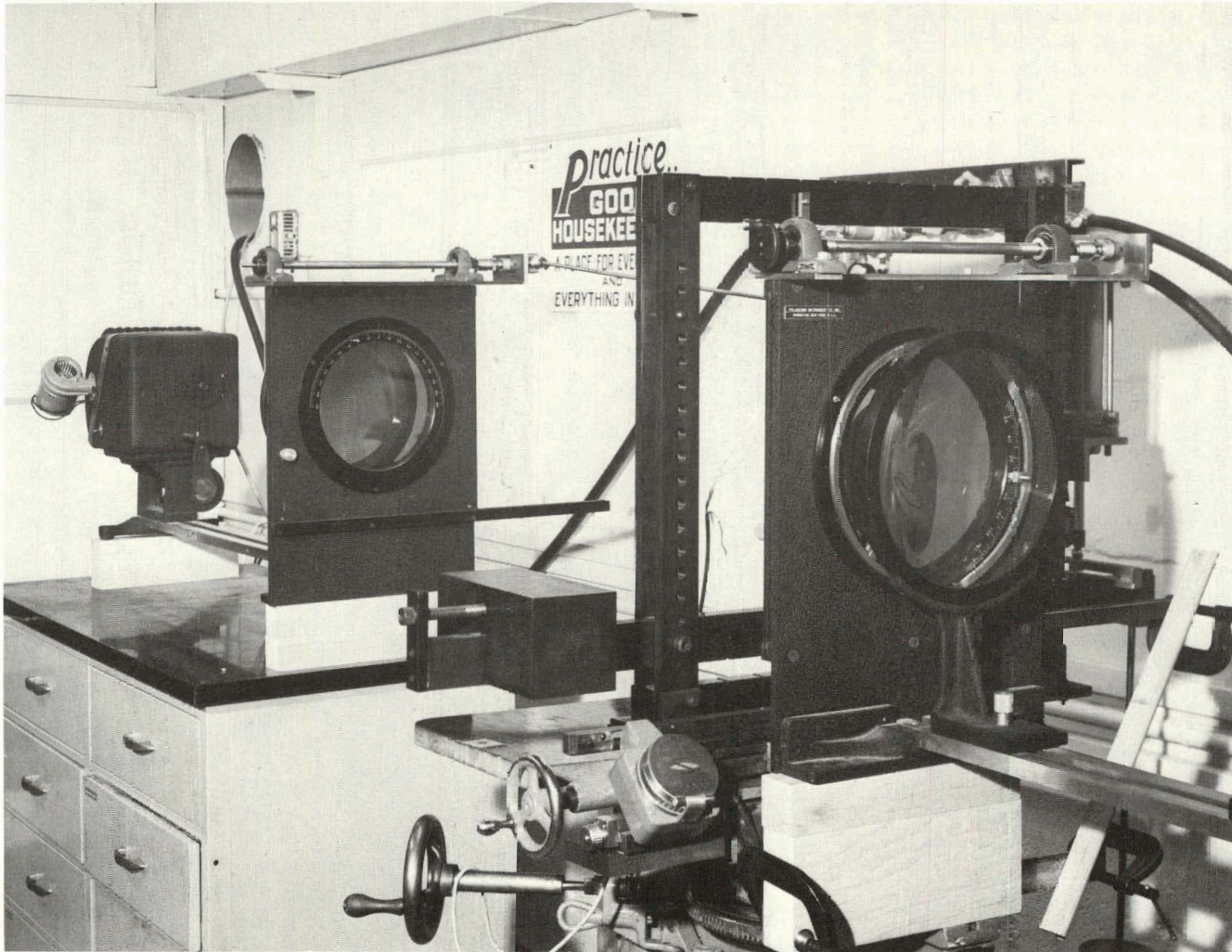
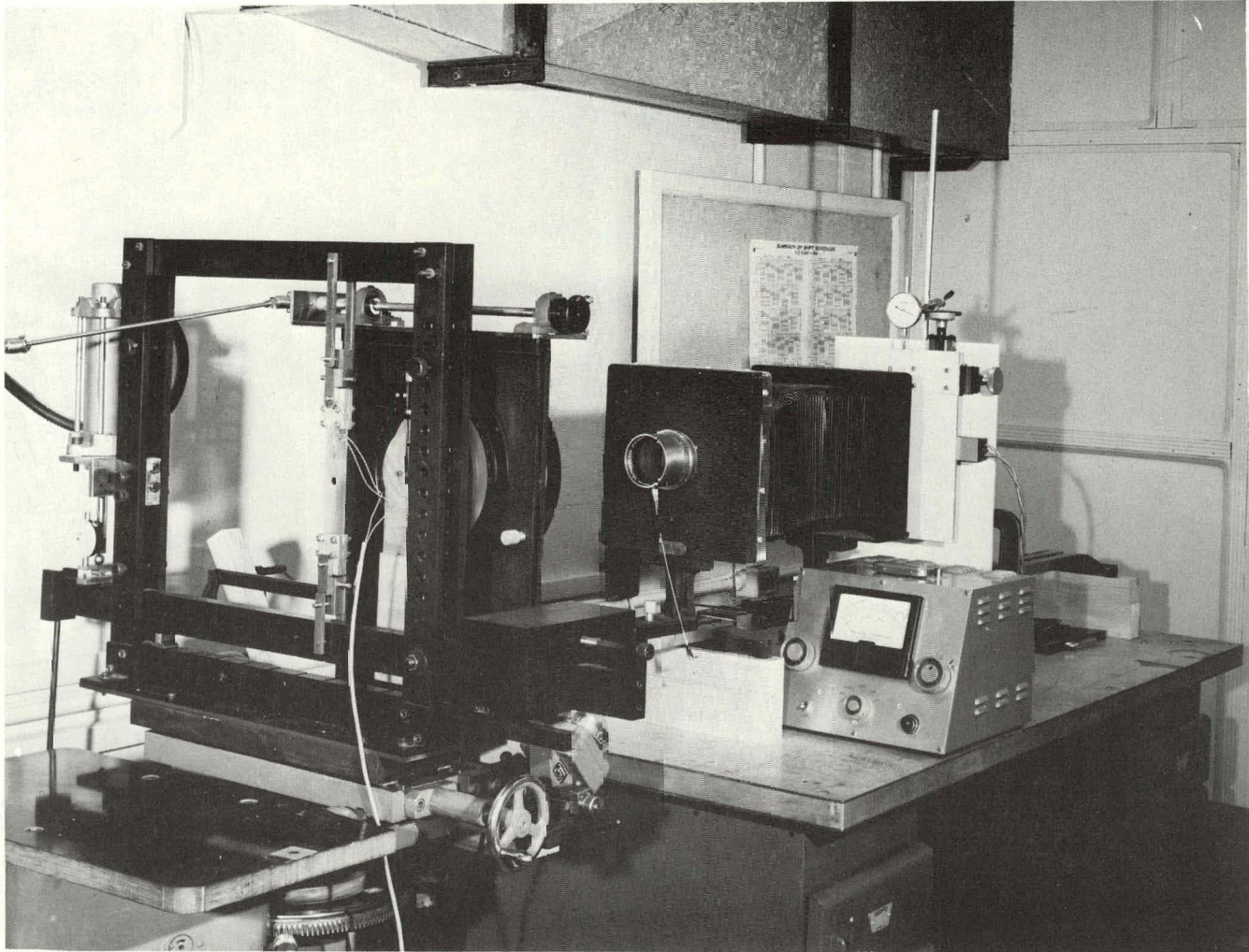


Figure 15. POLARISCOPE SHOWING THE LIGHT SOURCE, COUPLED POLARIZER AND ANALYZER, AND LOADING FRAME. 153059



153061

Figure 16. POLARISCOPE SHOWING THE LOADING FRAME, A LOADED SPECIMEN, THE CAMERA, AND PHOTOMETER.

$L/W > 5$ will give satisfactory results. This problem was most serious for the off-axis test because of shear coupling stresses and displacements.

The photoelastic-material properties were experimentally determined from data recorded when the specimen was loaded. Photoelastic data were obtained by conventional photoelastic methods. Experimental results were used to calculate the properties.

Experimental Determination of Photoelastic Properties

The tensile specimen was mounted in the loading frame and loaded incrementally. Incremental loading was used to determine the linear response range. Because the theories were based on the linear material behavior, the test was terminated when the response became nonlinear or the specimen fractured. Data were recorded at each increment.

The isoclinic angle was determined in a plane polariscope by rotating the coupled polarizer and analyzer until the minimum light intensity was indicated by the photometer. After determining the isoclinic angle, the compensator was inserted in the field and aligned with the principal birefringence direction. The fringe order was obtained by adjusting the compensator for minimum intensity on the photometer in a crossed, circular polariscope. White light was used so that the minimum light intensity was on the black, zero-order fringe.

The material produced in this research always had an initial birefringence with the isoclinic aligned with the fiber direction. This initial birefringence was usually small; and, in some cases, negligible. However, usually it must be extracted from the data. In the cases of 0 or 90-degree fiber orientation, the initial birefringence and load birefringence directly summed to produce the total measured birefringence. These data were easily corrected by subtraction. For off-axis tests, the initial birefringence and load birefringence combined in a more complex manner. Even small initial birefringence may have had a pronounced effect on the total birefringence, so the data must be corrected. The resulting correction formula and its derivation are presented in Appendix C.

The fiber-direction fringe value, f_1 , was determined by testing a 0-degree fiber orientation tensile specimen. The transverse fringe value, f_2 , was determined from a 90-degree fiber orientation specimen. The data were plotted with stress versus birefringence. A straight line was fitted to the data by the least-squares method. The slope, $d\sigma/dN$, times the thickness, t , gave the fringe value:

$$f = \frac{d\sigma}{dN} t, \quad (93)$$

where:

- f represents the material fringe value,
- $d\sigma$ the stress increment,
- dN the fringe increment, and
- t the thickness.

Correction for initial birefringence is unnecessary for the 0 and 90-degree tests. In fact, the intercept of the least-squares, straight-line fit of uncorrected data with the birefringence axis may be a more accurate value for the initial birefringence than a direct reading.

As mentioned before, two tests were tried for determining the shear fringe value, f_{12} . One of these is called the rail shear test. It is reported⁽¹⁶⁾ that the shear-stress field is sufficiently uniform if the geometry and material properties are within certain limits. If the aspect ratio (length/width) exceeds 10 or if the stiffness ratio (transverse stiffness/shear stiffness) $\gg 1$, then the shear stress should be uniform for most of the specimen. The test was conducted on specimens which satisfy these requirements, but the stress field judged by observing the fringe patterns was not even close to uniform. The calculated shear fringe value, assuming a uniform shear stress, is unreasonable.

Better results are achieved, however, by use of a strain-gage determination of the actual stress state at a specific point. This test is accomplished by mounting a strain-gage rosette at the point and measuring the birefringence at the corresponding symmetrical point. As implied, the stress field is symmetrical even though nonuniform. Results from the strain-gage rosette give the state of stress. The measured birefringence is used in Equation 58 with other properties previously determined to find f_{12} .

The test most used for shear properties is the off-axis tensile bar. Theoretically, any fiber orientation between 0 and 90 degrees is suitable for use in Equation 58 to find f_{12} . However, in order to minimize the effect of normal stress components in the equation, the orientation should be approximately in the range from 30 to 60 degrees.

When the tensile bar is loaded, the stress field should be a nearly uniform uniaxial stress along the bar if conditions on aspect ratio, loading devices, alignment, and normal test methods are followed. The test data are corrected for initial birefringence and fitted by least squares to a straight line. This treatment yields the material fringe value, f_{θ} , for that fiber angle, θ . The state of stress in the material principal axes is calculated by the stress-tensor transformation. The shear fringe value, f_{12} , is calculated from Equation 58 and previously determined properties. Note that Equation 58 may be utilized to select the fiber orientation angle which cancels the normal stress birefringence components. Once f_1 and f_2 are determined, the material fringe value, f_{θ} , divided by $2 \sin \theta \cos \theta$ at this calculated orientation equals the shear fringe value, f_{12} .

Experimental Determination of Elastic Properties

Determination of the elastic properties follows common methods used in composite materials technology. As the specimen is incrementally loaded, the strains are measured by strain gages. Strain components may then be used to calculate the properties.

Either biaxial or triaxial strain-gage rosettes were mounted on the tensile specimen. The gage installation procedure recommended by Micro-Measurements, Inc was followed. The specimen surface was prepared, the gage aligned, and the gage bonded with Micro-Measurements M-Bond 200 adhesive which is an Eastman 910-type adhesive.

A BLH Model 120 strain indicator and Model 225 switch and balance unit monitored the strains. A four-arm external-bridge arrangement was set up to reduce the gage voltage and

thus stabilize the gage response due to self heating on the poor heat-conducting materials. Two legs of the bridge used 1100-ohm resistors, and the gage and thermal compensator were 120 ohms. This arrangement reduced the indicator sensitivity by approximately a factor of three, but the readings were much more stable. Strain data were recorded at the same load increments as the photoelastic data and plotted to find the linear range.

Tests of 0 and 90-degree fiber-orientation specimens yielded the properties E_1 , E_2 , ν_{12} , and ν_{21} . Biaxial strain-gage rosettes measured the axial and transverse strains in the loaded specimen. Plots of the data were made and a least-squares straight-line fit of the linear stress-strain data gave the slopes required to calculate the properties. The 0-degree-specimen modulus of elasticity is E_1 and the Poisson's ratio is ν_{12} . Poisson's ratio, ν_{12} , is defined as the ratio of the transverse (2) strain to the longitudinal (1) strain produced by a longitudinal (1) stress. The 90-degree-specimen modulus of elasticity is E_2 and the Poisson's ratio is ν_{21} . As a check, since the stiffness matrix must be symmetric, then:

$$\frac{\nu_{21}}{E_2} = \frac{\nu_{12}}{E_1} \quad (94)$$

must be valid.

The shear modulus, G_{12} , completes the properties required for an analysis of a plane-stress problem. The off-axis tensile specimen is used to determine this property. A triaxial strain-gage rosette is mounted on the specimen, as described earlier, but with the gages oriented at 0, 45, and 90 degrees with respect to the fiber orientation.

The modulus of elasticity of the specimen in the loading direction, E_θ , is a function of the fiber orientation relative to the load. The elastic-property transformation equations give this relation as:

$$E_\theta = \left[\frac{m^4}{E_1} + \left(\frac{1}{G_{12}} - \frac{2\nu_{12}}{E_1} \right) m^2 n^2 + \frac{n^4}{E_2} \right]^{-1} \quad (95)$$

where:

θ represents the fiber orientation relative to the load direction,

$m = \cos \theta$, and

$n = \sin \theta$.

Since all the properties except E_θ are previously determined; then, with E_θ from the test, G_{12} is calculated from Equation 95.

Data from the triaxial gage rosette yield the complete state of strain in the loaded specimen. The only strain required for E_θ is the axial strain, ϵ_θ . Results from the complete rosette

check the accuracy of the assumed uniform uniaxial stress field. By mounting the rosettes aligned with the fiber coordinates and if $\theta = 45$ degrees was chosen ($\theta = 45$ degrees was chosen for most of the shear modulus tests here), then ϵ_θ is measured directly by the 45-degree gage. When other orientations are used, the axial strain may be calculated from the rosettes' values, or the gage may be applied with one gage in an axial orientation.

Uniaxial Loading Evaluation of Stress-Optic Laws

One of the experiments used to evaluate the proposed stress-optic laws was uniaxial stress loading of the tensile bars with different fiber orientations. The uniaxial stress, $\bar{\sigma}$, was applied to a specimen with a fiber orientation angle, θ . Equation 58, which only applies when the x and y coordinates are aligned with the material fiber direction, may be written:

$$N = t \sqrt{\left(\frac{\bar{\sigma}m^2}{f_1} - \frac{\bar{\sigma}n^2}{f_2}\right)^2 + \left(\frac{2\bar{\sigma}nm}{f_{12}}\right)^2} \quad (96)$$

The material fringe value is then:

$$f_\theta = \frac{\bar{\sigma}t}{N} = \left[\left(\frac{m^2}{f_1} - \frac{n^2}{f_2}\right)^2 + \left(\frac{2mn}{f_{12}}\right)^2 \right]^{-1/2} \quad (97)$$

Also, the isoclinic angle is a function of the fiber orientation angle. Equation 59 may be written:

$$\phi_\theta = \frac{1}{2} \tan^{-1} \frac{-\frac{2\bar{\sigma}mn}{f_{12}}}{\frac{\bar{\sigma}m^2}{f_1} - \frac{\bar{\sigma}n^2}{f_2}}, \quad (98)$$

which is the isoclinic angle, ϕ_θ , relative to the fiber coordinates.

The experiments were carried out on two material systems. The only difference between materials was the epoxy resin used. For the first material, the epoxy was DER 332/TETA/AGE (85/12/15 parts by weight). DER 332 is a Dow Chemical Company epoxy. TETA is triethylene Tetramine, designated by the CIBA Products Company as CIBA 951 Hardener. AGE is a reactive diluent, Allyl Glycidyl Ether, produced by the Shell Chemical Company. The second material uses Marblette 658/558 (100/50 parts by weight) epoxy produced by the Marblette Corporation.

Tensile specimens were cut from the material sheets at 15-degree increments of fiber orientation. They were mounted and loaded, as described earlier, for property determination. The recorded data were: birefringence, isoclinic angle, and strain. The photoelastic data were corrected for initial birefringence and plotted. Least-squares straight-line fits yielded the values necessary for calculating the material fringe value, f_θ .

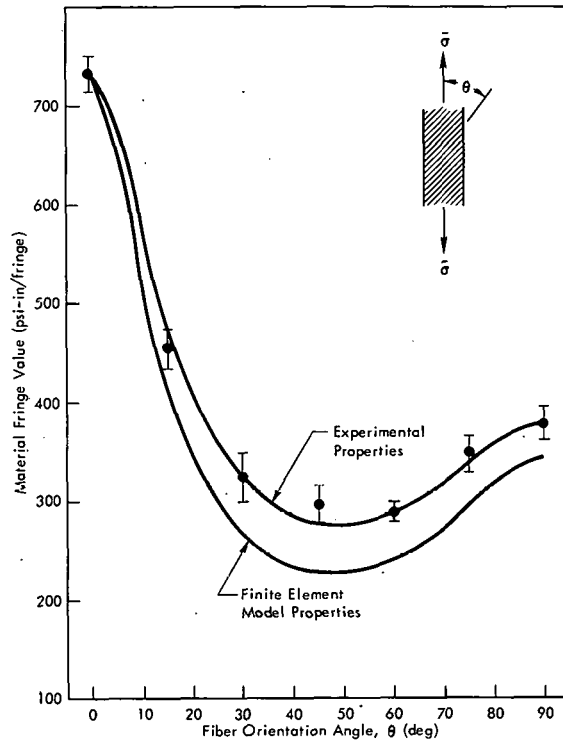


Figure 17. MATERIAL FRINGE VALUE AS A FUNCTION OF THE FIBER ORIENTATION FOR UNIAXIAL LOADING OF TENSILE BARS FROM MATERIAL 1.

Overall, the agreement was good and the verification of the proposed stress-optic laws seemed to be satisfactory. Material 2 had a lower initial birefringence and was a little more homogeneous than Material 1, so the results from Material 2 should be a little more reliable.

Plotted test points are the result of the average of a minimum of four tests; the bars give the 95% confidence intervals. The two solid curves in Figures 17 through 20 were calculated from Equations 97 and 98. One was determined using the finite-element-model calculated properties; the other was obtained using the experimentally determined properties, f_1 , f_2 , and f_{12} .

Satisfactory biaxial tests for plane-stress fields are very difficult to achieve. It was, therefore, decided to further evaluate the stress-optic relations in an orthotropic plane-stress problem. This phase of the study is presented in a subsequent section (Page 55).

SHEAR-DIFFERENCE METHOD FOR ORTHOTROPIC PHOTOELASTICITY

Before a general plane-stress problem can be solved by the use of photoelasticity, there must be a method for determining the individual normal-stress components. In isotropic photoelasticity, this is often accomplished by the shear-difference method,⁽¹⁷⁾ which is derived from the equilibrium equations. Therefore, it is equally applicable to orthotropic problems although the resulting equations in the two are different. Development of the equations for orthotropic materials is presented here.

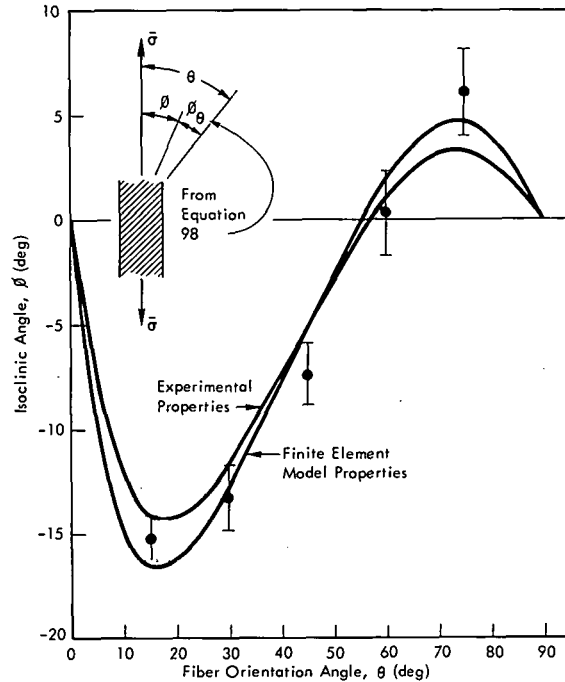


Figure 18. ISOCLINIC ANGLE AS A FUNCTION OF THE FIBER ORIENTATION FOR UNIAXIAL LOADING OF TENSILE BARS FROM MATERIAL 1.

The experimental data were compared with the results calculated from the finite element models (Figures 17 through 20).

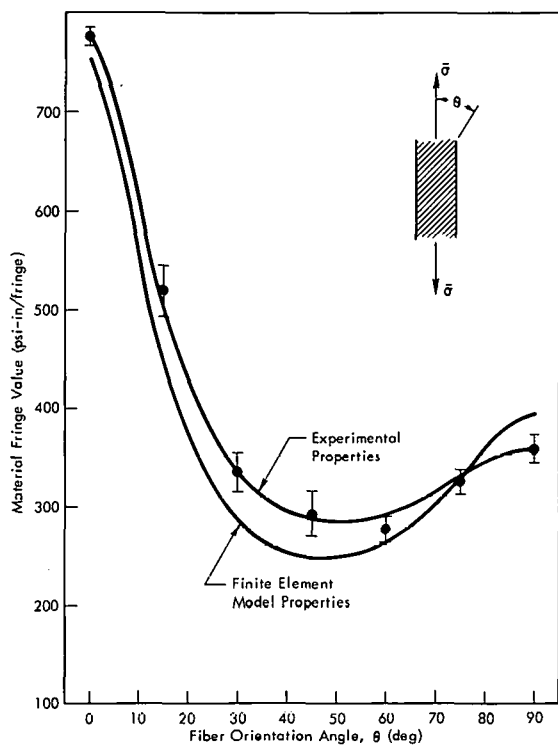


Figure 19. MATERIAL FRINGE VALUE AS A FUNCTION OF THE FIBER ORIENTATION FOR UNIAXIAL LOADING OF TENSILE BARS FROM MATERIAL 2.

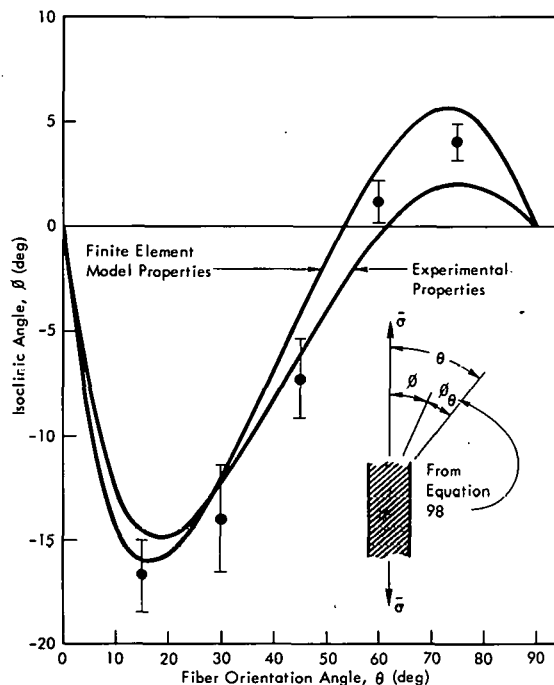
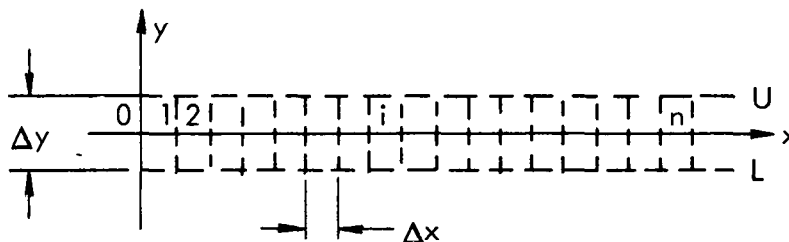


Figure 20. ISOCLINIC ANGLE AS A FUNCTION OF THE FIBER ORIENTATION FOR UNIAXIAL LOADING OF TENSILE BARS FROM MATERIAL 2.

Development of Equations

An x and y coordinate system is chosen such that x lies along the desired path of integration. The material fiber direction is at some angle, θ , relative to x. The unknown stress state must satisfy both the stress-optic laws and the equilibrium equations. To meet this requirement, the stress-optic laws are rearranged and substituted into the equilibrium equations. The resulting equations are numerically integrated along the x axis to determine σ_x . Substitution into the stress-optic laws then gives σ_y and τ_{xy} .

The geometrical arrangement for the path of integration is shown in the following diagram:



From Equation 47, the normal stress, σ_x , is:

$$\sigma_x = \frac{1}{C_1} [N \cos 2\phi + C_2\sigma_y - C_3\tau_{xy}] \tag{99}$$

Substituting into Equation 48, and solving for τ_{xy} , gives:

$$\tau_{xy} = \left(\frac{1}{\frac{C_4 C_3}{C_1} - C_6} \right) \left[\left(\frac{1}{2} \sin 2\phi + \frac{C_4}{C_1} \cos 2\phi \right) N + \left(C_5 + \frac{C_2 C_4}{C_1} \right) \sigma_y \right]. \quad (100)$$

Also, from Equation 47, the normal stress, σ_y , is:

$$\sigma_y = \frac{-1}{C_2} [N \cos 2\phi - C_1 \sigma_x - C_3 \tau_{xy}]. \quad (101)$$

Substituting into Equation 48, and solving for τ_{xy} , gives:

$$\tau_{xy} = \left(\frac{-1}{\frac{C_5 C_3}{C_2} + C_6} \right) \left[\left(\frac{1}{2} \sin 2\phi - \frac{C_5}{C_2} \cos 2\phi \right) N + \left(C_4 + \frac{C_5 C_1}{C_2} \right) \sigma_x \right]. \quad (102)$$

Taking the partial derivative with respect to x gives:

$$\frac{\partial \tau_{xy}}{\partial x} = \left(\frac{-1}{\frac{C_5 C_3}{C_2} + C_6} \right) \left\{ \frac{\partial}{\partial x} \left[\left(\frac{1}{2} \sin 2\phi - \frac{C_5}{C_2} \cos 2\phi \right) N \right] + \left(C_4 + \frac{C_5 C_1}{C_2} \right) \frac{\partial \sigma_x}{\partial x} \right\}. \quad (103)$$

Equilibrium in the y direction requires:

$$\frac{\partial \tau_{xy}}{\partial x} + \frac{\partial \sigma_y}{\partial y} = 0, \text{ or} \quad (104)$$

$$\frac{\partial \tau_{xy}}{\partial x} = - \frac{\partial \sigma_y}{\partial y}.$$

Taking the partial derivative of Equation 100 with respect to y gives:

$$\frac{\partial \tau_{xy}}{\partial y} = \left(\frac{1}{\frac{C_4 C_3}{C_1} - C_6} \right) \left\{ \frac{\partial}{\partial y} \left[\left(\frac{1}{2} \sin 2\phi + \frac{C_4}{C_1} \cos 2\phi \right) N \right] + \left(C_5 + \frac{C_2 C_4}{C_1} \right) \frac{\partial \sigma_y}{\partial y} \right\}. \quad (105)$$

Substituting Equations 103 and 104 into Equation 105 yields:

$$\begin{aligned}
\frac{\partial \tau_{xy}}{\partial y} = & \left(\frac{1}{\frac{C_4 C_3}{C_1} - C_6} \right) \left\{ \frac{\partial}{\partial y} \left[\left(\frac{1}{2} \sin 2\phi + \frac{C_4}{C_1} \cos 2\phi \right) N \right] \right. \\
& + \left(C_5 + \frac{C_2 C_4}{C_1} \right) \left(\frac{1}{\frac{C_5 C_3}{C_2} + C_6} \right) \left[\frac{\partial}{\partial x} \left(\frac{1}{2} \sin 2\phi - \right. \right. \\
& \left. \left. \frac{C_5}{C_2} \cos 2\phi \right) N \right] + \left(C_4 + \frac{C_5 C_1}{C_2} \right) \frac{\partial \sigma_x}{\partial x} \left. \right\}. \tag{106}
\end{aligned}$$

Equilibrium in the x direction requires:

$$\begin{aligned}
\frac{\partial \tau_{xy}}{\partial x} + \frac{\partial \sigma_x}{\partial x} = 0, \text{ or} \\
\frac{\partial \tau_{xy}}{\partial y} = - \frac{\partial \sigma_x}{\partial x}. \tag{107}
\end{aligned}$$

Equation 106 with Equation 107 can be solved for $\frac{\partial \sigma_x}{\partial x}$:

$$\frac{\partial \sigma_x}{\partial x} = \frac{A_2}{A_1} \left[\frac{\partial}{\partial y} (NB_2) - A_3 \frac{\partial}{\partial x} (NB_1) \right], \tag{108}$$

where:

$$A_1 = \left[1 - \left(\frac{C_4 C_2 + C_5 C_1}{C_6 C_1 - C_4 C_3} \right) \left(\frac{C_5 C_1 + C_4 C_2}{C_6 C_2 + C_5 C_3} \right) \right], \tag{109}$$

$$A_2 = \left(\frac{C_1}{C_6 C_1 - C_4 C_3} \right), \tag{110}$$

$$A_3 = - \left(\frac{C_4 C_2 + C_5 C_1}{C_6 C_2 + C_5 C_3} \right) \left(\frac{C_2}{C_1} \right), \tag{111}$$

$$B_1 = \left(\frac{\sin 2\phi}{2} - \frac{C_5}{C_2} \cos 2\phi \right), \text{ and} \tag{112}$$

$$B_2 = \left(\frac{\sin 2\phi}{2} + \frac{C_4}{C_1} \cos 2\phi \right) . \quad (113)$$

Using the difference form for numerical integration:

$$\begin{aligned} \sigma_x \Big|_n - \sigma_x \Big|_0 &= \frac{A_2}{A_1} \sum_{i=1}^n \left\{ \frac{\Delta X}{\Delta Y} \left[NB_2 \Big|_{\left[\frac{(i-1)+i}{2} \right]_U} \right. \right. \\ &\quad \left. \left. - NB_2 \Big|_{\left[\frac{(i-1)+i}{2} \right]_L} \right] + A_3 \left[NB_1 \Big|_i - NB_1 \Big|_{i-1} \right] \right\} , \end{aligned} \quad (114)$$

where:

$|_i$ denotes the value at Station i on the x axis, and
 $\left[\frac{(i-1)+i}{2} \right]_{U \text{ or } L}$ the average of values at Stations $(i-1)$ and i and is along the U or L lines, as shown in the sketch on Page 51.

After σ_x is found, τ_{xy} may be calculated from Equation 102 and σ_y may be calculated from Equation 101.

Application Along the Arbitrary Axes

Application of the shear-difference procedure is outlined in the following steps. The basic photoelastic constants for the material are determined in the material principal coordinate system. The transformation equations derived earlier are applied to the photoelastic property tensor to determine the constants (C_1 to C_6) in the x, y coordinate system. Birefringence and isoclinic data are collected incrementally along and parallel to the x axis. The data are corrected for initial birefringence and then used to compute the σ_x distribution. Finally, the σ_y and τ_{xy} distributions are calculated from the σ_x distribution.

Application Along the Principal Material Axes

If the x and y coordinates are chosen to align with the material principal axes, several simplifications can be made. For this case:

$$C_3 = C_4 = C_5 = 0 , \text{ and} \quad (115)$$

$$A_1 = 1, A_2 = \frac{1}{C_6}, A_3 = 0, B_1 = B_2 = \frac{1}{2} \sin 2\phi . \quad (116)$$

Equation 114 then reduces to the isotropic form of the shear-difference equation. If the x axis is also a line of load symmetry, only data along the x axis and one line parallel to x (say, u) are required. Symmetry requires that:

$$NB_2 \left| \left[\frac{(i-1)+i}{2} \right] U \right. = -NB_2 \left| \left[\frac{(i-1)+i}{2} \right] L \right. \quad (117)$$

If only the distributions along the material principal direction are required, regardless of the load direction or symmetries, then the conventional isotropic shear-difference form may be used.

APPLICATION OF ORTHOTROPIC PHOTOELASTICITY TO A PLANE-STRESS PROBLEM

Statement of the Problem

Solution of an orthotropic plane-stress problem may serve both as a demonstration of the photoelastic theory and further verification of the theory. There are several considerations for selecting the problem to be solved: (1) the problem should have a practical interest and should contribute to the general understanding of orthotropic materials; (2) general two-dimensional stress states should be involved in the problem; (3) agreement between the photoelastic solution and an analytical solution should provide further verification of the developed photoelastic analysis.

A strip with a central hole under uniaxial loading was the problem selected to be analyzed. The presence of a hole in a relatively uniform stress field has historically been and continues to be a significant practical problem. Premature failure due to stress concentrations caused by holes may even be more critical in the design with orthotropic materials than with isotropic materials because of directional strength properties.

The strips tested were 10 inches long, 1 1/2 inches wide, and 0.100 inch thick. The hole was 0.375 inch in diameter, giving a width-to-hole diameter ratio of 4. For this ratio, the analytical solution for an infinite-width plate should be a reasonable approximation. Three fiber orientations are sufficient for material-properties calibration as well as supplying distinctly different stress states. The data for photoelastic and elastic constants were collected in relatively undisturbed regions of the strip. Fiber orientations with respect to the loading directions of 0 and 90 degrees produce the effect of the hole on the uniform stress field when loaded in the material's stiffest and least-stiff directions. Loading at a 30-degree orientation eliminates the symmetry and provides a test for the shear-difference formulation of orthotropic materials.

Analytical Solution

The analytical solution may be realized by two methods: One is a closed-form elasticity solution, the other is a numerical solution. Of course, the closed-form solution is preferred, if it is available. Lekhnitskii⁽⁹⁾ gives the solution for a hole in an infinite orthotropic sheet

with a uniaxial stress field. Results from this solution are illustrated in Figure 21. The equation for the tangential stress around the edge of the hole is the only stress-distribution equation presented in final form. Howland⁽¹⁸⁾ solved the case of an isotropic strip of finite width with a hole. This solution gives the effect of finite width for isotropic materials and thus provides a feeling for the effect in orthotropic materials. A large amount of numerical data are presented in his paper. Complete field equations are not presented explicitly in either of the two proposed solutions. Since the problem here is not modeled precisely by either of these solutions, a finite-element solution was formulated.

The finite-element program used is the same as described earlier for an analysis of the micromodel for calculation of material properties. The program solves either axisymmetric or plane-stress problems. A built-in feature of the program allows arbitrary selection of the angle of the material principal orthotropic axes. The computer program will perform the coordinate transformation internally.

For the symmetric problem, only one quarter of the model would need to be analyzed. However, since the intermediate fiber-orientation angles between 0 and 90 degrees eliminate the material symmetry, the full strip is modeled. The same model is used for all three orientations: 0, 30, and 90 degrees. The model grid is refined until the calculated stress values are stabilized, especially in the high-stress-gradient region. The final model grid is shown in Figure 22.

Photoelastic Solution

The photoelastic solution proceeds in the same manner as for the handling of a conventional isotropic material. Some differences that have been noted in the prior text are described. The main difference is the use of multiple models to analyze the material-orientation effects. Of course, the analysis may be carried out for only one model with a given fiber orientation, but all the photoelastic constants for the model material must be found by some method. It was decided here to use models of 0, 30, and 90-degree fiber orientation and use data collected in regions relatively undisturbed by the hole discontinuity to determine the material properties.

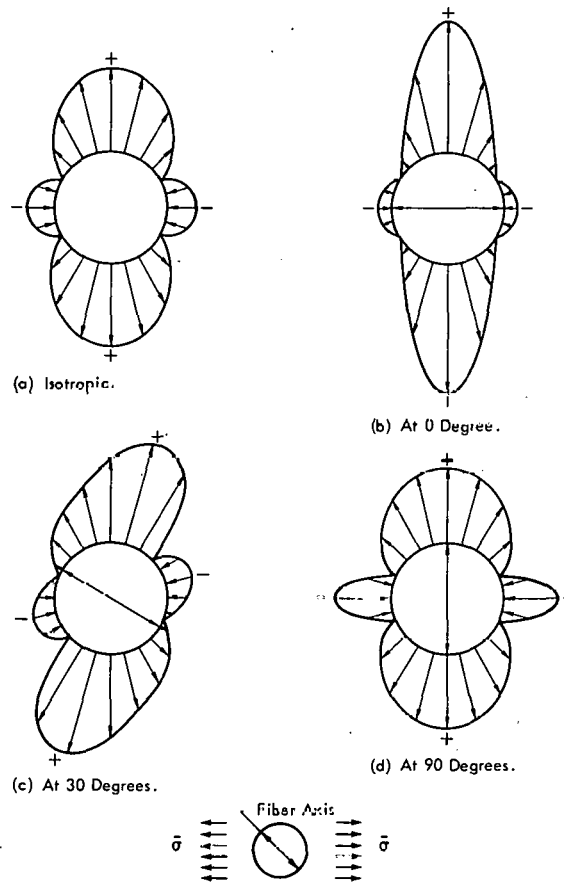


Figure 21. TANGENTIAL STRESS DISTRIBUTION ($\sigma_{\theta}/\bar{\sigma}$) AROUND A HOLE IN AN INFINITE ISOTROPIC OR ORTHOTROPIC SHEET FOR UNIAXIAL LOADING.

Calibration curves are generated in the same manner as for the earlier tensile specimen by incremental loading. Data are obtained at a centerline location halfway between the hole and the grips. In some cases, uniformity of the birefringence across the strip width was investigated and found to be good. Strain-gage rosettes were mounted at the symmetrical location on the specimen and used to check the state of stress and generate data to determine the elastic properties. The material properties were calculated from the calibration curves and the stress-optic or stress-strain relations.

The analysis was carried out for Lines a, b, and c in the specimen configuration presented in Figure 23. Symmetries in the 0 and 90-degree orientations allow some reduction of the data collection. In all cases, at least two sets of data were taken and the average values were used in the calculation. Data to apply the shear-difference method were required along Lines a and b. Intervals between points for data collection were, typically, 0.010 inch near the hole with an increasing interval size away from the hole as the stress gradient decreased. Data input to a computerized routine (which accounts for the initial birefringence) produced the stress distribution. Data were taken along Line c at 10-degree angular intervals. Data were corrected for initial birefringence; and, along with the transformed material fringe values, were used to calculate the tangential stress directly.

Comparison of Solutions

The photoelastic solutions were compared with the analytical solutions (Figures 24 through 26). Normalized stress distribution is shown for each specimen fiber orientation in each figure. Figures 24 and 25 compare finite-element and photoelastic-normalized stress distributions along Lines a and b, respectively; Figure 26 presents the closed-form solution⁽⁹⁾ along with finite element and photoelastic solutions along the hole boundary. It can be seen that the general agreement is good. The few significant differences are likely caused by material irregularities.

The vertical stress component in Figure 24 shows the maximum stress concentration at the hole boundary. The decay rate of this stress is seen to be different between fiber orientations. In all three specimens, the vertical stress has decayed to its nominal value at a distance of about three times the hole radius from the center. The finite-element and photoelastic data are in good agreement.

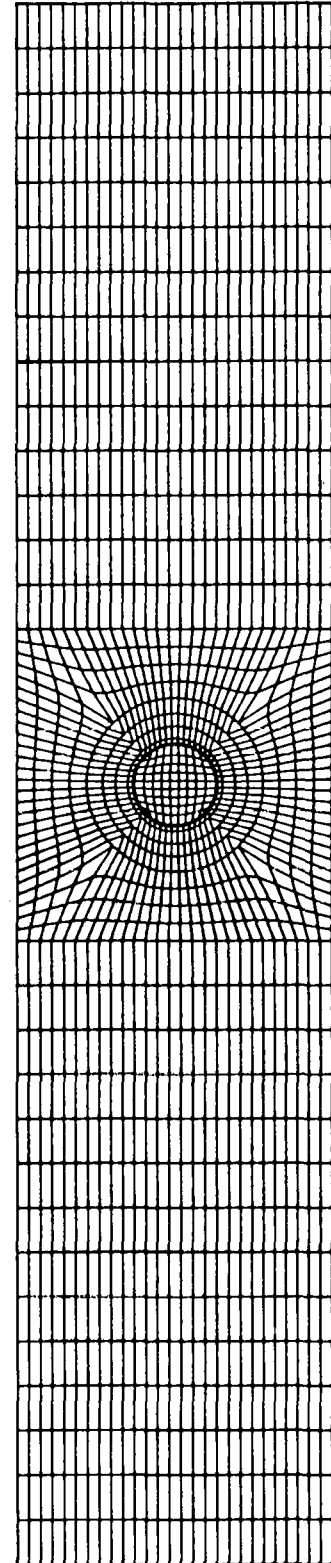


Figure 22. FINITE-ELEMENT MODEL OF A TENSILE STRIP WITH A CENTRAL HOLE.

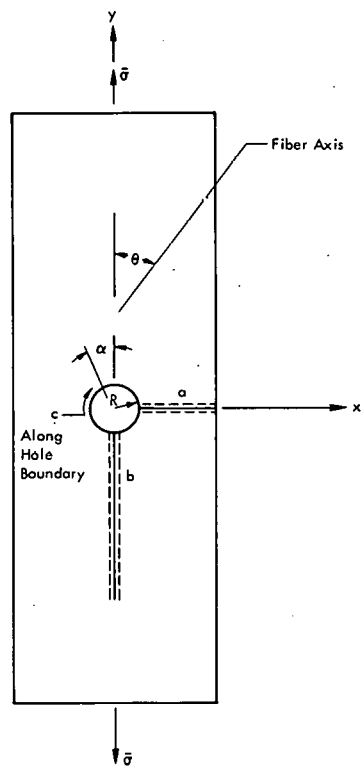
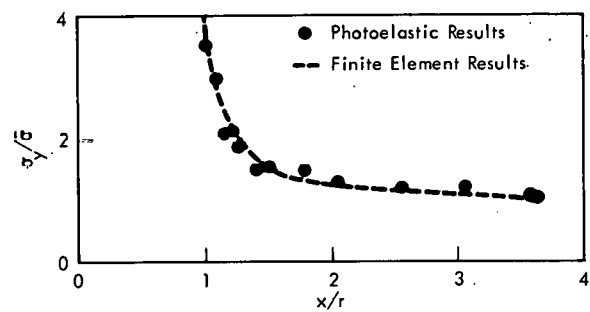
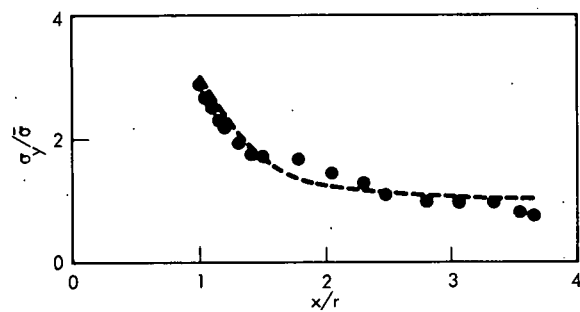


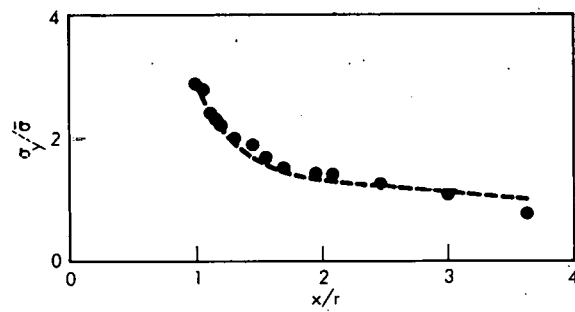
Figure 23. LOCATION OF PHOTO-ELASTIC SOLUTIONS.



(a) At 0 Degree.

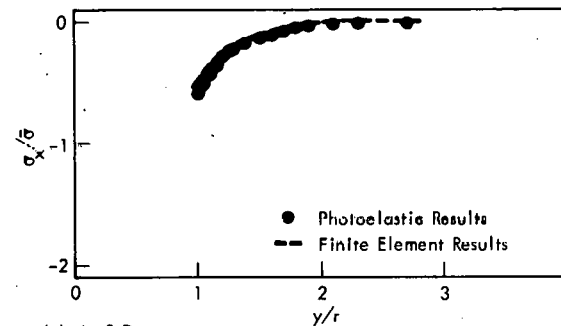


(b) At 30 Degrees.

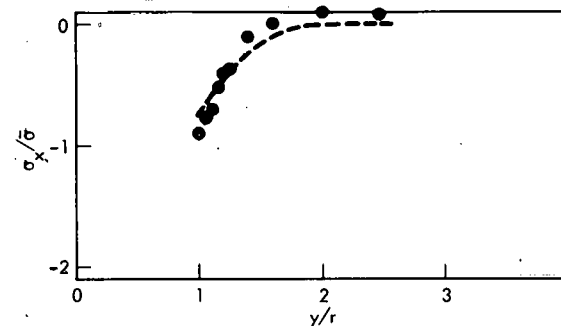


(c) At 90 Degrees.

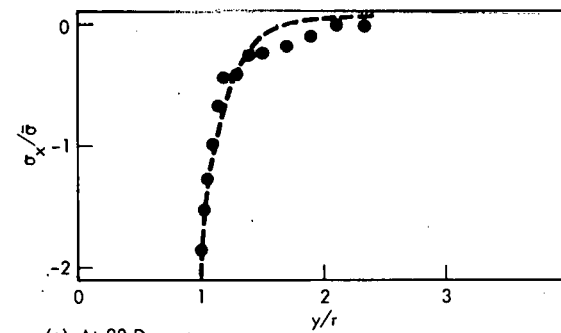
Figure 24. VERTICAL STRESS ($\sigma_y/\bar{\sigma}$) ALONG THE HORIZONTAL AXIS (x) FOR LINE a.



(a) At 0 Degree.

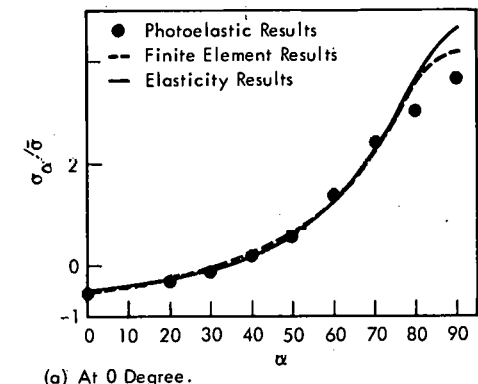


(b) At 30 Degrees.

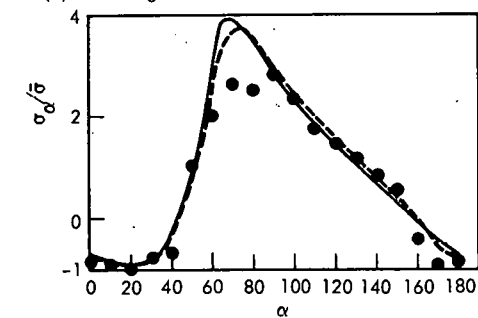


(c) At 90 Degrees.

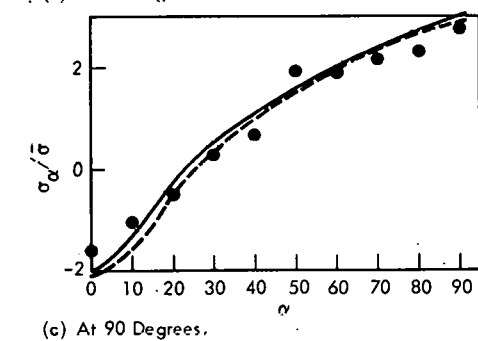
Figure 25. HORIZONTAL STRESS ($\sigma_x/\bar{\sigma}$) ALONG THE VERTICAL AXIS (y) FOR LINE b.



(a) At 0 Degree.



(b) At 30 Degrees.



(c) At 90 Degrees.

Figure 26. TANGENTIAL STRESS ($\sigma_\alpha/\bar{\sigma}$) AROUND THE HOLE BOUNDARY (LINE c).

The horizontal stress component along the vertical centerline in Figure 25 indicates the peak compressive stress on the hole boundary. The decay to nominal stress on this axis occurs at a distance about two times the hole radius from the center.

The tangential stress around the hole boundary in Figure 26 compares three solutions. Since the stresses decay away from the hole to nominal values before reaching the specimen edge, agreement between the elasticity and finite-element solutions is expected to be good. The major differences occur at the peak values. Photoelastic solutions for the most part are in closer agreement with the finite-element results. These comparisons substantially verify the orthotropic photoelasticity formulation.

CONCLUSIONS

The following conclusions can be stated as a result of this study:

1. The governing equations for orthotropic photoelasticity are established by utilizing the tensorial nature of stress, strain, and birefringence in the transparent composite material.
2. Condensation of the governing equations yields relations applicable to plane-stress problems for orthotropic materials.
3. The experimental data from tests with special biaxial stress conditions in the off-axis tensile specimen and the photoelastic solution of a general plane-stress problem verify the theoretical formulation.
4. The shear-difference method is reformulated to be applied in orthotropic photoelasticity to find separate stress components.
5. A composite material of fiberglass and epoxy can be manufactured with sufficient transparency and uniformity to use as a photoelastic model.
6. The photoelastic properties (also the elastic properties) can be calculated by use of a finite-element model of the material micro structure.
7. The other theories proposed to date in the literature are mostly correct under the special conditions for which they apply.

REFERENCES

- (1) Pih, H. and Knight, C. E.; "Photoelastic Analysis of Anisotropic Fiber Reinforced Composites", *Journal of Composite Materials*, 3, (1), pp 94 - 107; January 1969.
- (2) Sampson, R. C.; "A Stress-Optic Law for Photoelastic Analysis of Orthotropic Composites", *Experimental Mechanics*, 10, pp 210 - 215; May 1970.
- (3) Dally, J. W. and Prabhakaran, R.; "Photo-Orthotropic-Elasticity", *Experimental Mechanics*, 11, (8), pp 346 - 356; August 1971.
- (4) Bert, C. W.; "Theory of Photoelasticity for Birefringent Filamentary Composites", *Fibre Science and Technology*, 5, pp 165 - 171 (1972).
- (5) Bhagavantam, S.; *Crystal Symmetry and Physical Properties*; Academic Press, Inc, New York (1966).
- (6) Pipes, R. B. and Rose, J. L.; *Photo-Anisotropic-Elasticity—A Strain-Optic Law for Birefringent Composites*, Presented at the 1973 SESA Spring Meeting, May 13 - 18, Los Angeles, California.
- (7) Daniel, I. M., Rowlands, R. E., and Post, D.; "Strain Analysis of Composites by Moire Methods", *Experimental Mechanics*, 13, pp 246 - 254; June 1973.
- (8) Dally, J. W. and Alfirevich, I., "Application of Birefringent Coatings to Glass-Fiber-Reinforced Plastics", *Experimental Mechanics*, 9, pp 97 - 102 (1969).
- (9) Lekhnitskii, S. G.; *Theory of Elasticity of An Anisotropic Elastic Body*; Holden-Day, Inc, San Francisco, California (1963).
- (10) Zienkiewicz, O. C.; *The Finite Element Method in Engineering Science*, McGraw-Hill Publishing Co, London (1971).
- (11) Tsai, S. W.; *Mechanics of Composite Materials, Part II - Theoretical Aspects*, AFML-TR-66-149, Part II; Air Force Materials Laboratory, Wright-Patterson Air Force Base, Ohio; November 1966.
- (12) Hearmon, R. F. S.; *An Introduction to Applied Anisotropic Elasticity*; Oxford University Press, London (1961).
- (13) Boley, B. A. and Weiner, J. H.; *Theory of Thermal Stresses*, John Wiley and Sons, Inc, New York (1960).
- (14) Knight, C. E.; "Orthotropic Photoelastic Analysis of Residual Stresses in Filament-Wound Rings", *Experimental Mechanics*, 12, pp 107 - 112; February 1972.
- (15) Pagano, N. J. and Halpin, J. C.; "Influence of End Constraint in the Testing of Anisotropic Bodies", *Journal of Composite Materials*, 2, pp 18 - 31 (1968).

- (16) Whitney, J. M., Stansbarger, D. L., and Howell, H. B.; "Analysis of the Rail Shear Test-Application and Limitations", *Journal of Composite Materials*, 5, pp 24 - 34 (1971).
- (17) Frocht, M. M.; *Photoelasticity, I*, John Wiley and Sons, Inc, New York (1941).
- (18) Howland, R. C. J.; "On the Stresses in the Neighborhood of a Circular Hole in a Strip under Tension", *Phil Trans Royal Soc, London, Series A*, 229, pp 49 - 86; January 1930.

APPENDIX A

FINITE ELEMENT COMPUTER PROGRAM FOR NORMAL STRESS PROPERTIES

```

      IMPLICIT REAL*8 (A-H,O-Z)
C
C
      COMMON NUMNP,NUMEL,NUMMAT,NUMPC,ACELZ,ANGFQ,MBAND,MTYPE,TEMP,Q,
1 HED(12),E(8,8,12),RO(12),XXNN(12),R(900),Z(900),UR(900),UZ(900),
2 CODE(900),T(900),IBC(200),JBC(200),PR(200),ANGLE(4),NP
      COMMON /ARG/ RRR(5),ZZZ(5),S(10,10),P(10),TT(4),LM(4),CD(3,3),
1 HH(6,10),RR(4),ZZ(4),C(4,4),H(6,10),D(6,6),F(6,10),TP(6),XI(10)
2 ,EE(7),IX(800,5),EPS(800)
C
      HALF BAND WIDTH INCREASED TO 35, WIDTHB = 35
C
      COMMON /BANARG/ MBAN,NUMBLK,B(4*WIDTHB),A(4*WIDTHB,2*WIDTHB)
      COMMON /BANARG/ MBAN,NUMBLK,B(140),A(140,70)
      COMMON /PLANE/ NPP
      COMMON /STRES/ SIGT(5), SIGR(5), SIGZ(5), URM4, URM5, PNURZ,
1PNUTR, PNUTZ, ER, EZ, NNN
      DIMENSION UZP(900),URP(900)
      DO 5 I = 1,900
5 UZP(I) = 0.0
      REAL*4 CLASS(3)
      REAL*4 BUFF(5000)
40 CALL ZERO
      LENGTH=5000
      CALL PLOTS (BUFF,LENGTH)
C
C*****
C READ AND PRINT OF CONTROL INFORMATION AND MATERIAL PROPERTIES
C*****
50 READ (5,1000,END=3055) (HED(I),I=1,10),
1 NUMNP,NUMEL,NUMMAT,NUMPC,ACELZ,ANGFQ,
2 Q,NP,NPP,ICHECK,MSHPLT
      IF ( NP.EQ.0 ) NP = 1
      WRITE (6,2000) (HED(I),I=1,10),
1 NUMNP,NUMEL,NUMMAT,NUMPC,ACELZ,ANGFQ,
2 Q,NP,ICHECK,MSHPLT
C
      IF (NPP) 54,56,54
54 WRITE(6,2008)
56 DO 59 M=1,NUMMAT
      READ (5,1001) MTYPE,NUMTC,RO(MTYPE),XXNN(MTYPE)
      IF( NUMTC.EQ.0 ) NUMTC = 1
      WRITE(6,2011) MTYPE,NUMTC,RO(MTYPE),XXNN(MTYPE)
      READ (5,1005) ((E(I,J,MTYPE),J=1,8),I=1,NUMTC)
      WRITE(6,2010) ((E(I,J,MTYPE),J=1,8),I=1,NUMTC)
      DO 58 I=NUMTC,8
      DO 58 J=1,8
58 E(I,J,MTYPE)=E(NUMTC,J,MTYPE)
59 CONTINUE
C
C*****
C READ AND PRINT OF NODAL POINT DATA
C*****
      WRITE(6,2004)
      L=0
60 READ (5,1002) N,CODE(N),R(N),Z(N),UR(N),UZ(N),T(N)
      URP(N) = UR(N)
      UZP(N) = UZ(N)
      FA = 1.180
      RAD = DSQRT(R(N)**2 + Z(N)**2)
      IF(RAD .GT. 0.810) GO TO 62

```

```

R(N) = R(N)*FA
Z(N) = Z(N)*FA
GO TO 64
62 IF(R(N) .EQ. 0.) TH = 1.57079
IF(R(N) .NE. 0.) TH = DATAN(Z(N)/R(N))
IF(TH .LE. 45./57.2958) RP = 1./DCOS(TH)
IF(TH .GT. 45./57.2958) RP = 1./DSIN(TH)
FP = (RP - FA*0.800)/(RP - 0.800)
RAD = RP - FP*(RP - RAD)
R(N) = RAD*DCOS(TH)
Z(N) = RAD*DSIN(TH)
64 CONTINUE
R(N) = R(N) + 1000.
UR(N) = UR(N) *0.1
UZ(N) = UZ(N) *0.0
NL=L+1
IF( N.EQ.1 ) GO TO 70
ZX=N-L
DR=(R(N)-R(L))/ZX
DZ=(Z(N)-Z(L))/ZX
DT=(T(N)-T(L))/ZX
70 L=L+1
IF(N-L) 100,90,80
80 CODE(L)=0.0
R(L)=R(L-1)+DR
Z(L)=Z(L-1)+DZ
UR(L)=0.0
UZ(L)=0.0
T(L)=T(L-1)+DT
GO TO 70
90 WRITE(6,2002) (K,CODE(K),R(K),Z(K),UR(K),UZ(K),T(K),K=NL,N)
IF(NUMNP-N) 100,110,60
100 WRITE(6,2009) N
CALL EXIT
110 CONTINUE
C*****
C READ AND PRINT OF ELEMENT PROPERTIES
C*****
WRITE(6,2001)
N=0
130 READ(5,1003) M,(IX(M,I),I=1,5)
140 N=N+1
IF(M-N) 170,170,150
150 IX(N,1)=IX(N-1,1)+1
IX(N,2)=IX(N-1,2)+1
IX(N,3)=IX(N-1,3)+1
IX(N,4)=IX(N-1,4)+1
IX(N,5)=IX(N-1,5)
170 WRITE(6,2003) N,(IX(N,I),I=1,5)
IF(M-N)180,180,140
180 IF ( NUMEL - N ) 189,190,130
189 WRITE ( 6,2012 ) N
CALL EXIT
190 CONTINUE
C*****
C READ AND PRINT OF PRESSURE BOUNDARY CONDITIONS
C*****
IF(NUMPC)290,310,290
290 WRITE(6,2005)
DO 300 L=1,NUMPC
READ (5,1004) IBC(L),JBC(L),PR(L)
300 WRITE(6,2007) IBC(L),JBC(L),PR(L)
310 CONTINUE
C
C*****
C PLOT A MESH PLOT OF THE GEOMETRY, IF REQUESTED.
C*****
C
C (N1,N2) ARE FIRST AND LAST ELEMENTS NUMBERS TO BE PLOTTED
C SCALE IS FACTOR TO MAKE VERTICAL DIMENSION .LE. 10.0 INCHES

```

```

C (XD,YD) ARE COORDINATES OF ORIGIN ON PAPER (YD .GE. 0.5 )
C CLASS CONTAINS 0-12 HOLLERITH CHARACTERS. WRITTEN ON LEFT EDGE.
  IF (MSHPLT.LE.0) GO TO 346
  DO 345 M=1,MSHPLT
  READ (5,1006) N1,N2,SCALE,XD,YD,CLASS
  CALL GRDPLT (NUMNP,NUMEL,N1,N2,SCALE,XD,YD,HED,CLASS,IX,R,Z)
345 CONTINUE
346 IF (ICHECK.NE.0) GO TO 50
C
C*****
C DETERMINE BAND WIDTH
C*****
  J=0
  DO 340 N=1,NUMEL
  DO 340 I=1,4
  DO 325 L=1,4
  KK=IABS(IX(N,I)-IX(N,L))
  IF(KK-J)325,325,320
320 J=KK
325 CONTINUE
340 CONTINUE
  MBAND=2*J+2
  MBAN = MBAND
C*****
C SOLVE NON-LINEAR STRUCTURE BY SUCCESSIVE APPROXIMATIONS
C*****
  DO 350 N=1,NUMEL
350 EPS(N)=0.0
C
  DO 10 I = 1,5
  SIGT(I) = 0.0
  SIGR(I) = 0.0
  10 SIGZ(I) = 0.0
  DO 500 NNN=1,NP
  IF(NNN.EQ. 1) GO TO 400
  IF(NNN .EQ. 2)GO TO 390
  IF(NNN .EQ. 4)GO TO 370
  IF(NNN .EQ. 5)GO TO 380
  PNUTR = (SIGT(1)*SIGZ(2) - SIGT(2)*SIGZ(1))/(SIGR(1)*SIGZ(2)
1- SIGR(2)*SIGZ(1))
  PNUTZ = (SIGT(1)*SIGR(2) - SIGT(2)*SIGR(1))/(SIGZ(1)*SIGR(2)
1- SIGZ(2)*SIGR(1))
  DO 360 N = 1,NUMNP
  UR(N) = -URP(N)*PNUTR*0.1
  IF(CODE(N) .EQ. 1.0 .OR. CODE(N) .EQ. 3.0) UR(N) = UR(N) + 10.0
  UZ(N) = -UZP(N)*PNUTZ*0.1
360 CONTINUE
  GO TO 400
370 DO 375 N = 1,NUMNP
  UR(N) = URP(N)*0.1
  IF(CODE(N) .EQ. 1.0 .OR. CODE(N) .EQ. 3.0) UR(N) = UR(N) - URM4
  UZ(N) = -UZP(N)*PNURZ*0.1
375 CONTINUE
  GO TO 400
380 CONTINUE
  DO 385 N = 1,NUMNP
  UR(N) = -URP(N)*PNURZ*0.1*EZ/ER
  UZ(N) = UZP(N)*0.1
  IF(CODE(N) .EQ. 1.0 .OR. CODE(N) .EQ. 3.0) UR(N) = UR(N) - URM5
385 CONTINUE
  GO TO 400
390 DO 395 N = 1,NUMNP
  UR(N) = URP(N)*0.0
  UZ(N) = UZP(N)*0.1
395 CONTINUE
400 CONTINUE
C
C FORM STIFFNESS MATRIX
C
C CALL STIFF

```

```

C
C   SOLVE FOR DISPLACEMENTS
C
C   CALL BANSOL
C
C   WRITE (6,2006) (N,B(2*N-1),B(2*N),N=1,NUMNP)
C
C   COMPUTE STRESSES
C
C   CALL STRESS
C
C   500 CONTINUE
C*****
C   GO TO 40
C*****
1000 FORMAT(10A8/4I5,3F10.2,4I5)
1001 FORMAT (2I5,2F10.0)
1002 FORMAT (I5,F5.0,5F10.0)
1003 FORMAT (6I5)
1004 FORMAT (2I5,F10.0)
1005 FORMAT (8F10.0)
1006 FORMAT(2I5, 3F10.0, 3A4)
2000 FORMAT (1H1 10A8/
1 30H0 NUMBER OF NODAL POINTS----- I3 /
2 30H0 NUMBER OF ELEMENTS----- I3 /
3 30H0 NUMBER OF DIFF. MATERIALS--- I3 /
4 30H0 NUMBER OF PRESSURE CARDS---- I3 /
5 30H0 AXIAL ACCELERATION----- E12.4/
6 30H0 ANGULAR VELOCITY----- E12.4/
7 30H0 REFERENCE TEMPERATURE----- E12.4/
8 30H0 NUMBER OF APPROXIMATIONS---- I3/
9 '0 DATA CHECK ONLY (0=NO)-----',T31,I3/
A '0 NUMBER OF PLOTS-----',T31,I3)
2001 FORMAT (49H1ELEMENT NO.      I      J      K      L      MATERIAL )
2002 FORMAT (I12,F12.2,2F12.3,2E24.7,F12.3)
2003 FORMAT (11I3,4I6,11I2)
2004 FORMAT (109H1NODAL POINT      TYPE R-ORDINATE Z-ORDINATE R LO.
1AD OR DISPLACEMENT Z LOAD OR DISPLACEMENT TEMPERATURE I
2005 FORMAT (29H0PRESSURE BOUNDARY CONDITIONS/ 24H      I      J      PRESS
1URE )
2006 FORMAT (12H1N.P. NUMBER 18X 2HUR 18X 2HUR / (11I2,2F20.7))
2007 FORMAT (2I6,F12.3)
2008 FORMAT (23H0PLANE STRESS STRUCTURE )
2009 FORMAT (26H0NODAL POINT CARD ERROR N= I5)
2010 FORMAT (15H0 TEMPERATURE 10X 5HE(RZ) 9X 6HNU(RZ) 11X 4HE(T)
1 10X 5HNU(T) 6X 9HALPHA(RZ) 7X 8HALPHA(T) 15H YIELD STRESS /
2 (F15.2,7E15.5))
2011 FORMAT (17H0MATERIAL NUMBER= I3, 30H, NUMBER OF TEMPERATURE CARDS=
1 I3, 15H, MASS DENSITY= E12.4 ,16H,MODULUS RATIO= E12.4 )
2012 FORMAT ( 21H0ELEMENT ERROR FOR N= , I5 )
C
C   3055 CONTINUE
C   END

SUBROUTINE STIFF
IMPLICIT REAL*8 (A-H,O-Z)
C
COMMON NUMNP,NUMEL,NUMMAT,NUMPC,ACELZ,ANGFQ,MBAND,MTYPE,TEMP,Q,
1 HED(12),E(8,8,12),RO(12),XXNN(12),R(900),Z(900),UR(900),UZ(900),
2 CODE(900),T(900),IBC(200),JBC(200),PR(200),ANGLE(4),NP
COMMON /ARG/ RRR(5),ZZZ(5),S(10,10),P(10),TT(4),LM(4),DD(3,3),
1 HH(6,10),RR(4),ZZ(4),C(4,4),H(6,10),D(6,6),F(6,10),TP(6),XI(10)
2 ,EE(7),IX(800,5),EPS(800)
COMMON /BANARG/ MBAN,NUMBLK,B(140),A(140,70)
COMMON /PLANE/ NPP
C
C*****

```

```

C      INITIALIZATION
C*****
      REWIND 2
      NB = 35.
      ND=2*NB
      ND2=2*ND
      STOP=0.0
      NUMBLK=0

C
      DO 50 N=1,ND2
      B(N)=0.0
      DO 50 M=1,ND
      50 A(N,M)=0.0
C*****
C      FORM STIFFNESS MATRIX IN BLOCKS
C*****
      60 NUMBLK=NUMBLK+1
      NH=NB*(NUMBLK+1)
      NM=NH-NB
      NL=NM-NB+1
      KSHIFT=2*NL-2

C
      DO 210 N=1,NUMEL

C
      IF(IX(N,5)) 210,210,65
      65 DO 80 I=1,4
      IF(IX(N,I)-NL) 80,70,70
      70 IF(IX(N,I)-NM) 90,90,80
      80 CONTINUE
      GO TO 210

C
      90 CALL QUAD(N,VOL)

C
      IF(VOL) 142,142,144
      142 WRITE(6,2003) N
      STOP=1.0
      144 IF(IX(N,3)-IX(N,4)) 145,165,145
      145 DO 150 II=1,9
      CC=S(II,10)/S(10,10)
      P(II)=P(II)-CC*P(10)
      DO 150 JJ=1,9
      150 S(II,JJ)=S(II,JJ)-CC*S(10,JJ)

C
      DO 160 II=1,8
      CC=S(II,9)/S(9,9)
      P(II)=P(II)-CC*P(9)
      DO 160 JJ=1,8
      160 S(II,JJ)=S(II,JJ)-CC*S(9,JJ)

C
C      ADD ELEMENT STIFFNESS TO TOTAL STIFFNESS
C
      165 DO 166 I=1,4
      166 LM(I)=2*IX(N,I)-2

C
      DO 200 I=1,4
      DO 200 K=1,2
      II=LM(I)+K-KSHIFT
      KK=2*I-2+K
      B(II)=B(II)+P(KK)
      DO 200 J=1,4
      DO 200 L=1,2
      JJ=LM(J)+L-II+1-KSHIFT
      LL=2*J-2+L
      IF(JJ) 200,200,175
      175 IF(ND-JJ) 180,195,195
      180 WRITE(6,2004) N
      STOP=1.0
      GO TO 210
      195 A(II,JJ)=A(II,JJ)+S(KK,LL)
      200 CONTINUE

```

```

210 CONTINUE
C
C   ADD CONCENTRATED FORCES WITHIN BLOCK
C
      DO 250 N=NL,NM
      K=2*N-KSHIFT
      IF(K.GT. 2*NUMNP) GO TO 250
      B(K)=B(K)+UZ(N)
      B(K-1)=B(K-1)+UR(N)
250 CONTINUE
C
C   BOUNDARY CONDCITIONS
C
      1. PRESSURE B.C.
C
      IF(NUMPC) 260,310,260
260 DO 300 L=1,NUMPC
      I=IBC(L)
      J=JBC(L)
      PP=PR(L)/6.
      DZ=(Z(I)-Z(J))*PP
      DR=(R(J)-R(I))*PP
      RX=2.0*R(I)+R(J)
      ZX=R(I)+2.0*R(J)
      IF(NPP) 262,264,262
262 RX=3.0
      ZX=3.0
264 II=2*I-KSHIFT
      JJ=2*J-KSHIFT
      IF(II) 280,280,265
265 IF(II-ND)270,270,280
270 SINA=0.0
      COSA=1.0
      IF(CODE(I))271,272,272
271 SINA= DSIN(CCODE(I)/57.295779)
      COSA= DCCS(CODE(I)/57.295779)
272 B(II-1)=B(II-1)+RX*(COSA*DZ+SINA*DR)
      B(II)=B(II)-RX*(SINA*DZ-COSA*DR)
280 IF(JJ)300,300,285
285 IF(JJ-ND)290,290,300
290 SINA=0.0
      COSA=1.0
      IF(CODE(J))291,292,292
291 SINA= DSIN(CODE(J)/57.295779)
      COSA= DCCS(CODE(J)/57.295779)
292 B(JJ-1)=B(JJ-1)+ZX*(COSA*DZ+SINA*DR)
      B(JJ)=B(JJ)-ZX*(SINA*DZ-COSA*DR)
300 CONTINUE
C
C   2. DISPLACEMENT B.C.
C
310 DO 400 M=NL,NH
      IF(M-NUMNP) 315,315,400
315 U=UR(M)
      N=2*M-1-KSHIFT
      IF(CODE(M))390,400,316
316 IF(CODE(M)-1.)317,370,317
317 IF(CODE(M)-2.)318,390,318
318 IF(CODE(M)-3.) 390,380,390
370 CALL MODIFY(A,B,ND2,MBAND,N,U)
      GO TO 400
380 CALL MCDIFY(A,B,ND2,MBAND,N,U)
390 U=UZ(M)
      N=N+1
      CALL MODIFY(A,B,ND2,MBAND,N,U)
400 CONTINUE
C
C   WRITE BLOCK OF EQUATIONS ON TAPE AND SHIFT UP LOWER BLOCK
C
      WRITE(2) (B(N),(A(N,M),M=1,MBAND),N=1,ND)

```



```

C      DO 420 N=1,ND
        K=N+ND
        B(N)=B(K)
        B(K)=0.0
        DO 420 M=1,ND
          A(N,M)=A(K,M)
420    A(K,M)=0.0
C
C      CHECK FOR LAST BLOCK
C
        IF(NM-NUMNP) 60,480,480
480    CONTINUE
C*****
        IF(STOP)490,500,490
490    CALL EXIT
500    RETURN
C
2003  FORMAT (26HNEGATIVE AREA ELEMENT NO. 14)
2004  FORMAT (29HOBAND WIDTH EXCEEDS ALLOWABLE 14)
      END

      SUBROUTINE QUAD(N,VOL)
C
      IMPLICIT REAL*8 (A-H,O-Z)
      COMMON NUMNP,NUMEL,NUMMAT,NUMPC,ACELZ,ANGFQ,MBAND,MTYPE,TEMP,Q,
1 HED(12),E(8,8,12),RO(12),XXNN(12),R(900),Z(900),UR(900),UZ(900),
2 CODE(900),T(900),IBC(200),JBC(200),PR(200),ANGLE(4),NP
      COMMON /ARG/ RRR(5),ZZZ(5),S(10,10),P(10),TT(4),LM(4),DD(3,3),
1 HH(6,10),RR(4),ZZ(4),C(4,4),H(6,10),D(6,6),F(6,10),TP(6),XI(10)
2 ,EE(7),IX(800,5),EPS(800)
      COMMON /BANARG/ ND,NUMBLK,B(140),A(140,70)
      COMMON /PLANE/ NPP
      COMMON /AREAS/ AREA(800)
C
90    I=IX(N,1)
      J=IX(N,2)
      K=IX(N,3)
      L=IX(N,4)
      MTYPE=IX(N,5)
      IX(N,5)=-IX(N,5)
C
C      FORM STRESS-STRAIN RELATIONSHIP
C
      TEMP=(T(I)+T(J)+T(K)+T(L))/4.0
      DO 103 MM=2,8
        M = MM
        IF(E(M,1,MTYPE)-TEMP) 103,104,104
103    CONTINUE
104    RATIO=0.0
        DEN=E(M,1,MTYPE)-E(M-1,1,MTYPE)
        IF(DEN)70,71,70
        70 RATIO=(TEMP-E(M-1,1,MTYPE))/DEN
        71 DO 105 KK=1,7
105    EE(KK)=E(M-1,KK+1,MTYPE)+RATIO*(E(M,KK+1,MTYPE)-E(M-1,KK+1,MTYPE))
        TEMP=TEMP-Q
C
C
      EPSR=EE(7)/EE(1)
      IF(EPSR-EPS(N)) 106,106,108
106    RATIO=(EE(7)/(EPS(N)*EE(1)))+(1.0-XXNN(MTYPE))+XXNN(MTYPE)
      EE(1)=EE(1)*RATIO
      EE(3)=EE(3)*RATIO
108    CONTINUE
C
      IF(NPP)84,86,84
C      CHECK THERMAL SECTION FOR PLANE STRESS CASE
84    XX=EE(1)/EE(3)

```

```

COMM=EE(1)/(XX-EE(2)**2)
C(1,1)=COMM*XX
C(1,2)=COMM*EE(2)
C(1,3)=0.0
C(2,1)=C(1,2)
C(2,2)=COMM
C(2,3)=0.0
C(3,1)=0.0
C(3,2)=0.0
C(3,3)=0.0
C(4,4)=EE(4)
GO TO 88
C
86 C(1,1)=1.0/EE(1)
C(1,2)=-EE(2)/EE(1)
C(1,3)=-EE(4)/EE(3)
C(2,1)=C(1,2)
C(2,2)=C(1,1)
C(2,3)=C(1,3)
C(3,1)=C(1,3)
C(3,2)=C(2,3)
C(3,3)=1.0/EE(3)
CALL SYMINV(C,3)
C(4,4)=EE(1)/(2.0+2.0*EE(2))
C
88 DO 110 M=1,3
110 TT(M)=((C(M,1)+C(M,2))*EE(5)+C(M,3)*EE(6))*TT(M)
C
C FORM QUACRILATERAL STIFFNESS MATRIX
C
RRR(5)=(R(I)+R(J)+R(K)+R(L))/4.0
ZZZ(5)=(Z(I)+Z(J)+Z(K)+Z(L))/4.0
DO 94 M=1,4
MM=IX(N,M)
IF(NPP)93,89,93
89 IF(R(MM))93,91,93
91 R(MM)=.01*RRR(5)
IF(CODE(MM))93,92,93
92 CODE(MM)=1.0
93 RRR(M)=R(MM)
94 ZZZ(M)=Z(MM)
C
DO 100 II=1,10
P(II)=0.0
DO 95 JJ=1,6
95 HH(JJ,II)=0.0
DO 100 JJ=1,10
100 S(II,JJ)=0.0
DO 119 II=1,4
JJ=IX(N,II)
119 ANGLE(II)=CODE(JJ)/57.3
C
IF(K-L)125,120,125
120 CALL TRISTF(1,2,3)
RRR(5)=(RRR(1)+RRR(2)+RRR(3))/3.0
ZZZ(5)=(ZZZ(1)+ZZZ(2)+ZZZ(3))/3.0
VOL=XI(1)
GO TO 130
125 VOL=0.0
CALL TRISTF(4,1,5)
VOL=VOL+XI(1)
CALL TRISTF(1,2,5)
VOL=VOL+XI(1)
CALL TRISTF(2,3,5)
VOL=VOL+XI(1)
CALL TRISTF(3,4,5)
VOL=VOL+XI(1)
AREA(N) = VOL
IF(NPP .EQ. 0) AREA(N) = AREA(N)/RRR(5)
C

```

```

      DO 140 II=1,6
      DO 140 JJ=1,10
140  HH(II,JJ)=HH(II,JJ)/4.0
C
130  RETURN
C
      END

      SUBROUTINE TRISTF(II,JJ,KK)
C
      IMPLICIT REAL*8 (A-H,O-Z)
      COMMON NUMNP,NUMEL,NUMMAT,NUMPC,ACELZ,ANGFQ,MBAND,MTYPE,TEMP,Q,
1  HED(12),E(8,8,12),RO(12),XXNN(12),R(900),Z(900),UR(900),UZ(900),
2  CODE(900),T(900),IBC(200),JBC(200),PR(200),ANGLE(4),NP
      COMMON /ARG/ RRR(5),ZZZ(5),S(10,10),P(10),TT(4),LM(4),DD(3,3),
1  HH(6,10),RR(4),ZZ(4),C(4,4),H(6,10),D(6,6),F(6,10),TP(6),XI(10)
2  ,EE(7),IX(800,5),EPS(800)
      COMMON /PLANE/ NPP
C
      1.  INITIALIZATION
C
      LM(1)=II
      LM(2)=JJ
      LM(3)=KK
C
      RR(1)=RRR(II)
      RR(2)=RRR(JJ)
      RR(3)=RRR(KK)
      RR(4)=RRR(II)
      ZZ(1)=ZZZ(II)
      ZZ(2)=ZZZ(JJ)
      ZZ(3)=ZZZ(KK)
      ZZ(4)=ZZZ(II)
C
      85  DO 100 I=1,6
          DO 90 J=1,10
              F(I,J)=0.0
          90  H(I,J)=0.0
              DO 100 J=1,6
100     D(I,J)=0.0
C
      3.  FORM INTEGRAL(G)T*(C)*(G)
C
      CALL INTER(XI,RR,ZZ)
C
      D(2,6)=XI(1)*(C(1,2)+C(2,3))
      D(3,5)=XI(1)*C(4,4)
      D(5,5)=XI(1)*C(4,4)
      D(6,6)=XI(1)*C(2,2)
      IF(NPP)104,106,104
104  D(2,2)=XI(1)*C(1,1)
      D(3,3)=XI(1)*C(4,4)
      GO TO 108
106  D(1,1)=XI(3)*C(3,3)
      D(1,2)=XI(2)*(C(1,3)+C(3,3))
      D(1,3)=XI(5)*C(3,3)
      D(1,6)=XI(2)*C(2,3)
      D(2,2)=XI(1)*(C(1,1)+2.0*C(1,3)+C(3,3))
      D(2,3)=XI(4)*(C(1,3)+C(3,3))
      D(3,3)=XI(6)*C(3,3)+XI(1)*C(4,4)
      D(3,6)=XI(4)*C(2,3)
C
108  DO 110 I=1,6
          DO 110 J=I,6

```

```

110 D(J,I)=D(I,J)
C
C      4. FORM COEFFICIENT-DISPLACEMENT TRANSFORMATION MATRIX
C
COMM=RR(2)*(ZZ(3)-ZZ(1))+RR(1)*(ZZ(2)-ZZ(3))+RR(3)*(ZZ(1)-ZZ(2))
DD(1,1)=(RR(2)*ZZ(3)-RR(3)*ZZ(2))/COMM
DD(1,2)=(RR(3)*ZZ(1)-RR(1)*ZZ(3))/COMM
DD(1,3)=(RR(1)*ZZ(2)-RR(2)*ZZ(1))/COMM
DD(2,1)=(ZZ(2)-ZZ(3))/COMM
DD(2,2)=(ZZ(3)-ZZ(1))/COMM
DD(2,3)=(ZZ(1)-ZZ(2))/COMM
DD(3,1)=(RR(3)-RR(2))/COMM
DD(3,2)=(RR(1)-RR(3))/COMM
DD(3,3)=(RR(2)-RR(1))/COMM
C
DO 120 I=1,3
J=2*LM(I)-1
H(1,J)=DD(1,I)
H(2,J)=DD(2,I)
H(3,J)=DD(3,I)
H(4,J+1)=DD(1,I)
H(5,J+1)=DD(2,I)
120 H(6,J+1)=DD(3,I)
C
C      ROTATE UNKNOWNNS IF REQUIRED
C
DO 125 J=1,2
I=LM(J)
IF(ANGLE(I))122,125,125
122 SINA= DSIN(ANGLE(I))
COSA= DCOS(ANGLE(I))
IJ=2*I
DO 124 K=1,6
TEM=H(K,IJ-1)
H(K,IJ-1)=TEM*COSA+H(K,IJ)*SINA
124 H(K,IJ)=-TEM*SINA+H(K,IJ)*COSA
125 CONTINUE
C
C      5. FORM ELEMENT STIFFNESS MATRIX (H)T*(D)*(H)
C
DO 130 J=1,10
DO 130 K=1,6
IF(H(K,J))128,130,128
128 DO 129 I=1,6
129 F(I,J)=F(I,J)+D(I,K)*H(K,J)
130 CONTINUE
C
DO 140 I=1,10
DO 140 K=1,6
IF(H(K,I))138,140,138
138 DO 139 J=1,10
139 S(I,J)=S(I,J)+H(K,I)*F(K,J)
140 CONTINUE
C
C      6. FORM THERMAL LOAD MATRIX
C
IF(NPP)145,150,145
145 TT(3)=0.0
COMM=XI(1)*EE(4)
150 COMM=RO(MTYPE)*ANGFQ**2
TP(1)=COMM*XI(7)+XI(2)*TT(3)
TP(2)=COMM*XI(9)+XI(1)*(TT(1)+TT(3))
TP(3)=COMM*XI(10)+XI(4)*TT(3)
COMM=-RO(MTYPE)*ACELZ
TP(4)=COMM*XI(1)
TP(5)=COMM*XI(7)
TP(6)=COMM*XI(8)+XI(1)*TT(2)
C
DO 160 I=1,10
DO 160 K=1,6

```

```

160 P(I)=P(I)+H(K,I)*TP(K)
C
C
C   FORM STRAIN TRANSFORMATION MATRIX
C
400 DO 410 I=1,6
    DO 410 J=1,10
410 HH(I,J)=HH(I,J)+H(I,J)
C
    RETURN
C
    END

SUBROUTINE STRESS
C
    IMPLICIT REAL*8 (A-H,O-Z)
    COMMON NUMNP,NUMEL,NUMMAT,NUMPC,ACELZ,ANGFQ,MBAND,MTYPE,TEMP,Q,
1 HED(12),E(8,8,12),RO(12),XXNN(12),R(900),Z(900),UR(900),UZ(900),
2 CODE(900),T(900),IBC(200),JBC(200),PR(200),ANGLE(4),NP
    COMMON /ARG/ RRR(5),ZZZ(5),S(10,10),P(10),TT(4),LM(4),DD(3,3),
1 HH(6,10),RR(4),ZZ(4),C(4,4),H(6,10),D(6,6),F(6,10),TP(6),XI(10)
2 ,EE(7),IX(800,5),EPS(800)
    COMMON /BANARG/ ND,NUMBLK,B(140),A(140,70)
    COMMON /PLANE/ NPP
    COMMON /AREAS/ AREA(800)
    COMMON /STRES/ SIGT(5),SIGR(5),SIGZ(5),URM4,URM5,PNURZ,
1PNUTR,PNUTZ,ER,EZ,NNN
    DIMENSION SIG(10)
C*****
C   COMPUTE ELEMENT STRESSES
C*****
    XKE=0.0
    XPE=0.0
    MPRINT=0
    IFR = 1
    FRNGRT = 0.
    FRNGZT = 0.
    SIGRT = 0.0
    SIGZT = 0.0
    SIGTT = 0.
    AREAT = 0.

C
    DO 300 M=1,NUMEL
C
        N=M
        IX(N,5)=IABS(IX(N,5))
        MTYPE=IX(N,5)
C
        CALL QUAD(N,VOL)
        IX(N,5)=MTYPE
C
        DO 120 I=1,4
            II=2*I
            JJ=2*IX(N,I)
            P(II-1)=B(JJ-1)
120 P(II)=B(JJ)
C
            DO 150 I=1,2
                RR(I)=F(I+8)
                DO 150 K=1,8
150 RR(I)=RR(I)-S(I+8,K)*P(K)
C
                COMM=S(9,9)*S(10,10)-S(9,10)*S(10,9)
                IF(COMM)155,160,155
155 P(9)=(S(10,10)*RR(1)-S(9,10)*RR(2))/COMM
                P(10)=(-S(10,9)*RR(1)+S(9,9)*RR(2))/COMM
C
160 DO 170 I=1,6

```

```

      TP(I)=0.0
      DO 170 K=1,10
170  TP(I)=TP(I)+HH(I,K)*P(K)
C
C
      RR(1)=TP(2)
      RR(2)=TP(6)
      RR(3)=(TP(1)+TP(2)*RRR(5)+TP(3)*ZZZ(5))/RRR(5)
      RR(4)=TP(3)+TP(5)
C
176  DO 180 I=1,3
      SIG(I)=-TT(I)
      DO 180 K=1,3
180  SIG(I)=SIG(I)+C(I,K)*RR(K)
      SIG(4)=C(4,4)*RR(4)
C
C      CALCULATE PHOTOELASTIC TERMS
C
      SIG(1) = SIG(1) - SIGRT
      SIG(2) = SIG(2) - SIGZT
      SIG(3) = SIG(3) - SIGTT
      SIGT(NNN) = SIGT(NNN) + SIG(3)*AREA(N)
      FRINGZ = ((SIG(1)-SIG(3))/E(1,8,MTYPE))*AREA(N)
      FRINGR = ((SIG(2)-SIG(3))/E(1,8,MTYPE))*AREA(N)
      FRNGRT = FRNGRT + FRINGR
      FRNGZT = FRNGZT + FRINGZ
      IF(N .NE. 25*IFR) GO TO 190
      IFR = IFR + 1
      SIGR(NNN) = SIGR(NNN) + SIG(1)/25.
190  IF(N .LE. 600) GO TO 195
      SIGZ(NNN) = SIGZ(NNN) + SIG(2)/25.
195  SIG(8) = SIG(3)
      SIG(9) = FRINGZ/AREA(N)
      SIG(10) = AREA(N)
      AREAT = AREAT + AREA(N)
C
C      CALCULATE ENERGY TERMS
C
      DO 250 I=1,10
      COMM=0.0
      DO 200 K=1,10
200  COMM=COMM+S(I,K)*P(K)
250  XPE=XPE+COMM*P(I)
      XKE=XKE+VOL*RO(MTYPE)*(P(9)**2+P(10)**2)
C
C      CALCULATE EFFECTIVE STRAIN
C
      IF(NPP)251,252,251
251  RR(3)=-{(SIG(1)+SIG(2))*EE(2)/EE(1)}
252  CC=(RR(1)+RR(2))/2.0
      CR= DSQRT(((RR(2)-RR(1))/2.0)**2+(RR(4)/2.0)**2)
      RR(1)=CC+CR
      RR(2)=CC-CR
      EPS(N)= DSQRT((RR(1)-RR(2))**2+(RR(1)-RR(3))**2+(RR(2)-RR(3))**2)
      I *.707/(1.0+EE(2))
C
C*****
C      OUTPUT STRESSES
C*****
C
C      CALCULATE PRINCIPAL STRESSES
C
      CC=(SIG(1)+SIG(2))/2.0
      BB=(SIG(1)-SIG(2))/2.0
      CR= DSQRT(BB**2+SIG(4)**2)
      SIG(5)=CC+CR
      SIG(6)=CC-CR
      SIG(7)= 28.648*DATAN2(SIG(4),BB)
C
C      STRESSES PARALLEL TO LINE I-J

```

```

C
  GO TO 104
  I=IX(N,1)
  J=IX(N,2)
  ANG= 2.*DATAN2(Z(J)-Z(I),R(J)-R(I))
  COS2A= DCOS(ANG)
  SIN2A= DSIN(ANG)
  CX=.5*(SIG(1)-SIG(2))
  SIG(8)=CX*COS2A+SIG(4)*SIN2A+CC
  SIG(9)=2.*CC-SIG(8)
  SIG(10)=-CX*SIN2A+SIG(4)*COS2A
C
104 IF(MPRINT)110,105,110
105 WRITE(6,2000)
  MPRINT=50
110 MPRINT=MPRINT-1
C
305 WRITE(6,2001)N,RRR(5),ZZZ(5),(SIG(I),I=1,10)
300 CONTINUE
  WRITE(6,2005) SIGRT,SIGZT,SIGTT,AREAT,SIGR(NNN),SIGZ(NNN),
  1SIGT(NNN),E(1,8,1),E(1,8,2),FRNGZT
  IF(NNN .EQ. 1) GO TO 306
  IF(NNN .EQ. 2) GO TO 306
  IF(NNN .EQ. 4) GO TO 303
  IF(NNN .EQ. 5) GO TO 304
  ET = SIGT(3)*100.
  FTR= SIGT(3)/FRNGZT
  FTZ= SIGT(3)/FRNGRT
  ER = (SIGZ(2)*SIGR(1) - SIGR(2)*SIGZ(1))/(SIGZ(2)*0.01 - PNUTR*
  1(SIGT(2)*SIGZ(1) - SIGT(1)*SIGZ(2))/ET)
  PNURZ = (SIGR(2) - PNUTR*ER*SIGT(2)/ET)/SIGZ(2)
  EZ = SIGZ(2)/(0.01 + PNURZ*SIGR(2)/ER + PNUTZ*SIGT(2)/ET)
  URM4 = 10.*PNUTR*ER/ET
  URM5 = 10.*PNUTZ*EZ/ET
  GO TO 306
303 FR = SIGR(4)/FRNGZT
  GO TO 306
304 FZ = SIGZ(5)/FRNGRT
306 CONTINUE
  IF(NNN .EQ. 5) WRITE(6,2007) ER,EZ,ET,PNUTR,PNUTZ,PNURZ,FR,FZ,FTR,
  1FTZ
C
  IF(XKE)310,320,310
310 W= DSQRT(XPE/XKE)
  WRITE(6,2006)W
C
320 RETURN
C
2000 FORMAT (7H1EL.NO. 7X 1HR 7X 1HZ 4X 8HR-STRESS 4X 8HZ-STRESS 4X
  1 8HT-STRESS 3X 9HRZ-STRESS 2X 10HMAX-STRESS 2X 10HMIN-STRESS
  2 37H ANGLE SIGZ FRINGE AREA )
2001 FORMAT (I7,2F8.2,1P6E12.4,0P1F7.2,1P3E10.2)
2006 FORMAT (36HO APPROXIMATE FUNDAMENTAL FREQUENCY = E12.5)
2005 FORMAT(1H1/
  A25HO SUPERIMP. SIGMA R.....= , E11.4,4H PSI/
  B25HO SUPERIMP. SIGMA Z.....= , E11.4,4H PSI/
  225HO SUPERIMP. SIGMA T.....= , E11.4,4H PSI/
  325HO CROSS-SECTIONAL AREA.= , E11.4,7H SQ.IN./
  425HO AVERAGE SIGMA R.....= , E11.4,4H PSI/
  525HO AVERAGE SIGMA Z.....= , E11.4,4H PSI/
  125HO AVERAGE SIGMA T.....= , E11.4,4H PSI/
  625HO FIBER FRINGE VALUE...= , E11.4,15H PSI IN./FRINGE/
  725HO MATRIX FRINGE VALUE..= , E11.4,15H PSI IN./FRINGE/
  825HO TOTAL FRINGE ORDER...= , E11.4,8H FRINGES)
2007 FORMAT(1HO/
  125HO R MODULUS.....= , E11.4, 4H PSI/
  225HO Z MODULUS.....= , E11.4, 4H PSI/
  325HO T MODULUS.....= , E11.4, 4H PSI/
  425HO NUTR.....= , E11.4/
  525HO NUTZ.....= , E11.4/

```

```

625HO NUHZ.....= , E11.4/
725HO R    FRINGE VALUE...= , E11.4, 15H PSI IN./FRINGE/
825HO Z    FRINGE VALUE...= , E11.4, 15H PSI IN./FRINGE/
925HO TR   FRINGE VALUE...= , E11.4, 15H PSI IN./FRINGE/
A25HO TZ   FRINGE VALUE...= , E11.4, 15H PSI IN./FRINGE)
C
  END

  SUBROUTINE SYMINV(A,NMAX)
C
  IMPLICIT REAL*8 (A-H,O-Z)
  DIMENSION A(4,4)
C
  DO 200 N=1,NMAX
C
  D=A(N,N)
  DO 100 J=1,NMAX
100 A(N,J)=-A(N,J)/D
C
  DO 150 I=1,NMAX
  IF(N-I)110,150,110
110 DO 140 J=1,NMAX
  IF(N-J)120,140,120
120 A(I,J)=A(I,J)+A(I,N)*A(N,J)
140 CONTINUE
150 A(I,N)=A(I,N)/D
C
  A(N,N)=1.0/D
C
200 CONTINUE
C
  RETURN
C
  END

  SUBROUTINE INTER(XI,RR,ZZ)
C
  IMPLICIT REAL*8 (A-H,O-Z)
  DIMENSION RR(1),ZZ(1),XI(1),XM(6),R(6),Z(6),XX(6)
  COMMON /PLANE/ NPP
  DATA XX/3*1.000,3*3.000/
C
  COMM=RR(2)*(ZZ(3)-ZZ(1))+RR(1)*(ZZ(2)-ZZ(3))+RR(3)*(ZZ(1)-ZZ(2))
  COMM=COMM/24.0
  R(1)=RR(1)
  R(2)=RR(2)
  R(3)=RR(3)
  R(4)=(R(1)+R(2))/2.
  R(5)=(R(2)+R(3))/2.
  R(6)=(R(3)+R(1))/2.
C
  Z(1)=ZZ(1)
  Z(2)=ZZ(2)
  Z(3)=ZZ(3)
  Z(4)=(Z(1)+Z(2))/2.
  Z(5)=(Z(2)+Z(3))/2.
  Z(6)=(Z(3)+Z(1))/2.
C
  IF(NPP)10,30,10
10 DO 20 I=1,6
20 XM(I)=XX(I)
  GO TO 40
30 DO 35 I=1,6
35 XM(I)=XX(I)*R(I)
C
40 DO 50 I=1,10

```



```

50 XI(I)=0.0
C
DO 100 I=1,6
XI(1)=XI(1)+XM(I)
XI(2)=XI(2)+XM(I)/R(I)
XI(3)=XI(3)+XM(I)/(R(I)**2)
XI(4)=XI(4)+XM(I)*Z(I)/R(I)
XI(5)=XI(5)+XM(I)*Z(I)/(R(I)**2)
XI(6)=XI(6)+XM(I)*Z(I)**2/(R(I)**2)
XI(7)=XI(7)+XM(I)*R(I)
XI(8)=XI(8)+XM(I)*Z(I)
XI(9)=XI(9)+XM(I)*R(I)**2
XI(10)=XI(10)+XM(I)*R(I)*Z(I)
100 CONTINUE
C
DO 150 I=1,10
150 XI(I)=XI(I)*COMM
C
RETURN
C
END

SUBROUTINE MODIFY(A,B,NEQ,MBAND,N,U)
C
IMPLICIT REAL*8 (A-H,O-Z)
DIMENSION A(140,70),B(140)
C
DO 250 M=2,MBAND
K=N-M+1
IF(K)235,235,230
230 B(K)=B(K)-A(K,M)*U
A(K,M)=0.0
235 K=N+M-1
IF(NEQ-K)250,240,240
240 B(K)=B(K)-A(N,M)*U
A(N,M)=0.0
250 CONTINUE
A(N,1)=1.0
B(N)=U
RETURN
C
END

SUBROUTINE BANSOL
C
IMPLICIT REAL*8 (A-H,O-Z)
COMMON /BANARG/ MM,NUMBLK,B(140),A(140,70)
C
NN = 2.*35.
NL=NN+1
NH=NN+NN
REWIND 1
REWIND 2
NB=0
GO TO 150
C*****
C REDUCE EQUATIONS BY BLOCKS
C*****
C
C 1. SHIFT BLOCK OF EQUATIONS
C
100 NB=NB+1
DO 125 N=1,NN
NM=NN+N
B(N)=B(NM)
B(NM)=0.0

```

```

      DO 125 M=1,MM
      A(N,M)=A(NM,M)
125  A(NM,M)=0.0
C
C      2. READ NEXT BLOCK OF EQUATIONS INTO CORE
C
      IF(NUMBLK-NB)150,200,150
150  READ(2)(B(N),(A(N,M),M=1,MM),N=NL,NH)
      IF(NB)200,100,200
C
C      3. REDUCE BLOCK OF EQUATIONS
C
200  DO 300 N=1,NN
      IF(A(N,1))225,300,225
225  B(N)=B(N)/A(N,1)
      DO 275 L=2,MM
      IF(A(N,L))230,275,230
230  C=A(N,L)/A(N,1)
      I=N+L-1
      J=0
      DO 250 K=L,MM
      J=J+1
250  A(I,J)=A(I,J)-C*A(N,K)
      B(I)=B(I)-A(N,L)*B(N)
      A(N,L)=C
275  CONTINUE
300  CONTINUE
C
C      4. WRITE BLOCK OF REDUCED EQUATIONS ON TAPE 2
C
      IF(NUMBLK-NB)375,400,375
375  WRITE(1)(B(N),(A(N,M),M=2,MM),N=1,NN)
      GO TO 100
C*****
C      BACK-SUBSTITUTION
C*****
400  DO 450 M=1,NN
      N=NN+1-M
      DO 425 K=2,MM
      L=N+K-1
425  B(N)=B(N)-A(N,K)*B(L)
      NM=N+NN
      B(NM)=B(N)
450  A(NM,NB)=B(N)
      NB=NE-1
      IF(NB)475,500,475
475  BACKSPACE 1
      READ(1)(B(N),(A(N,M),M=2,MM),N=1,NN)
      BACKSPACE 1
      GO TO 400
C*****
C      ORDER UNKNOWNAS IN B ARRAY
C*****
500  K=0
      DO 600 NB=1,NUMBLK
      DO 600 N=1,NN
      NM=N+NN
      K=K+1
600  B(K)=A(NM,NB)
C
      RETURN
C
      END

      SUBROUTINE GRDPLT (NN,NE,N1,N2,SCALE,XD,YD,HED,CLASS,IX,R,Z)
C**** ROUTINE TO PLOT THE FINITE ELEMENT GRID FOR WILSON'S CODE.
C

```

```

REAL*8 R(900),Z(900),SCALE,XD,YD
C
DIMENSION IX(800,5),HED(20),END(4),CLASS(3),DATE(2)
C
C
MAXDIF=0
WRITE (6,50) N1,N2,SCALE,XD,YD,CLASS
50 FORMAT(' MESH PLOT REQUESTED FOR ELEMENTS',I5,' TO ',I5/
1      'OSCALE=',T10,F10.6/
2      ' XD=',T10,F10.6/
3      ' YD=',T10,F10.6/
4      ' CLASS=',T10,3A4)
C
C**** PLOT ONLY THE ELEMENTS BETWEEN N1 AND N2, INCLUSIVE.
C
      N1=MAXO(N1,1)
      N2=MINO(N2,NE)
C
C**** FIND MINIMUM COORDINATES.
C
      XMIN=1.E75
      YMIN=XMIN
      DO 100 M=N1,N2
      DO 75 I=1,4
      K=IX(M,I)
      IF (K.LT.1 .OR. K.GT.NN) GO TO 75
      XMIN=AMIN1(XMIN,SNGL(R(K)))
      YMIN=AMIN1(YMIN,SNGL(Z(K)))
      75 CONTINUE
      100 CONTINUE
      WRITE (6,600) XMIN,YMIN
      600 FORMAT('OMINIMUM COORDINATES ARE',2E15.6)
C
C**** WRITE TITLES ON PLOT
C
      CALL SYMBOL(-1.0,4.0,0.105,CLASS(1),90.0,12)
      CALL ICAY(CATE)
      CALL SYMBOL(-1.0,6.0,0.105,DATE(1),90.0,8)
      CALL SYMBOL (0.0,0.5,0.105,HED(1),0.0,72)
C
C**** PLOT THE ELEMENTS.
C
      DO 200 M=N1,N2
      I=IX(M,1)
      J=IX(M,2)
      K=IX(M,3)
      L=IX(M,4)
      MAXDIF=MAXO(MAXDIF, IABS(I-J), IABS(I-K), IABS(I-L),
1      IABS(J-K), IABS(J-L), IABS(K-L))
      L=4
      IF (IX(M,4).EQ.IX(M,3)) L=3
      K=IX(M,L)
      IF (K.LT.1 .OR. K.GT.NN) GO TO 200
      XP=SCALE*(R(K)-XMIN)+XD
      YP=SCALE*(Z(K)-YMIN)+YD
      CALL PLOT (XP,YP,3)
      DO 150 I=1,L
      K=IX(M,I)
      IF (K.LT.1 .OR. K.GT.NN) GO TO 200
      XP=SCALE*(R(K)-XMIN)+XD
      YP=SCALE*(Z(K)-YMIN)+YD
      CALL PLOT (XP,YP,2)
      150 CONTINUE
      200 CONTINUE
      WRITE (6,2000) MAXDIF
      2000 FORMAT('OGRID PLOT FINISHED.  MAXIMUM NODE DIFFERENCE WAS',I3)
      CALL PLOT (17.0,0.0,-3)
      RETURN
      END

```

```
SUBROUTINE ZERO
  IMPLICIT REAL*8 (A-H,O-Z)
  COMMON Z1(6617)
  COMMON /ARG/ Z2(3198)
  COMMON /BANARG/ Z3(9941)
  DO 10 I=1,6617
10  Z1(I)=0.0
  DO 20 J=1,3198
20  Z2(J)=0.0
  DO 30 K=1,9941
30  Z3(K)=0.0
  RETURN
  END
```

APPENDIX B

FINITE ELEMENT COMPUTER PROGRAM FOR SHEAR STRESS PROPERTIES

```

C
C
C
COMMON B(700),X(700),Y(700),T(700),D(700),KODE(700),
1 HED(20),LM(5),IX(3),E(3,3),KX(4),P(5),S(5,5),DD(5),
2 XCOND(20),SPHT(20),DENS(20),QX(20)
COMMON /SYMARG/ NUMNP,MBAND,A(700,27),Q(700)
DIMENSION LMI(1250), LMJ(1250), LMK(1250), MTyp(1250), AREA(1250)
DIMENSION TXZ(1250), TYZ(1250)
DIMENSION JX(1250,5)
REAL*4 CLASS(3)
REAL*4 BUFF(5000)
LENGTH=5000
CALL PLOTS (BUFF,LENGTH)
C*****HEAT0006
C READ AND PRINT OF CONTROL INFORMATION HEAT0007
C*****HEAT0008
50 READ (5,1000) HED,NUMNP,NUMEL,NUMCBC,KAT,NUMMAT,NDT,INTER,DT, HEAT0009
1 ICHECK, MSHPL7
IF (KAT) 54,56,54 HEAT0010
54 WRITE (6,2010) HEAT0011
GO TO 58 HEAT0012
56 WRITE (6,2011) HEAT0013
58 WRITE (6,2000) HED,NUMNP,NUMEL,NUMCBC,NUMMAT,NDT,INTER,DT, HEAT0014
1 ICHECK, MSHPL7
C HEAT0015
READ (5,1003) (M,XCOND(M),SPHT(M),DENS(M),QX(M),N=1,NUMMAT) HEAT0016
WRITE(6,2009) (M,XCOND(M),SPHT(M),DENS(M),QX(M),M=1,NUMMAT) HEAT0017
C*****HEAT0018
C READ OR GENERATE NODAL POINT INFORMATION HEAT0019
C*****HEAT0020
WRITE (6,2001) HEAT0021
L=1 HEAT0022
HEAT0023
C HEAT0024
60 READ (5,1001) N,KODE(N),X(N),Y(N),T(N)
FA = 0.6308
RAD = SQRT(X(N)**2 + Y(N)**2)
IF(RAD .GT. 0.010) GO TO 62
X(N) = X(N)*FA
Y(N) = Y(N)*FA
GO TO 64
62 IF(X(N) .EQ. 0.) TH = 1.57079
IF(X(N) .NE. 0.) TH = ATAN(Y(N)/X(N))
IF(TH .LE. 45./57.2958) RP = 1./ COS(TH)
IF(TH .GT. 45./57.2958) RP = 1./ SIN(TH)
FP = (RP - FA*0.800)/(RP - 0.800)
RAD = RP - FP*(RP - RAD)
X(N) = RAD* COS(TH)
Y(N) = RAD* SIN(TH)
64 CONTINUE
DIFF=N+1-L
IF (N-L) 65,80,70
65 WRITE (6,2020) N
GO TO 60
70 DX=(X(N)-X(L-1))/DIFF
DY=(Y(N)-Y(L-1))/DIFF
75 KODE(L)=0
X(L)=X(L-1)+DX
HEAT0025
HEAT0026
HEAT0027
HEAT0028
HEAT0029
HEAT0030
HEAT0031
HEAT0032

```

```

      Y(L)=Y(L-1)+DY
      T(L)=0.0
80  WRITE (6,2002) L,KODE(L),X(L),Y(L),T(L)
      L=L+1
      IF (N-L) 90,80,75
90  IF (NUMNP+1-L) 100,100,60
100 CONTINUE
C*****
C  FORM CONDUCTIVITY MATRIX FOR COMPLETE BODY
C*****
      DO 110 I=1,NUMNP
      D(I)=0.0
      B(I)=0.0
      DO 110 J=1,27
110  A(I,J)=0.0
      MBAND=0
      NUM=0
      WRITE (6,2003)
C
      DO 200 N=1,NUMEL
C
C  1. READ OR GENERATE ELEMENT PROPERTIES
C
      IF (NUM-N) 120,121,121
120  READ (5,1002) NUM,KX(1),KX(2),KX(3),KX(4),MTYPE
      IF (NUM-((NUM-1)/32)*32 .GT. 24 .OR. NUM .GT. 384) MTYPE = 2
C
121  DO 122 I=1,4
122  LM(I)=LM(I)+1
C
      IF (NUM-N) 123,124,126
123  WRITE (6,2021) NUM
      GO TO 120
C
124  DO 125 I=1,4
125  LM(I)=KX(I)
      COND=XCOND(MTYPE)
C
126  WRITE (6,2004) N,LM(1),LM(2),LM(3),LM(4),MTYPE
      LMI(N) = LM(1)
      LMJ(N) = LM(2)
      LMK(N) = LM(3)
      MTYP(N) = MTYPE
      JX(N,1) = LM(1)
      JX(N,2) = LM(2)
      JX(N,3) = LM(3)
      JX(N,4) = LM(4)
      JX(N,5) = MTYPE
C
C  2. FORM ELEMENT CONDUCTIVITY MATRIX
C
      DO 150 I=1,5
      DD(I)=0.0
      P(I)=0.0
      DO 150 J=1,5
150  S(I,J)=0.0
C
      I=LM(1)
      J=LM(2)
      K=LM(3)
      L=LM(4)
      LM(5)=I
C
      XX=(X(I)+X(J)+X(K)+X(L))/4.
      YY=(Y(I)+Y(J)+Y(K)+Y(L))/4.
C
      DO 152 K=1,4
C
      I=LM(K)
      J=LM(K+1)

```

```

HEAT0033
HEAT0034
HEAT0035
HEAT0036
HEAT0037
HEAT0038
HEAT0039
HEAT0040
HEAT0041
HEAT0042
HEAT0043
HEAT0044
HEAT0045
HEAT0046
HEAT0047
HEAT0048
HEAT0049
HEAT0050
HEAT0051
HEAT0052
HEAT0053
HEAT0054
HEAT0055
HEAT0056
HEAT0058
HEAT0059
HEAT0060
HEAT0061
HEAT0062
HEAT0063
HEAT0064
HEAT0065
HEAT0066
HEAT0067
HEAT0068
HEAT0069
HEAT0070
HEAT0071
HEAT0072
HEAT0073
HEAT0074
HEAT0075
HEAT0076
HEAT0077
HEAT0078
HEAT0079
HEAT0080
HEAT0081
HEAT0082
HEAT0083
HEAT0084
HEAT0085
HEAT0086
HEAT0087
HEAT0088
HEAT0089
HEAT0090
HEAT0091
HEAT0092

```

```

      IF (I-J) 135,152,135
135  AJ=X(J)-X(I)
      AK=XX-X(I)
      BJ=Y(J)-Y(I)
      BK=YY-Y(I)
      C=BJ-BK
      DX=AK-AJ
C
      XMUL=1.0
      IF (KAT) 136,137,136
136  XMUL=XMUL*(X(I)+X(J)+XX)/3.0
C
137  XLAM=AJ*BK-AK*BJ
      COMM=.5*COND*XMUL/XLAM
      QQ=XLAM*XMUL*QX(MTYPE)/4.0
      QSTORE=XLAM*XMUL*SPHT(MTYPE)*DENS(MTYPE)/4.0
C
      E(1,1)=C**2+DX**2
      E(1,2)=BK*C-AK*DX
      E(1,3)=-BJ*C+AJ*DX
      E(2,1)=E(1,2)
      E(2,2)=BK**2+AK**2
      E(2,3)=-BJ*BK-AJ*AK
      E(3,1)=E(1,3)
      E(3,2)=E(2,3)
      E(3,3)=BJ**2+AJ**2
C
      IX(1)=K
      IX(2)=K+1
      IF (K-4) 145,140,145
140  IX(2)=1
145  IX(3)=5
C
      DO 151 I=1,3
      II=IX(I)
      P(II)=P(II)+QQ
      DD(II)=DD(II)+QSTORE
      DO 151 J=1,3
      JJ=IX(J)
151  S(II,JJ)=S(II,JJ)+E(I,J)*COMM
C
152  CONTINUE
C
      DO 155 I=1,4
      DO 155 J=1,4
155  S(I,J)=S(I,J)-S(I,5)*S(J,5)/S(5,5)
C
3.  ADD ELEMENT CONDUCTIVITY TO COMPLETE CONDUCTIVITY MATRIX
C
      DO 175 L=1,4
      I=LM(L)
      D(I)=D(I)+DD(L)
      B(I)=B(I)+P(L)
      DO 175 M=1,4
      J=LM(M)-I+1
      IF (27-J) 123,158,158
158  IF(MBAND-J) 160,165,165
160  MBAND=J
165  IF(J) 175,175,170
170  A(I,J)=A(I,J)+S(L,M)
175  CONTINUE
C
200  CONTINUE
C*****
C  BOUNDARY CONDITIONS
C*****
C  1. CONVECTION BOUNDARY CONDITIONS
C
      IF (NUMCBC) 220,220,205

```

```

HEAT0093
HEAT0094
HEAT0095
HEAT0096
HEAT0097
HEAT0098
HEAT0099
HEAT0100
HEAT0101
HEAT0102
HEAT0103
HEAT0104
HEAT0105
HEAT0106
HEAT0107
HEAT0108
HEAT0109
HEAT0110
HEAT0111
HEAT0112
HEAT0113
HEAT0114
HEAT0115
HEAT0116
HEAT0117
HEAT0118
HEAT0119
HEAT0120
HEAT0121
HEAT0122
HEAT0123
HEAT0124
HEAT0125
HEAT0126
HEAT0127
HEAT0128
HEAT0129
HEAT0130
HEAT0131
HEAT0132
HEAT0133
HEAT0134
HEAT0135
HEAT0136
HEAT0137
HEAT0138
HEAT0139
HEAT0140
HEAT0141
HEAT0142
HEAT0143
HEAT0144
HEAT0145
HEAT0146
HEAT0147
HEAT0148
HEAT0149
HEAT0150
HEAT0151
HEAT0152
HEAT0153
HEAT0154
HEAT0155
HEAT0156
HEAT0157
HEAT0158
HEAT0159
HEAT0160
HEAT0161
HEAT0162

```

```

205 WRITE (6,2006)
DO 215 N=1,NUMCBC
WRITE(6,2004) NUMNP,NUMCBC,N
READ (5,1007) I,J,H,TEMP
WRITE (6,2007) I,J,H,TEMP
XL=SQRT((X(J)-X(I))**2+(Y(J)-Y(I))**2)
IF (KAT) 206,207,206
206 XL=XL*(X(I)+X(J))/2.
207 TEMP=H*XL*TEMP/2.
H=H*XL/4.
B(I)=B(I)+TEMP
B(J)=B(J)+TEMP
A(I,1)=A(I,1)+H
A(J,1)=A(J,1)+H
K=J-I+1
IF (K) 212,212,210
210 A(I,K)=A(I,K)+H
GO TO 215
212 K=I-J+1
A(J,K)=A(J,K)+H
215 CONTINUE
220 CONTINUE
C
C 2. TEMPERATURE BOUNDARY CONDITIONS
C
DO 300 N=1,NUMNP
B(N)=B(N)+T(N)
IF(KODE(N)) 225,300,225
225 DO 250 M=2,MBAND
K=N-M+1
IF(K) 235,235,230
230 B(K)=B(K)-A(K,M)*T(N)
A(K,M)=0.0
235 L=N+M-1
IF(NUMNP-L) 245,240,240
240 B(L)=B(L)-A(N,M)*T(N)
245 A(N,M)=0.0
250 CONTINUE
A(N,1)=1.0
B(N)=T(N)
300 CONTINUE
C*****
C PLOT A MESH PLOT OF THE GEOMETRY, IF REQUESTED.
C*****
C
C (N1,N2) ARE FIRST AND LAST ELEMENTS NUMBERS TO BE PLOTTED
C SCALE IS FACTOR TO MAKE VERTICAL DIMENSION .LE. 10.0 INCHES
C (XD,YD) ARE COORDINATES OF ORIGIN ON PAPER (YD .GE. 0.5 )
C CLASS CONTAINS 0-12 HOLLERITH CHARACTERS. WRITTEN ON LEFT EDGE.
IF (MSHPLT.LE.0) GO TO 346
DO 345 M=1,MSHPLT
READ (5,1006) N1,N2,SCALE,XD,YD,CLASS
CALL GRDPLT (NUMNP,NUMEL,N1,N2,SCALE,XD,YD,HED,CLASS,JX,X,Y)
345 CONTINUE
346 IF (ICHECK.NE.0) GO TO 50
C
C*****
C SOLVE FOR NODAL POINT TEMPERATURES HEAT0204
C***** HEAT0205
C FORM EFFECTIVE CONDUCTIVITY MATRIX FOR TIME INCREMENT HEAT0206
C HEAT0207
C HEAT0208
IF (DT) 700,700,304 HEAT0209
304 DT2=1.0/DT HEAT0210
DO 320 N=1,NUMNP HEAT0211
T(N)=0.0 HEAT0212
IF (KODE(N)) 320,305,320 HEAT0213
305 IF (D(N)) 310,320,310 HEAT0214
310 D(N)=DT2*D(N) HEAT0215
A(N,1)=A(N,1)+D(N) HEAT0216
320 CONTINUE HEAT0217

```



```

C          CALL SYMSOL(1)
C          CALCULATE TEMPERATURE AT THE END OF EACH TIME INCREMENT
C          TIME=0.0
C          LL=0
C          DD 600 L=1,NDT
C          1. CALCULATE EFFECTIVE LOAD MATRIX
C          DD 400 I=1,NUMNP
C          Q(I)=B(I)
C          IF (KODE(I)) 400,395,400
395 Q(I)=B(I)+D(I)*T(I)
400 CONTINUE
C          2. SOLVE FOR TEMPERATURES
C          CALL SYMSOL(2)
C          DO 500 I=1,NUMNP
500 T(I)=Q(I)
C          TIME=TIME+DT
C          LL=LL+1
C          IF (LL-INTER) 600,550,550
550 WRITE (6,2005) TIME,(N,T(N),N=1,NUMNP)
C          LL=0
600 CONTINUE
C          GO TO 50
C          STEADY STATE SOLUTION
C          700 DO 800 I=1,NUMNP
800 Q(I)=B(I)
C          CALL SYMSOL(1)
C          CALL SYMSOL(2)
C          WRITE (6,2005) TIME,(N,Q(N),N=1,NUMNP)
C          AREAT = 0.0
C          AREAM = 0.0
C          AREAF = 0.0
C          TXZA = 0.0
C          TXZAF = 0.0
C          TXZAM = 0.0
C          IP = 1
C          FRING = 0.0
C          DO 900 II = 1,NUMEL
C          I = LMI(II)
C          J = LMJ(II)
C          K = LMK(II)
C          M = MTP(II)
C          AREA(II) = (X(J)*Y(K) - Y(J)*X(K) - X(I)*Y(K) + Y(I)*X(K) + X(I)*
1Y(J) - Y(I)*X(J))/2.0
C          AREAT = AREAT + AREA(II)
C          IF (M .EQ. 1) AREAF = AREAF + AREA(II)
C          IF (M .EQ. 2) AREAM = AREAM + AREA(II)
C          BI = Y(J) - Y(K)
C          BJ = Y(K) - Y(I)
C          BK = Y(I) - Y(J)
C          CI = X(K) - X(J)
C          CJ = X(I) - X(K)
C          CK = X(J) - X(I)
C          PHIX = (BI*Q(I) + BJ*Q(J) + BK*Q(K))/(2.0*AREA(II))
C          PHIY = (CI*Q(I) + CJ*Q(J) + CK*Q(K))/(2.0*AREA(II))
C          TXZ(II) = XCOND(M)*PHIX
C          TYZ(II) = XCOND(M)*PHIY
C          FRING = FRING + 2.0*TXZ(II)*AREA(II)/SPHT(M)
C          TXZA = TXZA + TXZ(II)*AREA(II)

```

```

HEAT0218
HEAT0219
HEAT0220
HEAT0221
HEAT0222
HEAT0223
HEAT0224
HEAT0225
HEAT0226
HEAT0227
HEAT0228
HEAT0229
HEAT0230
HEAT0231
HEAT0232
HEAT0233
HEAT0234
HEAT0235
HEAT0236
HEAT0237
HEAT0238
HEAT0239
HEAT0240
HEAT0241
HEAT0242
HEAT0243
HEAT0244
HEAT0245
HEAT0246
HEAT0247
HEAT0248
HEAT0249
HEAT0250
HEAT0251
HEAT0252
HEAT0253
HEAT0254
HEAT0255
HEAT0256
HEAT0257

```

```

IF(M.EQ. 1) TXZAF = TXZAF + TXZ(II)*AREA(II)
IF(M.EQ. 2) TXZAM = TXZAM + TXZ(II)*AREA(II)
850 CONTINUE
900 CONTINUE
WRITE(6,2030) (II, AREA(II), TXZ(II), TYZ(II), II = 1,NUMEL)
WRITE(6,2031) AREAT, FRING, TXZA, TXZAF, TXZAM, AREAF, AREAM
2030 FORMAT( I5, 3E15.3)
2031 FORMAT(8H1AREA = , F6.3/16H FRINGE ORDER = , E10.3 /21H AVG. SHEAR
1 STRESS = , E10.3/27H AVG. FIBER SHEAR STRESS = ,E10.3/28H AVG. MA
2TRIX SHEAR STRESS = ,E10.3/14H FIBER AREA = ,F6.3/15H MATRIX AREA
3= ,F6.3)
GO TO 50
C
C
C
C
1000 FORMAT (20A4/7I5,E15.6,2I5)
1001 FORMAT (2I5,3F10.0)
1002 FORMAT (6I5)
1003 FORMAT (I10,4F10.0)
1007 FORMAT (2I5,2F10.0)
1006 FORMAT(2I5, 3F10.0, 3A4)
C
2000 FORMAT (1H0 20A4// 25HNUMBER OF NODAL POINTS-- I4/
1 25H NUMBER OF ELEMENTS----- I4 / 25H NUMBER OF CONVECTION BC-I4/HEAT0268
2 25H NUMBER OF MATERIALS----- I4 / 25H NUMBER OF INCREMENTS----I4/HEAT0270
3 25H OUTPUT INTERVAL----- I4 / 20H TIME INTERVAL----- E10.3/ HEAT0271
4 25H DATA CHECK ONLY (0=NO)-- I4/
5 25H NUMBER OF PLOTS----- I4)
2001 FORMAT (20H0 N.P. NO. CODE 14X,1HX,14X,1HY,14X,1HT) HEAT0272
2002 FORMAT (2I10,3E15.6) HEAT0273
2003 FORMAT (35H0 N I J K L MATERIAL ) HEAT0274
2004 FORMAT (5I5,I10) HEAT0275
2005 FORMAT (6H0TIME= E12.5/ (I6,E14.6,I6,E14.6,I6,E14.6,I6,E14.6,
1 I6,E14.6,I6,E14.6)) HEAT0276
2006 FORMAT (40H0 I J H TEMPERATURE ) HEAT0277
2007 FORMAT (2I5,2E15.6) HEAT0278
2009 FORMAT (4H0 M 14X 1HK 14X 1HC 14X 1HD 14X 1H0/ (I4,4E15.6)) HEAT0279
2010 FORMAT (25H1AXISYMMETRIC SOLID BODY ) HEAT0280
2011 FORMAT (27HITWO DIMENSIONAL PLANE BODY ) HEAT0281
C
2020 FORMAT (10H0CARD NO. I4, 13H OUT OF ORDER ) HEAT0282
2021 FORMAT (13H0BAD CARD NO. I4) HEAT0283
C
C
C
C
END HEAT0284
HEAT0285
HEAT0286
HEAT0287

SUBROUTINE SYMSOL (KKK) HEAT0289
C
COMMON /SYMARG/ NN,MM,A(700,27),B(700) HEAT0290
C
GO TO (1000,2000),KKK HEAT0291
C
REDUCE MATRIX HEAT0292
C
REDUCE MATRIX HEAT0293
C
REDUCE MATRIX HEAT0294
C
REDUCE MATRIX HEAT0295
C
REDUCE MATRIX HEAT0296
1000 DO 280 N=1,NN HEAT0297
DO 260 L=2,MM HEAT0298
C=A(N,L)/A(N,1) HEAT0299
I = N+L-1 HEAT0300
IF(NN-I) 260,240,240 HEAT0301
240 J=0 HEAT0302
DO 250 K=L,MM HEAT0303
J=J+1 HEAT0304
250 A(I,J)=A(I,J)-C*A(N,K) HEAT0305
260 A(N,L)=C HEAT0306
280 CONTINUE HEAT0307
GO TO 500 HEAT0308
C
REDUCE VECTOR HEAT0309
C
REDUCE VECTOR HEAT0310
C
REDUCE VECTOR HEAT0311

```

```

2000 DO 290 N=1,NN
      DO 285 L=2,MM
        I=N+L-1
        IF(NN-I) 290,285,285
285  B(I)=B(I)-A(N,L)*B(N)
290  B(N)=B(N)/A(N,1)
C
C    BACK SUBSTITUTION
C
      N=NN
300  N = N-1
      IF(N) 350,500,350
350  DO 400 K=2,MM
        L = N+K-1
        IF(NN-L) 400,370,370
370  B(N) = B(N) - A(N,K) * B(L)
400  CONTINUE
      GO TO 300
C
500  RETURN
C
      END

```

HEAT0312
HEAT0313
HEAT0314
HEAT0315
HEAT0316
HEAT0317
HEAT0318
HEAT0319
HEAT0320
HEAT0321
HEAT0322
HEAT0323
HEAT0324
HEAT0325
HEAT0326
HEAT0327
HEAT0328
HEAT0329
HEAT0330
HEAT0331
HEAT0332
HEAT0333

```

      SUBROUTINE GRDPLT (NN,NE,N1,N2,SCALE,XD,YD,HED,CLASS,IX,R,Z)
C
C**** ROUTINE TO PLOT THE FINITE ELEMENT GRID FOR WILSON'S CODE.
C
      REAL*4 R(700),Z(700),SCALE,XD,YD
C
      DIMENSION IX(1250,5),HED(20),END(4),CLASS(3),DATE(2)
C
C
      MAXDIF=0
      WRITE (6,50) N1,N2,SCALE,XD,YD,CLASS
50  FORMAT(' MESH PLOT REQUESTED FOR ELEMENTS',I5,' TO ',I5/
1    ' OSCALE=',T10,F10.6/
2    ' XD=',T10,F10.6/
3    ' YD=',T10,F10.6/
4    ' CLASS=',T10,3A4)
C
C**** PLOT ONLY THE ELEMENTS BETWEEN N1 AND N2, INCLUSIVE.
C
      N1=MAX0(N1,1)
      N2=MIN0(N2,NE)
C
C**** FIND MINIMUM COORDINATES.
C
      XMIN = 1.0E50
      YMIN=XMIN
      DO 100 M=N1,N2
      DO 75 I=1,4
        K=IX(M,I)
        IF (K.LT.1 .OR. K.GT.NN) GO TO 75
        XMIN=AMINI(XMIN,R(K))
        YMIN=AMINI(YMIN,Z(K))
75  CONTINUE
100 CONTINUE
      WRITE (6,600) XMIN,YMIN
600 FORMAT(' MINIMUM COORDINATES ARE',2E15.6)
C
C**** WRITE TITLES ON PLOT
C
      CALL SYMBOL(-1.0,4.0,0.105,CLASS(1),90.0,12)
      CALL IDAY(DATE)
      CALL SYMBOL(-1.0,6.0,0.105,DATE(1),90.0,8)
      CALL SYMBOL (0.0,0.5,0.105,HED(1),0.0,72)
C
C**** PLOT THE ELEMENTS.

```

C

```
DO 200 M=N1,N2
I=IX(M,1)
J=IX(M,2)
K=IX(M,3)
L=IX(M,4)
MAXDIF=MAX0(MAXDIF, IABS(I-J), IABS(I-K), IABS(I-L),
1 IABS(J-K), IABS(J-L), IABS(K-L))
L=4
IF (IX(M,4).EQ.IX(M,3)) L=3
K=IX(M,L)
IF (K.LT.1 .OR. K.GT.NN) GO TO 200
XP=SCALE*(R(K)-XMIN)+XD
YP=SCALE*(Z(K)-YMIN)+YD
CALL PLOT (XP,YP,3)
DO 150 I=1,L
K=IX(M,I)
IF (K.LT.1 .OR. K.GT.NN) GO TO 200
XP=SCALE*(R(K)-XMIN)+XD
YP=SCALE*(Z(K)-YMIN)+YD
CALL PLOT (XP,YP,2)
150 CONTINUE
200 CONTINUE
WRITE (6,2000) MAXDIF
2000 FORMAT('OGRID PLOT FINISHED. MAXIMUM NODE DIFFERENCE WAS',I3)
CALL PLOT (17.0,0.0,-3)
RETURN
END
```

APPENDIX C

EXTRACTION OF INITIAL BIREFRINGENCE

Load-induced birefringence is the total birefringence minus the initial birefringence. This relationship may be written:

$$[N] = [N_T] - [N_I] \quad , \quad (C-1)$$

where:

$[N]$ represents the load birefringence tensor,

$[N_T]$ the total or observed birefringence tensor, and

$[N_I]$ the initial birefringence tensor.

From Equation 42, the tensors may be expressed in terms of their principal components and orientation angle with respect to the chosen coordinate system:

$$\begin{bmatrix} N_p \cos^2 \phi + N_q \sin^2 \phi \\ N_p \sin^2 \phi + N_q \cos^2 \phi \\ (N_q - N_p) \sin \phi \cos \phi \end{bmatrix} = \begin{bmatrix} N_{pT} \cos^2 \phi_T + N_{qT} \sin^2 \phi_T \\ N_{pT} \sin^2 \phi_T + N_{qT} \cos^2 \phi_T \\ (N_{qT} - N_{pT}) \sin \phi_T \cos \phi_T \end{bmatrix} \quad (C-2)$$

$$\begin{bmatrix} N_{pI} \cos^2 \phi_I + N_{qI} \sin^2 \phi_I \\ N_{pI} \sin^2 \phi_I + N_{qI} \cos^2 \phi_I \\ (N_{qI} - N_{pI}) \sin \phi_I \cos \phi_I \end{bmatrix}$$

where:

p and q represents the principal birefringence directions, and

ϕ the isoclinic angle relative to the coordinate system.

The first two terms in the birefringence matrix are summed to find one of the stress-optic relations. When this summation is accomplished:

$$\begin{aligned} (N_p - N_q) (\cos^2 \phi - \sin^2 \phi) &= (N_{pT} - N_{qT}) (\cos^2 \phi_T - \sin^2 \phi_T) \\ &- (N_{pI} - N_{qI}) (\cos^2 \phi_I - \sin^2 \phi_I) \end{aligned} \quad (C-3)$$

The third terms yield:

$$\begin{aligned} (N_q - N_p) \sin\phi \cos\phi &= (N_{qT} - N_{pT}) \sin\phi_T \cos\phi_T \\ &- (N_{qI} - N_{pI}) \sin\phi_I \cos\phi_I \end{aligned} \quad (C-4)$$

Squaring Equations C-3 and C-4 and using trigonometric identities and Equation 46 gives the expression for the load birefringence:

$$N = \sqrt{N_T^2 + N_I^2 - 2N_T N_I \cos 2(\phi_T - \phi_I)} \quad (C-5)$$

Dividing Equation C-4 by C-3 gives the load isoclinic:

$$\phi = \frac{1}{2} \tan^{-1} \left[\frac{N_T \sin 2\phi_T - N_I \sin 2\phi_I}{N_T \cos 2\phi_T - N_I \cos 2\phi_I} \right] \quad (C-6)$$

The load-induced birefringence and isoclinic are used for the analysis.

ACKNOWLEDGEMENTS

The author wishes to express his appreciation to his advisor, Dr. Hui Pih, for his guidance and many helpful discussions throughout this research. The author also gratefully acknowledges the opportunity which the Development Division of the Oak Ridge Y-12 Plant extended to conduct this research. A special thanks is due the author's supervisors, W. S. Dritt and F. W. Jones, for their support and encouragement.

DISTRIBUTION**Atomic Energy Commission - Oak Ridge**

Hickman, H. D.
 Leed, R. E.
 Zachry, D. S., Jr

Lawrence Livermore Laboratory

Broadman, G. A.
 Chiao, T. T.
 Garner, B. L.

Los Alamos Scientific Laboratory

Hockett, J. E.

Oak Ridge Gaseous Diffusion Plant

Blake, H. W.
 Douglass, T. E.
 Keyser, R. M.
 Waters, D. A.
 Wilcox, W. J., Jr
 Winkel, R. A.

Oak Ridge Y-12 Plant

Alvey, H. E.
 Burditt, R. B.
 Burkhart, L. E.
 Denny, A.
 Dritt, W. S.
 Ebert, T. H.
 Ellingson, R. D.
 Fraser, R. J.
 Gritzner, V. D.
 Huddleston, R. L.
 Jones, F. W.
 Kahl, K. G.
 Keith, A.
 Knight, C. E., Jr (15)
 Lundin, M. I.
 Oakes, R. E., Jr
 Phillips, L. R.
 Poore, M. W.

Reeves, C. A.
 Schreyer, J. M.
 Smith, H. F., Jr
 Smith, R. D.
 Stoner, H. H.
 Tewes, W. E.
 Weathersby, W. E.
 Yaggi, W. J./Googin, J. M.
 Y-12 Central Files (5)
 Y-12 Central Files (master copy)
 Y-12 Central Files (route copy)
 Y-12 Central Files (Y-12RC)
 Zerby, C. D.

Paducah Gaseous Diffusion Plant

Levin, R. W.

Sandia - Albuquerque

Gerstle, F. P.
 Schuster, D. M.

In addition, this report is distributed in accordance with the category UC-25, **Materials**, as given in the *USAEC Standard Distribution Lists for Unclassified Scientific and Technical Reports*, TID-4500.